STRUCTURAL AND FUNCTIONAL ASPECTS OF SPERM HEAD MORPHOLOGY IN THE PLAINS MOUSE, *Pseudomys australis*

A thesis submitted for the degree of Doctor of Philosophy in the University of Adelaide

by

SEAN P. FLAHERTY (BSc. Hons.)

DEPARTMENT OF ANATOMY AND HISTOLOGY

UNIVERSITY OF ADELAIDE

VOLUME 2

January, 1986

LIST OF ABBREVIATIONS

A	Type A spermatogonium
Ac	Acrosome
Am	Amorphous structure
An	Annulus
AP	Acrosomal projection
AS	Apical segment
Ax	Axoneme
AZ	Acrosomal zonule
B	Type B spermatogonium
Bl	Bleb
BP	Basal plate
C	Core of acrosomal contents
CC	Cumulus cell
CG	Cortical granule
CP	Connecting piece
CPD	Cytoplasmic droplet
D	Dorsal hook
DG	Dense cortical granule
DL	Post-acrosomal dense lamina
DR	Sub-acrosomal dorsal ridge
ECM	Extra-cellular matrix
EPS	Sertoli cell ectoplasmic specializations
ES	Equatorial segment
F	Filament
FS	Fibrous sheath
G	Golgi
GG	Granular cortical granule
Gr	ECM granule
Gx	Glycocalyx
I	Intermediate spermatogonium
L	Leptotene primary spermatocyte
Li	Lipid droplet
M	Spermatocyte completing first meiotic division
Mc	Mitochondria
Mf	Microfilaments
MP	Middle piece
Mv	Microvilli
MW	Membrane whorl
N	Nucleus
NE	Nuclear envelope
NV	Nuclear vacuole
O	Oocyte
ODF	Outer dense fibres
OMM	Outer mitochondria membrane
P	Periodic stuctures
PAR	Post-acrosomal region
PB	Polar body
Pc	Pachytene primary spermatocyte
PM	Plasma membrane
Pn	Pronucleus
Po	Zona pore
Pp	Pseudoperforatorium
Pr	Projections from dense lamina

LIST OF ABBREVIATIONS (continued)

PR	Posterior ring
PS	Principal segment
PVS	Peri-vitelline space
R	Resting primary spermatocyte
RER	Rough endoplasmic reticulum
Ri	Ribosome
RNE	Redundant nuclear envelope
RSt	Round spermatid
S	Secondary spermatocyte
SAM	Sub-acrosomal material
SAS	Sub-acrosomal space
SER	Smooth endoplasmic reticulum
Sp	Meiotic spindle
Sr	Strand of ECM
St	Spermatid
Sz	Spermatozoa
TBC	Tubulobulbar complexe
TS	Tubular structures
V	Ventral Hooks
VAP	Ventral acrosomal plate
VGM	Variable glycocalyx material
Vi	Vitellus
VS	Ventral spur
Z	Zygotene primary spermatocyte
ZP	Zona pellucida

PLATE 1

Fig. 1. Phase contrast micrograph of an unwashed cauda epididymal spermatozoon. The three hooks lie close together on the apical margin of the sperm head.
Bar = 10 µm. x 2,990

Fig. 2. Phase contrast micrograph of a washed spermatozoon, showing the hooks spread apart. There is a single dorsal hook (D), and two ventral hooks (V) which are united caudally.
Bar = 10 µm. x 2,990

Fig. 3. Scanning electron micrograph of the sperm head, showing the extent of the equatorial segment (ES) of the acrosome, and the post-acrosomal region (PAR). A ventral spur (VS) is located on the ventral surface of the sperm head, immediately anterior to the point of tail insertion. There is a deep depression on either side of the sperm head at the base of the hooks (arrow).
Bar = 1 µm. x 21,280

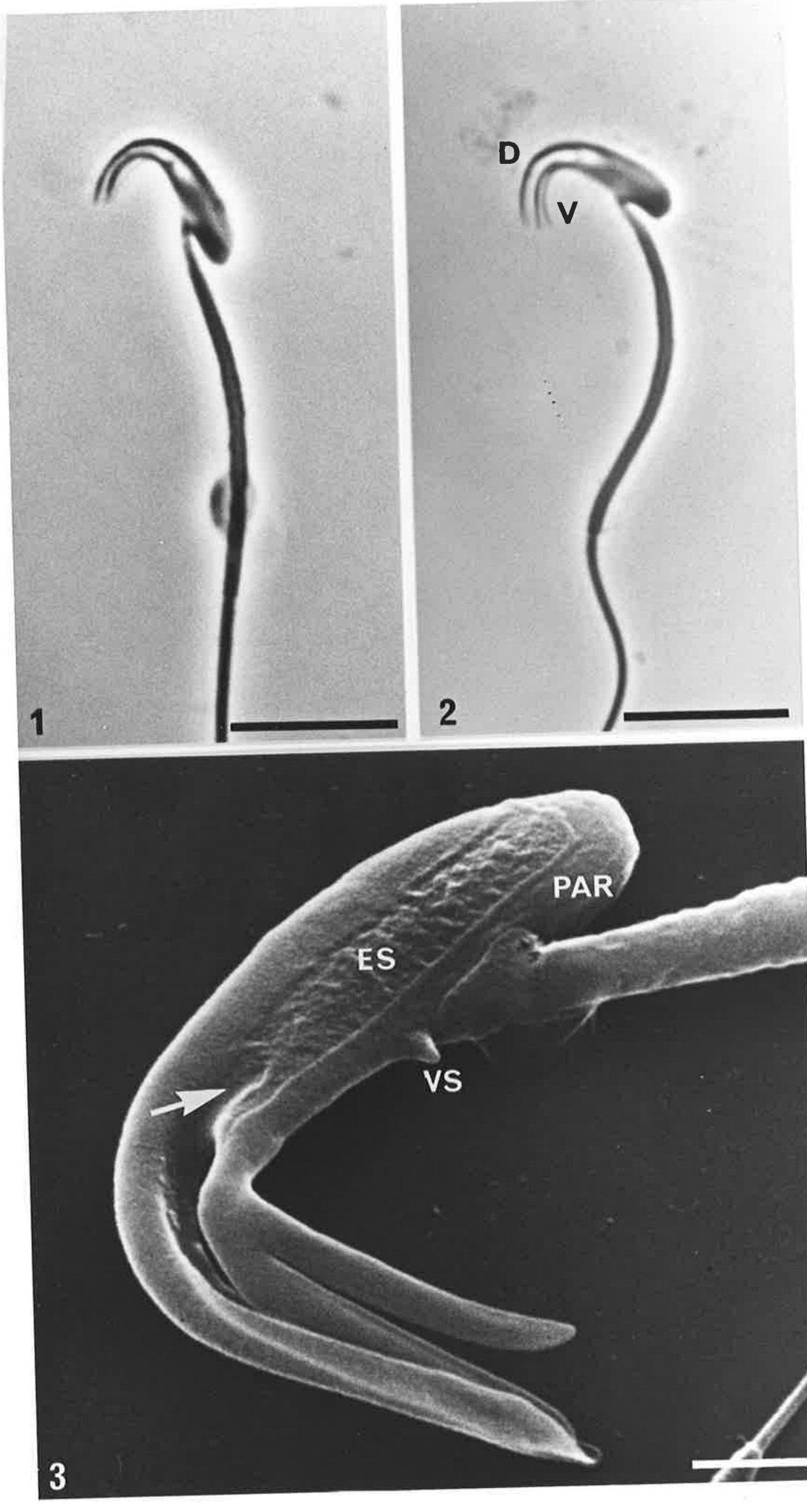
1
2
D
V
3
PAR
ES
VS

PLATE 2

Fig. 4. Scanning electron micrograph of the three hooks. The lines indicate the approximate planes of section in Fig. 5.
Bar = 1 µm. x 14,620

Fig. 5. A series of transverse sections cut through the hooks at the levels indicated in Fig. 5, showing the variation in the size, shape and structure of the hooks. The dorsal hook contains nuclear material (N), and a thick layer of sub-acrosomal material (SAM). The principal segment (PS) of the acrosome caps the dorsal margin, and is indented by one or two sub-acrosomal ridges (DR), whilst the remainder appears to be an extension of the equatorial segment (ES). There is also an isolated plate of acrosome (VAP) on the ventral surface of the hook. The sub-acrosomal material projects beyond the termination of the nucleus as a crescent-shaped rod or pseudoperforatorium (Pp). The nucleus (N) is only present at the base of the ventral hooks. They appear to consist largely of material of similar electron density to the sub-acrosomal material (SAM) in the dorsal hook. Two thin projections of acrosome (AP) extend into the base of the ventral hooks, but terminate caudal to the point of bifurcation.
No OsO_4 post-fixation.
Bar = 0.5 µm. x 47,580

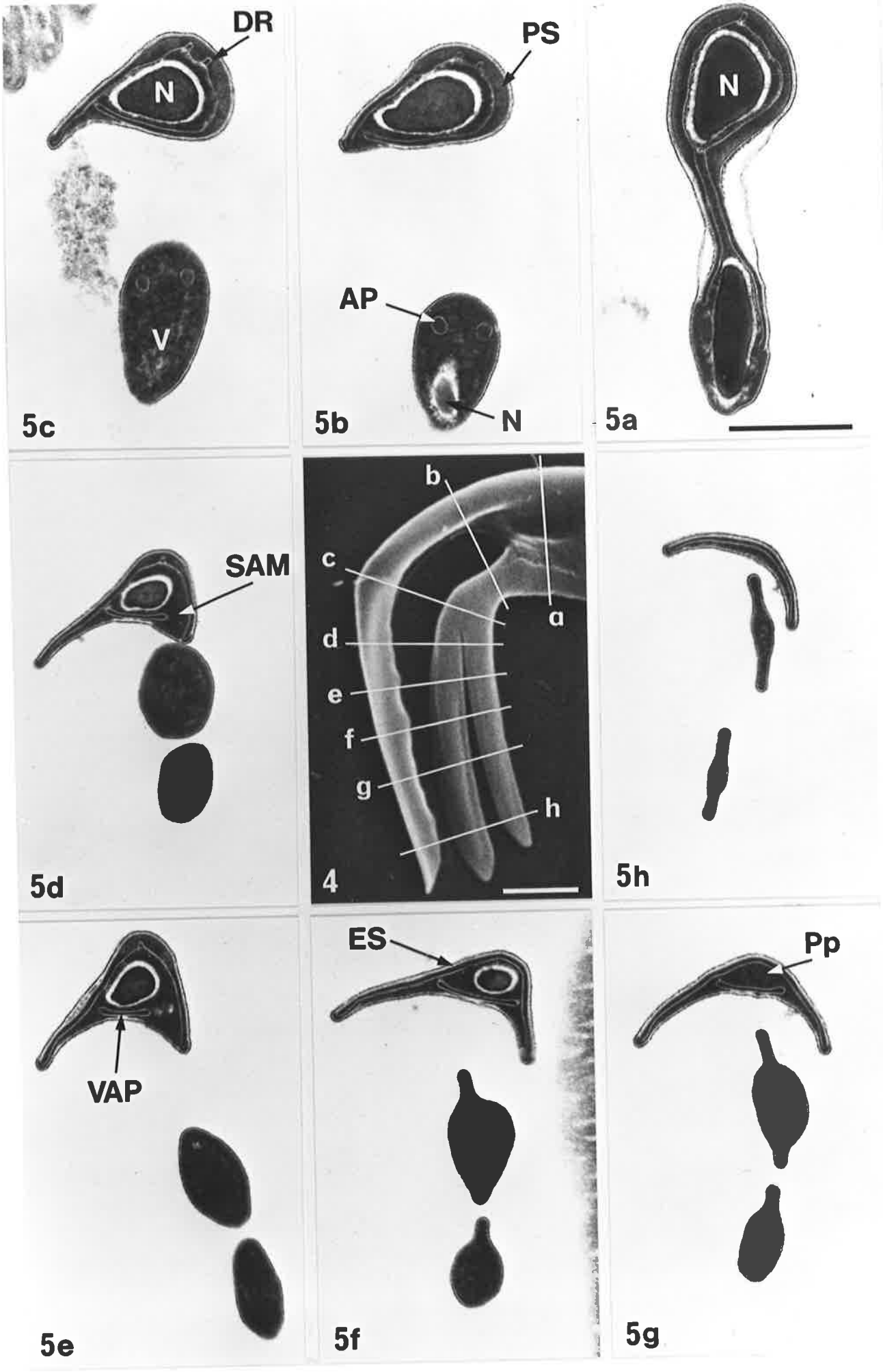
DR
N
V
5c
PS
AP
N
5b
N
5a
SAM
5d
b
c
a
d
e
f
g
h
4
5h
VAP
5e
ES
5f
Pp
5g

PLATE 3

Fig. 6. Transverse section cut through the dorsal hook, showing the nucleus (N), nuclear envelope (NE), sub-acrosomal material (SAM), and equatorial segment (ES). The plasma membrane (PM) is loosely applied over the acrosome, but tightly adherant to the ventral surface of the hook (arrow).
Bar = 0.2 µm. x 87,870

Fig. 7. In the dorsal hook, the inner leaflet of the inner acrosomal membrane is of increased density (arrow), the plasma membrane (PM) is closely associated with the ventral surface of the hook, and periodic structures (P) occur on the lateral tip of the hook.
Bar = 0.1 µm. 150,450

Fig. 8. Higher magnification of the periodic structures (P) on the tip of the dorsal hook.
Bar = 0.05 µm. x 220,100

Figs. 9, 10. The material in the ventral hooks is confluent with the sub-acrosomal material (SAM) in the remainder of the sperm head. Two thin acrosomal projections (AP), which arise from the equatorial segment (ES), extend into the hooks for a distance of up to 1 µm, then terminate in a slightly bulbous region (arrow).
No OsO_4 post-fixation. Bar = 0.5 µm. x 46,790 (9)
x 42,850 (10)

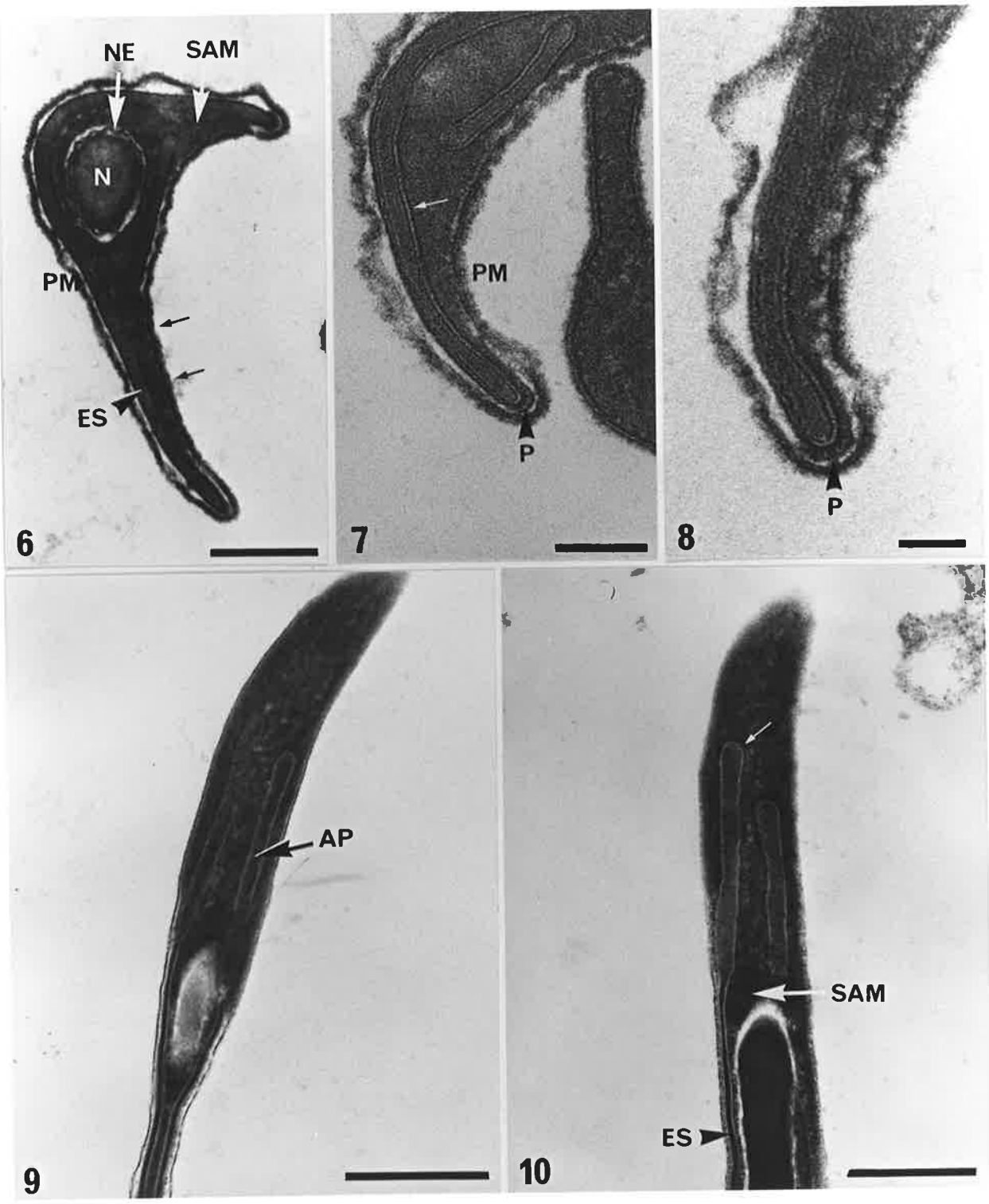
NE
SAM
N
PM
ES
6
PM
P
7
P
8
AP
9
SAM
ES
10

PLATE 4

Fig. 11. This transverse section of the ventral hooks shows that a less homogeneous zone (arrowhead) demarcates the core and peripheral layers. Sub-membranous projections (Pr) link the plasma membrane to the peripheral layer.
Bar = 0.1 µm. x 96,890

Fig. 12. Longitudinal section of the sperm head, revealing that the peripheral layer of the ventral hooks is a continuation of the post-acrosomal dense lamina (DL) on the ventral surface of the sperm head.
No OsO_4 post-fixation. Bar = 0.5 µm. x 36,350

Figs. 13, 14. The projections (Pr) are regularly arranged, with a centre-centre spacing of 14-15 nm, and are found along the entire length of the ventral hooks.
Bar = 0.1 µm. x 121,340

Figs. 15-17. Higher magnifications of the ventral hooks, showing that the projections are roughly square or triangular in outline, and appear to fuse with the inner leaflet of the plasma membrane (PM), which is of increased electron density (arrow).
Bar = 0.05 µm. x 193,780

Fig. 18. The acrosomal projections (AP) at the base of the ventral hooks are about 70 nm in diameter. The outer leaflet of the acrosomal membrane which is in contact with the sub-acrosomal material (SAM), is of higher density (arrow).
Bar = 0.05 µm. x 193,780

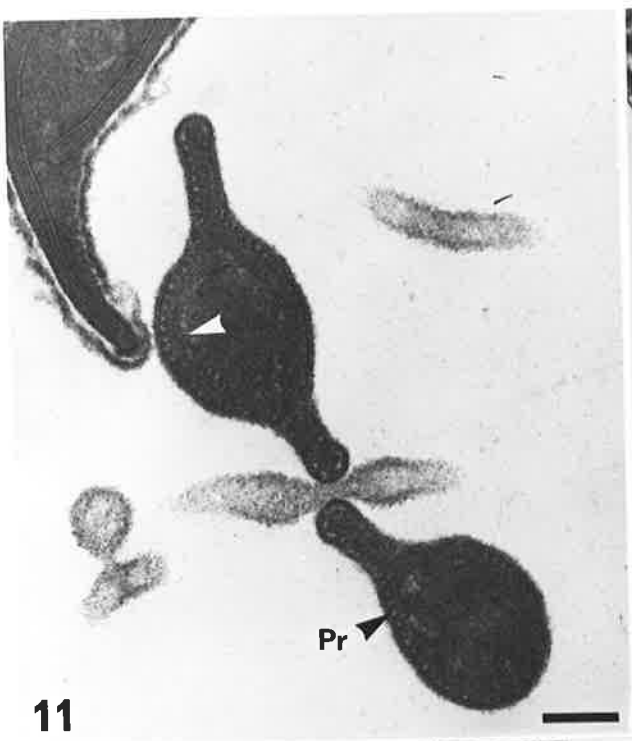

11

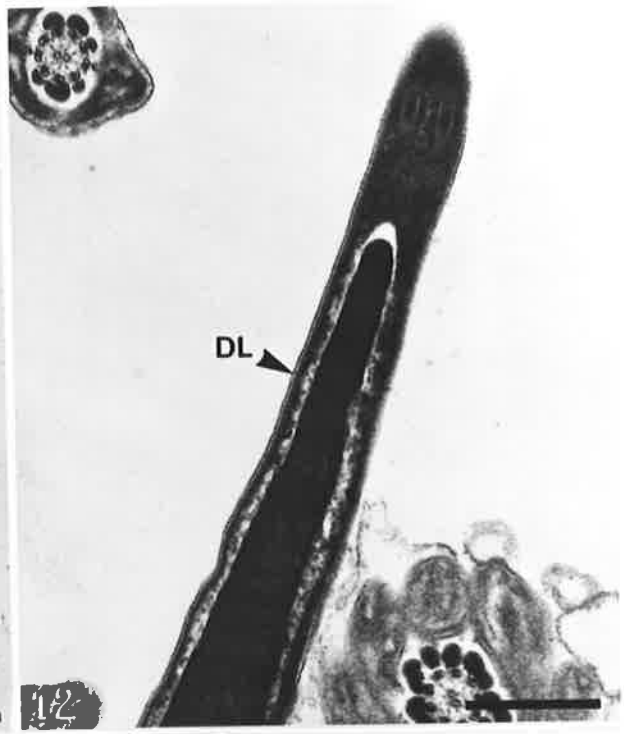

12

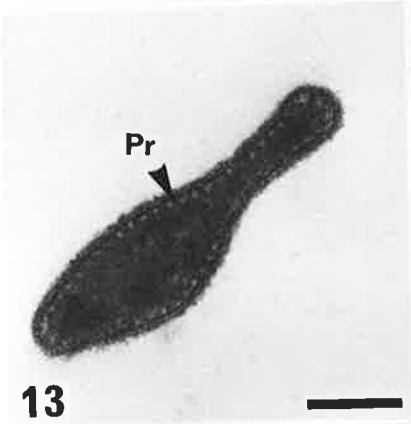

13

14

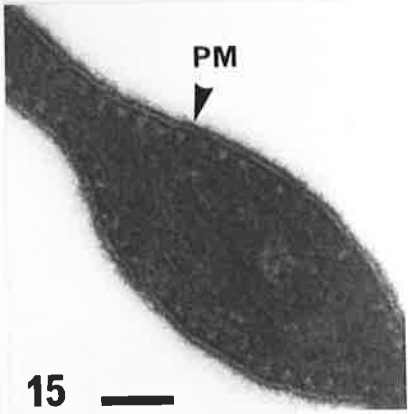

15

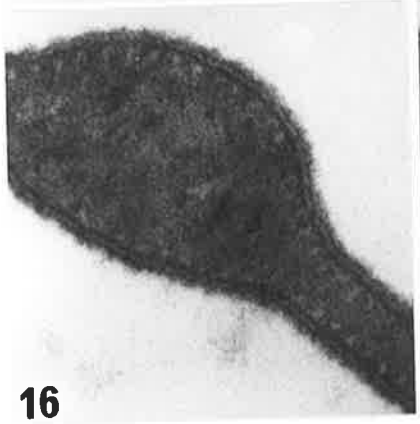

16

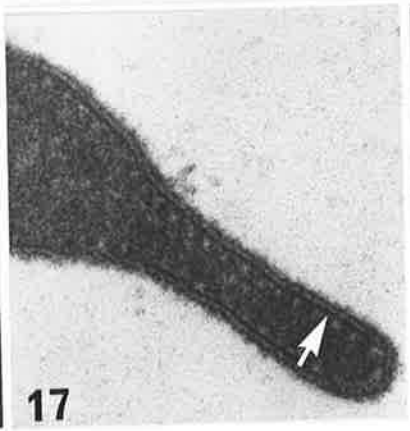

17

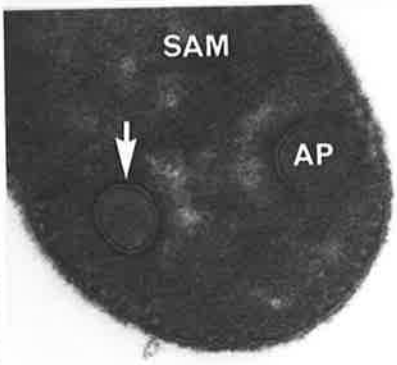

18

PLATE 5

Fig. 19. Scanning electron micrograph of the sperm head. The lines indicate the approximate planes of section in Fig. 20.
Bar = 1 µm. x 15,940

Fig. 20. A series of transverse sections cut through the sperm head at the levels indicated in Fig. 19, showing the shape and structure of the sperm head caudal to the hooks. It is bilaterally flattened, with a rounded dorsal margin. Caudal to the tail insertion, the ventral aspect becomes broadened (d,e). An indentation of the sperm head (arrow) marks the border of the principal (PS) and equatorial (ES) segments. The extent of the post-acrosomal region (PAR) is shown. The nucleus is homogeneous, though small nuclear vacuoles or inconsistencies are apparent (arrow-heads). There is a narrow sub-acrosomal space (SAS), with an accumulation of sub-acrosomal material on the dorsal margin of the sperm head, forming two dorsal ridges (DR) which indent the acrosome. The asymmetrical distribution of the acrosomal segments on the two surfaces of the sperm head is marked by the small bars.
Bar = 0.5 µm. x 26,310

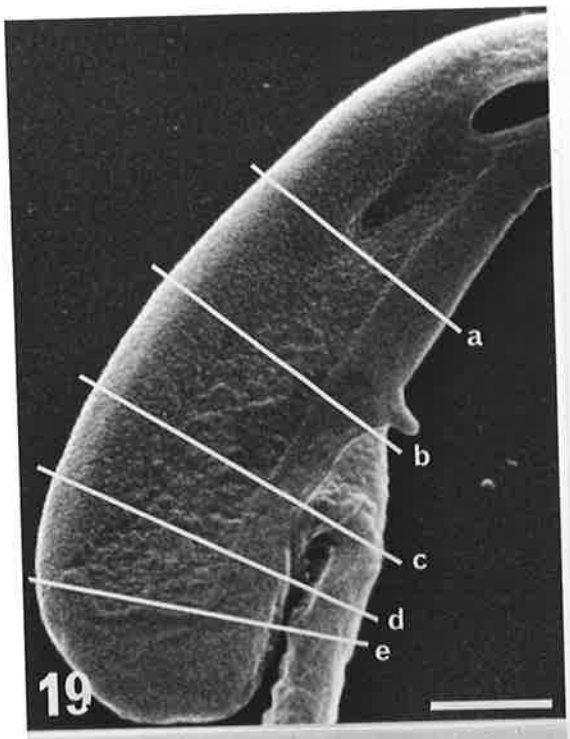
a
b
c
d
e
19

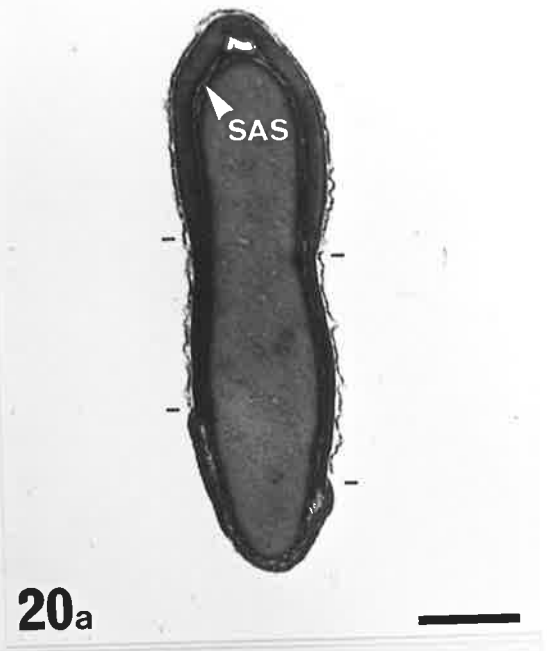
SAS
20a

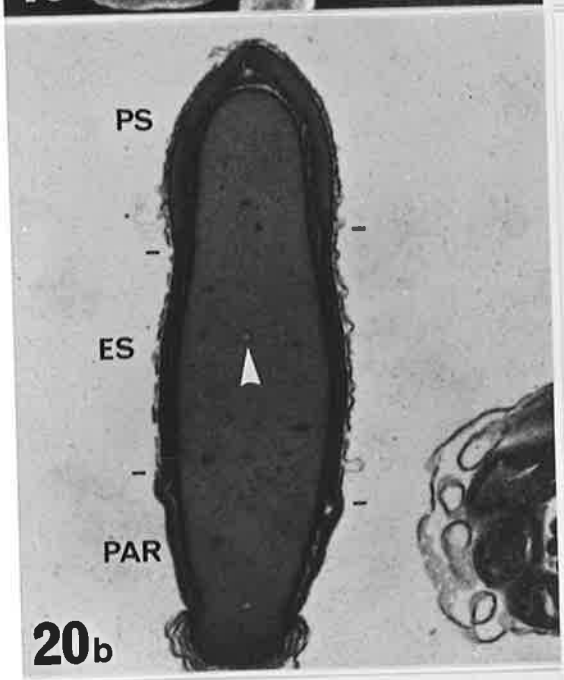
PS
ES
PAR
20b

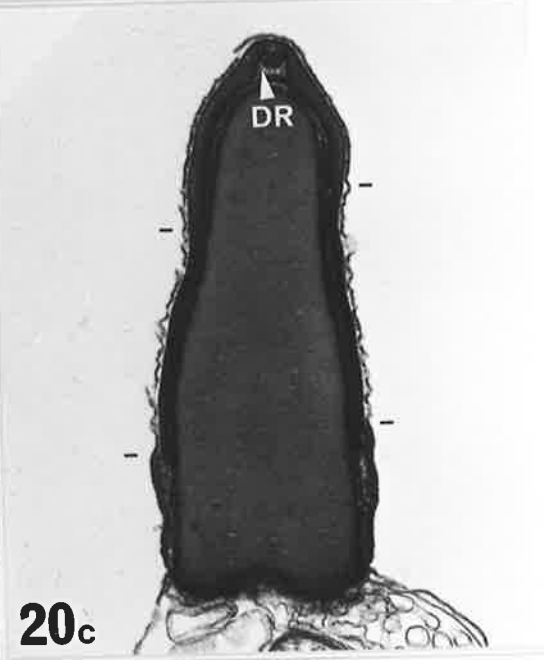
DR
20c

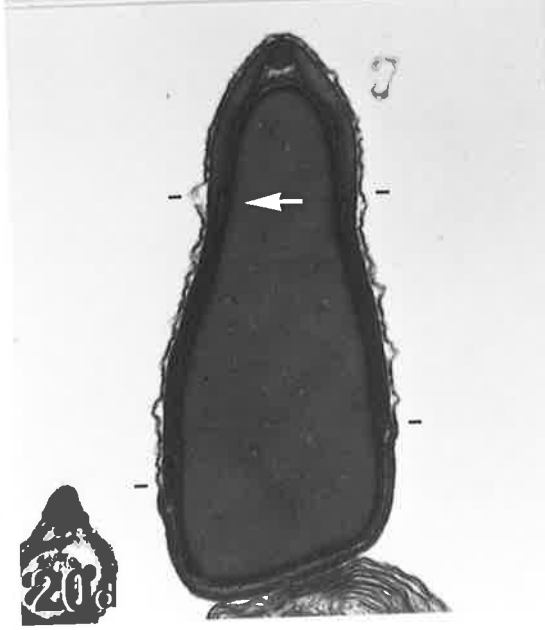
20d


20e

PLATE 6

Figs. 21, 22. Transverse sections cut through sperm heads which were not post-fixed in OsO_4. Although the nucleus (N) is homogeneous, it is more electron-dense in the ventral nuclear extention (asterisk). The sub-acrosomal space is expanded, but a thin layer of sub-acrosomal material (SAM) is attached to the inner aspect of the acrosome. The dorsal ridges (DR) are a prominent feature on the dorsal margin. The contents of the acrosome are heterogeneous, with more electron-dense patches occurring in the principal segment, and near the dorsal ridges (arrows). The contents of the equatorial segment (ES) are also of increased electron density.
Bar = 0.5 µm. x 50,830

Fig. 23. This micrograph shows the structure of the nucleus (N), the wavy nuclear envelope (NE), and the acrosome (Ac). The dorsal ridges (DR) are clearly bounded by the inner acrosomal membrane. The contents of the equatorial segment (ES) are more electron-dense, whilst the outer zone in the principal segment is less homogeneous (arrows). The plasma membrane (PM) is smooth and closely applied to the principal segment, but is wavy over the equatorial segment.
Bar = 0.2 µm. x 68,230

Figs. 24, 25. Higher magnifications of the equatorial segment, showing the wavy outline of the plasma membrane (PM), the thicker inner acrosomal membrane (arrow), and also the nuclear envelope (NE).
Bar = 0.1 µm. x 191,040 (24)
0.05 µm. x 262,400 (25)

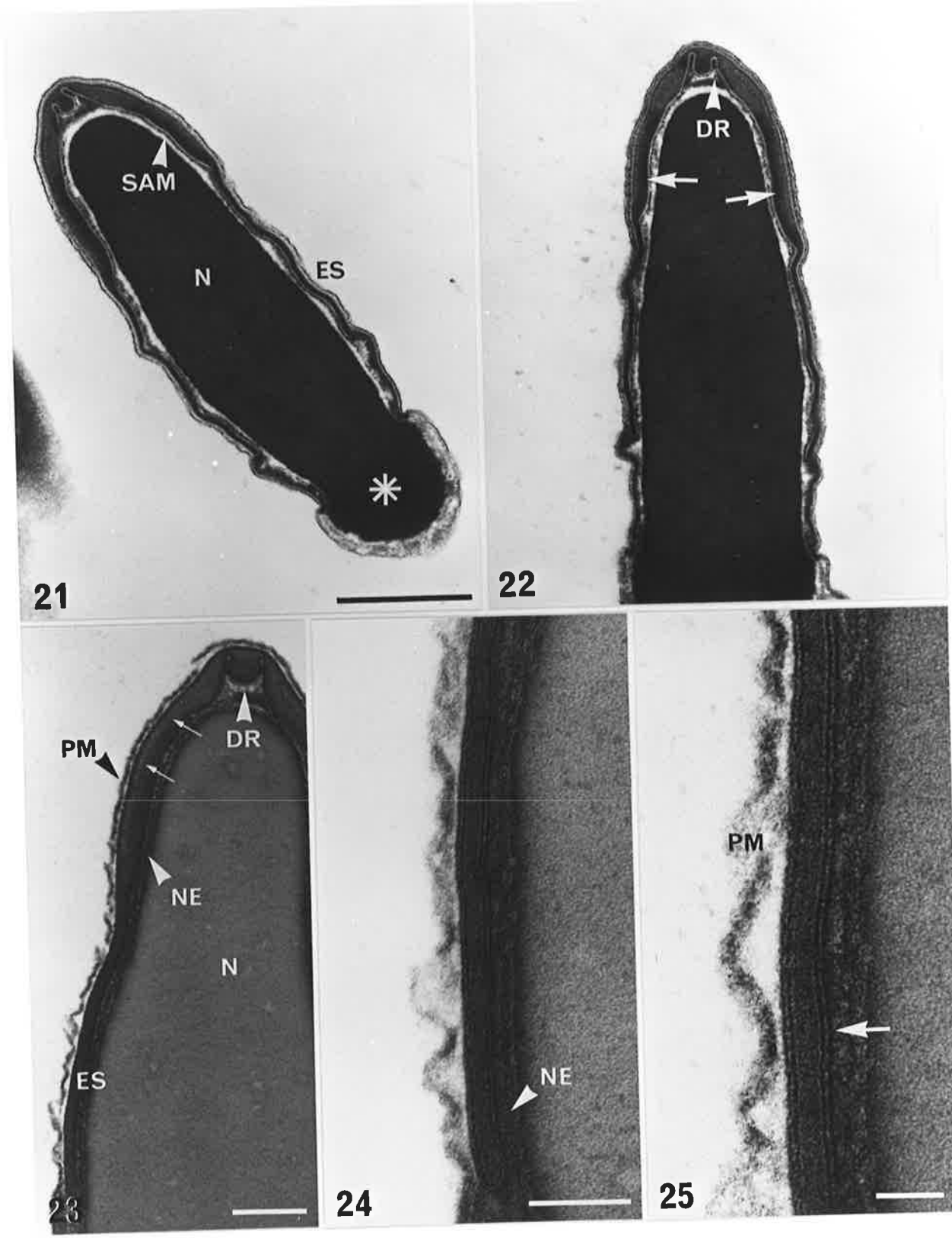
SAM
N
ES
21
DR
22
PM
DR
NE
N
ES
23
NE
24
PM
25

PLATE 7

Figs. 26-30. These micrographs show the structural features of the ventral border of the equatorial segment (ES), and the post-acrosomal region. The inner and outer acrosomal membranes are continuous at the ventral border of the equatorial segment. There is an accumulation of sub-acrosomal material (SAM) at this point, which attaches to the inner aspect of the post-acrosomal dense lamina (DL), and causes the lamina to bulge out (arrow). The dense lamina is about 14 nm thick, and is usualy closely associated with the plasma membrane, except when this is damaged as in Fig. 30. The lamina is separated from the nuclear envelope by a continuation of the sub-acrosomal space. This often contains dense, lamellar structures which are attached to the nuclear envelope (arrowheads). The position of the posterior ring (PR) is also shown.
Bar = 0.1 µm. x 105,050

Fig. 31. Transverse section cut through the caudal region of the sperm head, revealing the projections (Pr) which link the dense lamina and plasma membrane, as well as the lamellar structures (arrows) associated with the nuclear envelope.
Bar = 0.1 µm. x 105,050

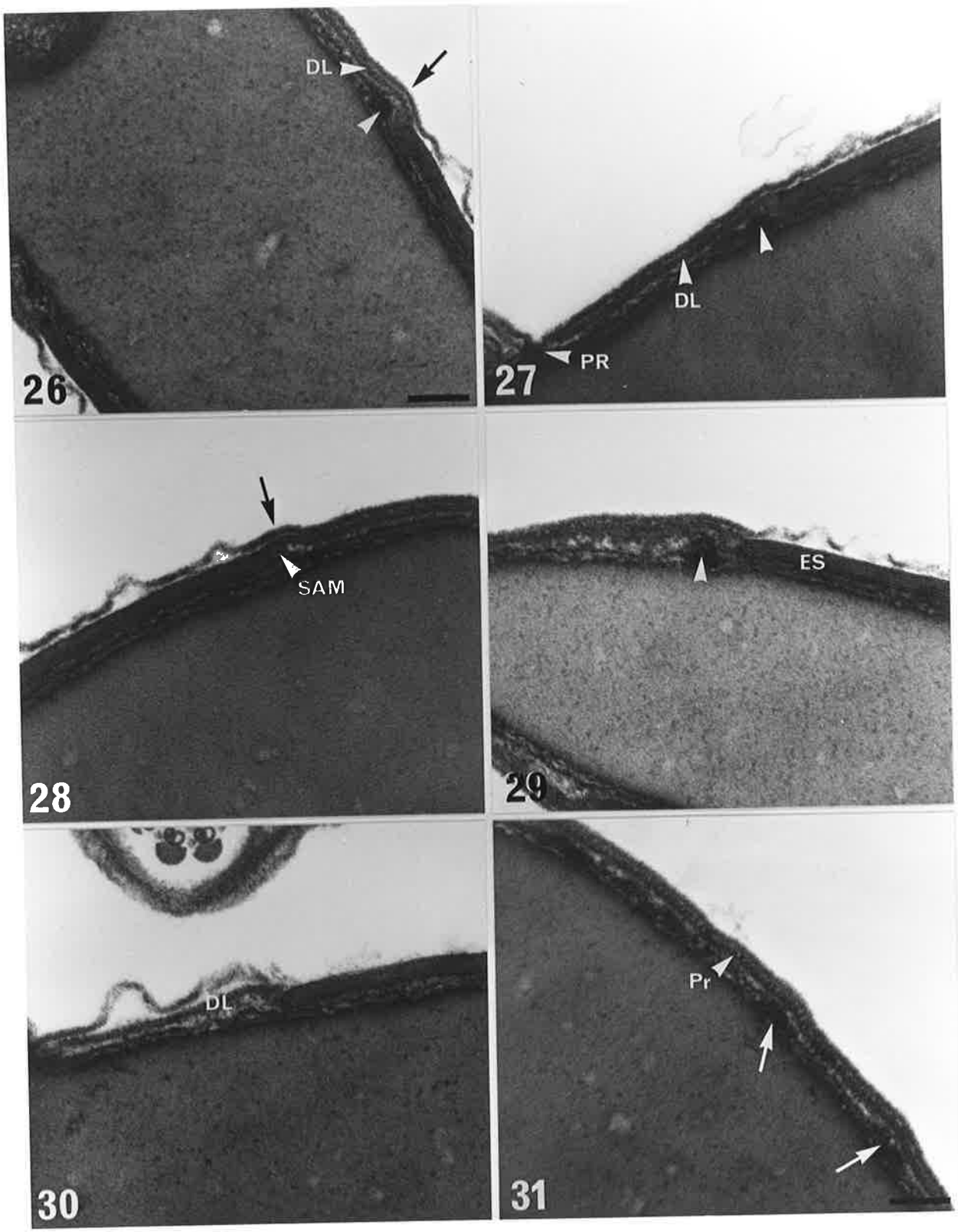
DL
26
DL
PR
27
SAM
28
ES
29
DL
30
Pr
31

PLATE 8

Figs. 32, 33. Longitudinal sections cut through the ventral margin of the sperm head. The regular spacing of the projections, and the close association of the plasma membrane can be observed. Fig. 32 shows that the thickness of the lamina increases to 20-40 nm near the base of the ventral hooks.
Bar = 0.1 µm. x 113,000

Fig. 34. This is a sagittal section through the implantation fossa and neck region. The increased density of the chromatin in the ventral nuclear extension is shown (asterisk), as well as the 30 nm thick basal plate (BP).
Bar = 0.2 µm. x 51,860

Figs. 35, 36. These sperm were <u>en bloc</u> stained with tannic acid before dehydration. This method reveals a continuous and uniform glycocalyx (Gx) on the entire surface of the sperm head and tail.
Bar = 0.5 µm. x 40,670 (35)
x 55,520 (36)

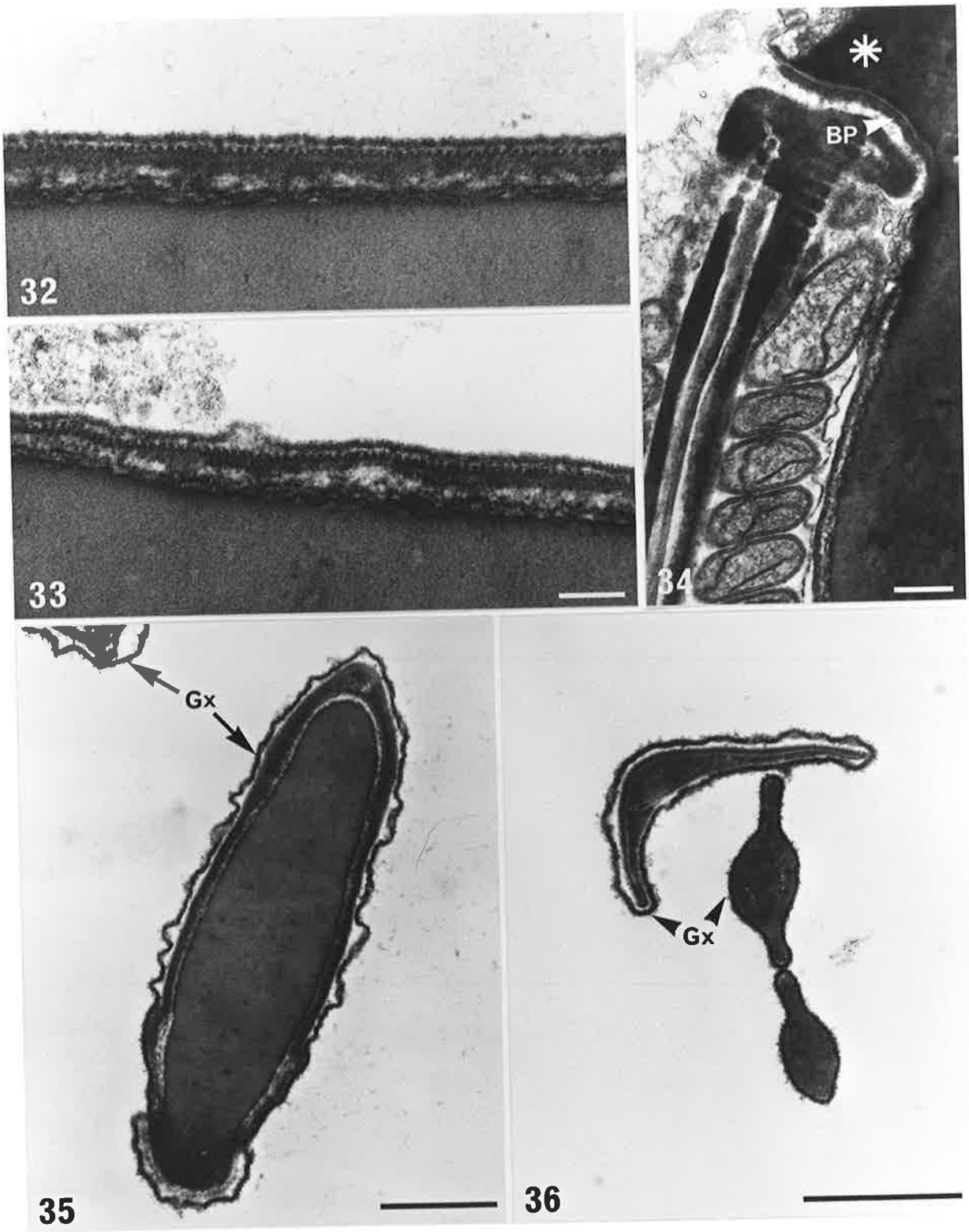
32
33
BP
34
Gx
35
Gx
36

PLATE 9

Figs. 37, 38. Scanning electron micrographs reveal the deep indentation at the base of the hooks (arrow), a ridge that marks the junction of the equatorial segment and post-acrosomal region (arrowheads), the ventral spur (VS), the posterior ring (PR), nuclear pores in the redundant nuclear envelope (RNE), and the point of entry of the acrosomal projections (AP) into the ventral hooks. The post-acrosomal region (PAR) and ventral hooks have a fine, granular texture, whilst the surface overlying the acrosome (Ac) is ruffled.
Bar = 0.5 µm. x 27,550 (37)
x 28,940 (38)

Fig. 39. Platinum/carbon surface replicas reveal the above mentioned features with greater resolution. In particular, the surface of the equatorial segment (ES) and post-acrosomal region (PAR) exhibits a definite sub-structure.
Bar = 1 µm. x 17,700

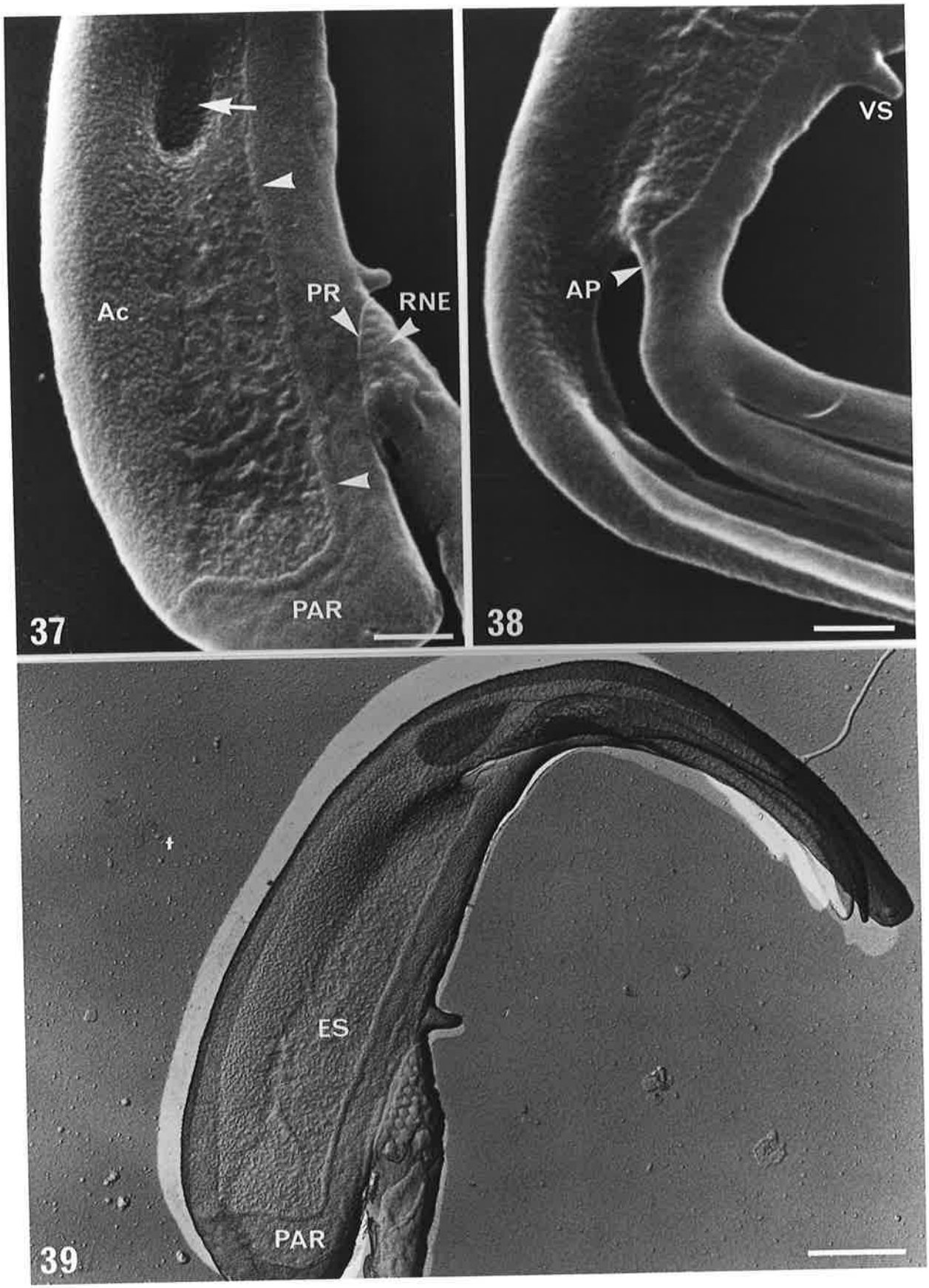
Ac
PR
RNE
PAR
37
VS
AP
38
ES
PAR
39

PLATE 10

Figs. 40-46. Platinum/carbon surface replicas of cauda epididymal sperm.

Figs. 40, 41. The surface of the plasma membrane overlying the principal segment (PS) features a ruffled appearance, whereas the equatorial segment (ES) is characterized by short rod-like structures, and particles with a 17 nm spacing (arrows).
Bar = 0.5 µm. x 25,120 (40)
0.2 µm. x 78,200 (41)

Figs. 42, 43. The surface features of the equatorial segment extend onto the lateral surfaces of the dorsal hook (arrow), with a similar array of particles and rod-like structures.
Bar = 0.5 µm. x 27,100 (42)
0.2 µm. x 78,200 (43)

Figs. 44-46. The characteristics of the post-acrosomal region (PAR) and ventral hooks (V) is entirely different to the acrosome. The surface appears as a random array of ridges and furrows, although the pattern is not identical in the two regions.
Bar = 0.5 µm. x 27,100 (44)
0.2 µm. x 57,870 (45,46)

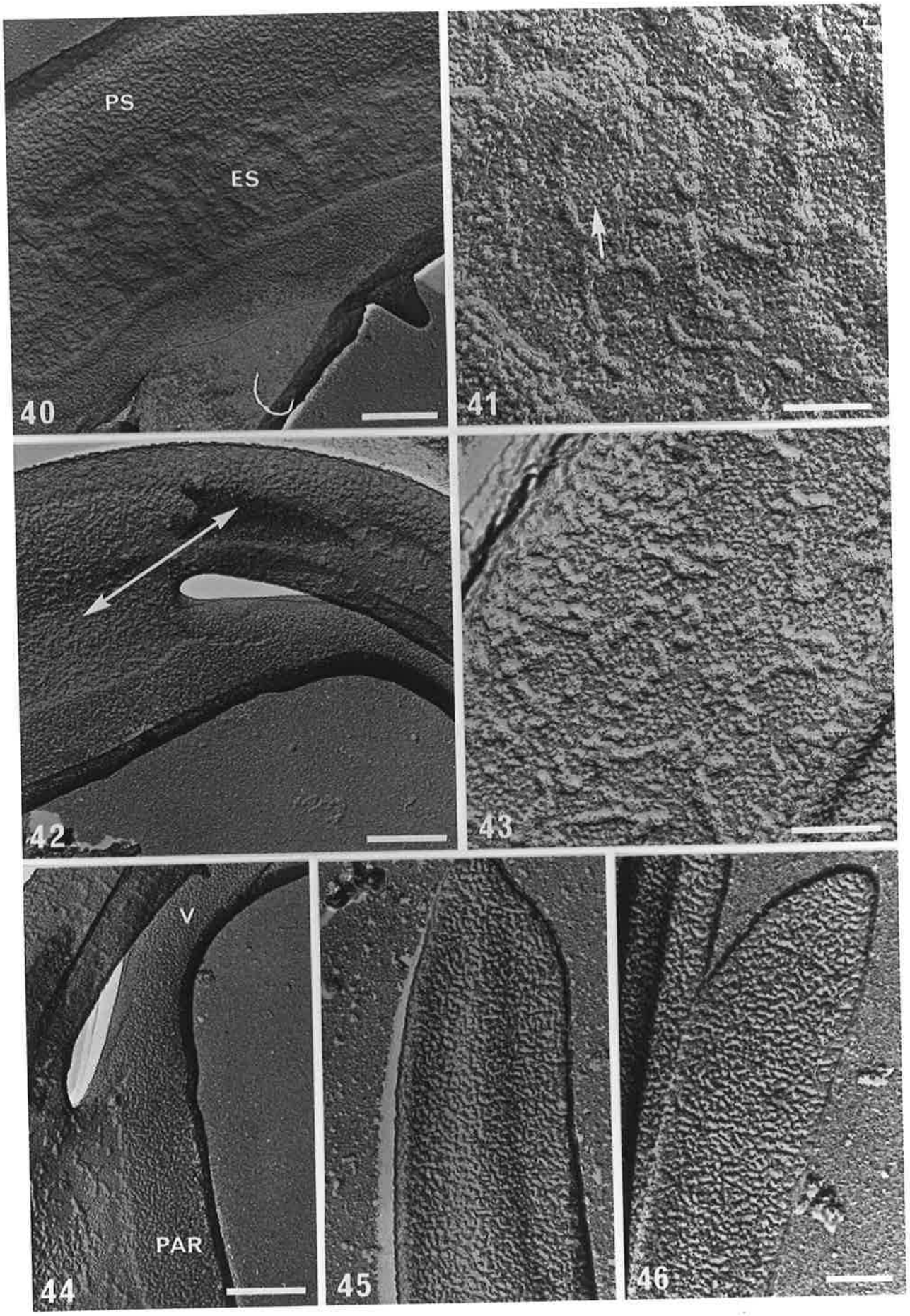
PS
ES
40
41
42
43
V
PAR
44
45
46

PLATE 11

Figs. 47-49. Platinum/carbon surface replicas of cauda epididymal sperm in which the plasma membrane has been removed during processing.

Fig. 47. In the principal segment (PS) of the acrosome, the outer acrosomal membrane has a rough appearance. The surface of the OAM in the equatorial segment (ES) consists of parallel rows of small particles, which are oriented in the dorso-ventral plane (arrows).
Bar = 0.5 µm. x 52,230

Fig. 48. Higher magnification of the equatorial segment. The particles are hexagonally packed with a centre-centre spacing of 19 nm.
Bar = 0.2 µm. x 105,000

Fig. 49. On the lateral surfaces of the dorsal hook, the rows of particles are aligned at an angle of about 55° to the long axis of the hook (arrows).
Bar = 0.5 µm. x 52,230

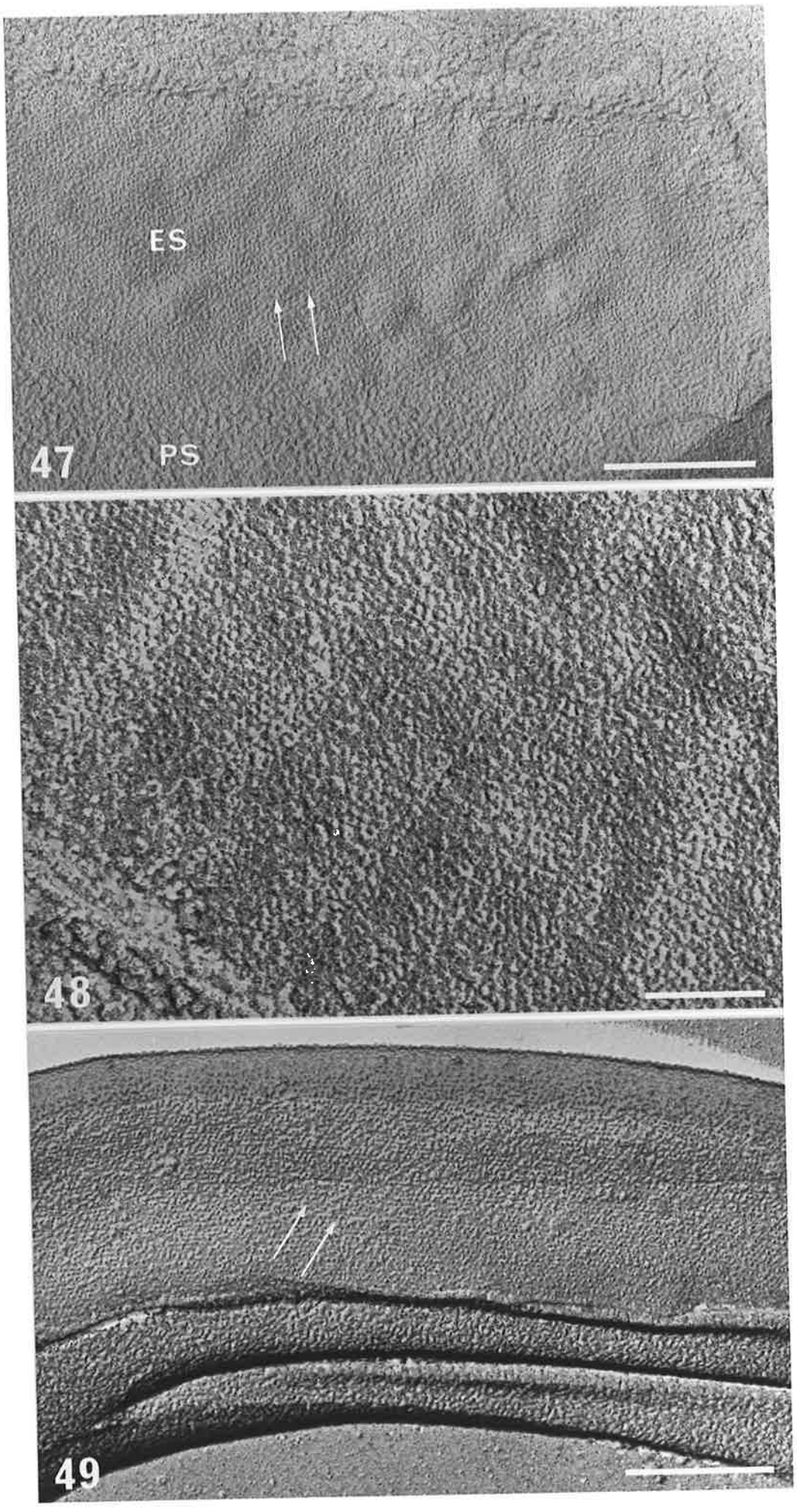
ES
47
PS
48
49

PLATE 12

Figs. 50-55. Platinum/carbon surface replicas of cauda epididymal sperm treated with Triton X-100 and DTT to remove the plasma membrane.

Fig. 50. Low magnification micrograph showing that the contents of the acrosome (Ac) have been solubilized. The nuclear pores in the redundant nuclear envelope (RNE) are evident. In the post-acrosomal region (PAR) on the ventral margin of the sperm head, there are parallel ridges oriented in the dorso-ventral plane.
Bar = 0.5 µm. x 21,230

Fig. 51. Higher magnification of the ridges, which are spaced about 16 nm apart.
Bar = 0.1 µm. x 95,100

Fig. 52. On the caudal margin of the sperm head, the ridges are oriented in the long axis of the sperm head.
Bar = 0.2 µm. x 55,940

Fig. 53. A periodic sub-structure is evident at the border of the equatorial segment (ES) and post-acrosomal region (PAR).
Bar = 0.1 µm. x 94,300

Figs. 54, 55. In the ventral hooks, the ridges are oriented in the long axis, but are difficult to visualize (arrows).
Bar = 0.2 µm. x 51,540 (54)
x 25,560 (55)

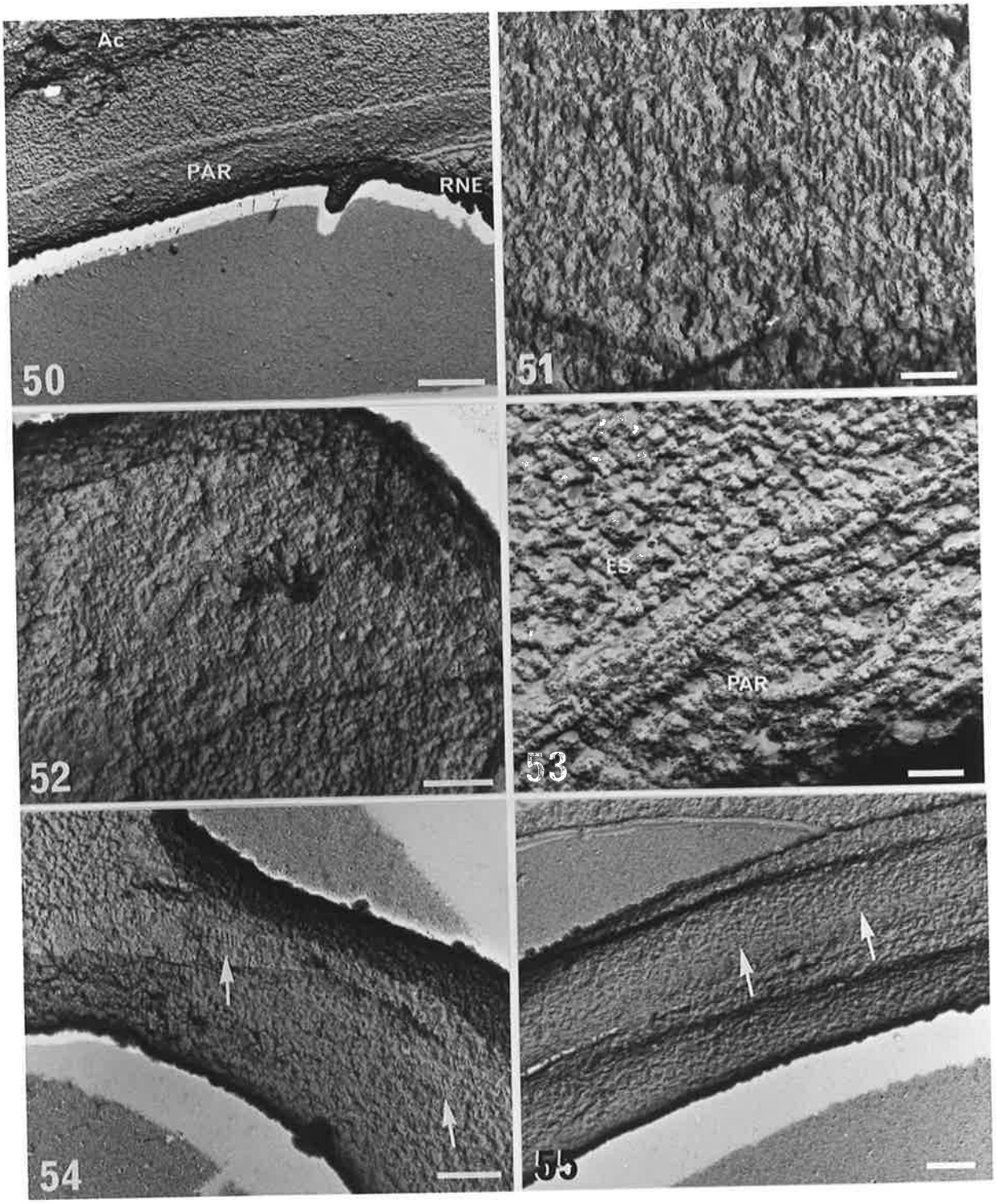
Ac
PAR
RNE
50
51
52
ES
PAR
53
54
55

PLATE 13

Figs. 56, 57. Cauda epididymal sperm stained with silver nitrate. The post-acrosomal region, ventral spur and ventral hooks are intensely argyrophilic, whilst the principal segment of the acrosome and lateral edges of the dorsal hook (arrows) display a less intense reaction.
Bar = 10 µm. x 1,420

Figs. 58-60. Paired phase contrast (a) and fluorescence (b) micrographs of sperm stained with NBD-phallacidin. The two ventral hooks (V) are intensely fluorescent, and a short band of fluorescence extends dorsally from the base of the hooks, whilst another extends caudally along the ventral margin of the sperm head (arrows). The dorsal hook is negative, and the middle piece (MP) is moderately fluorescent.
Bar = 10 µm. x 1,580 (58,59)
x 2,250 (60)

Fig. 61. Paired phase contrast (a) and fluorescence (b) micrographs of control sperm. There is no fluorescence in the ventral hooks (V) or any part of the sperm head, but the middle piece (MP) exhibits a low to moderate degree of fluorescence.
Bar = 10 µm. x 1,580

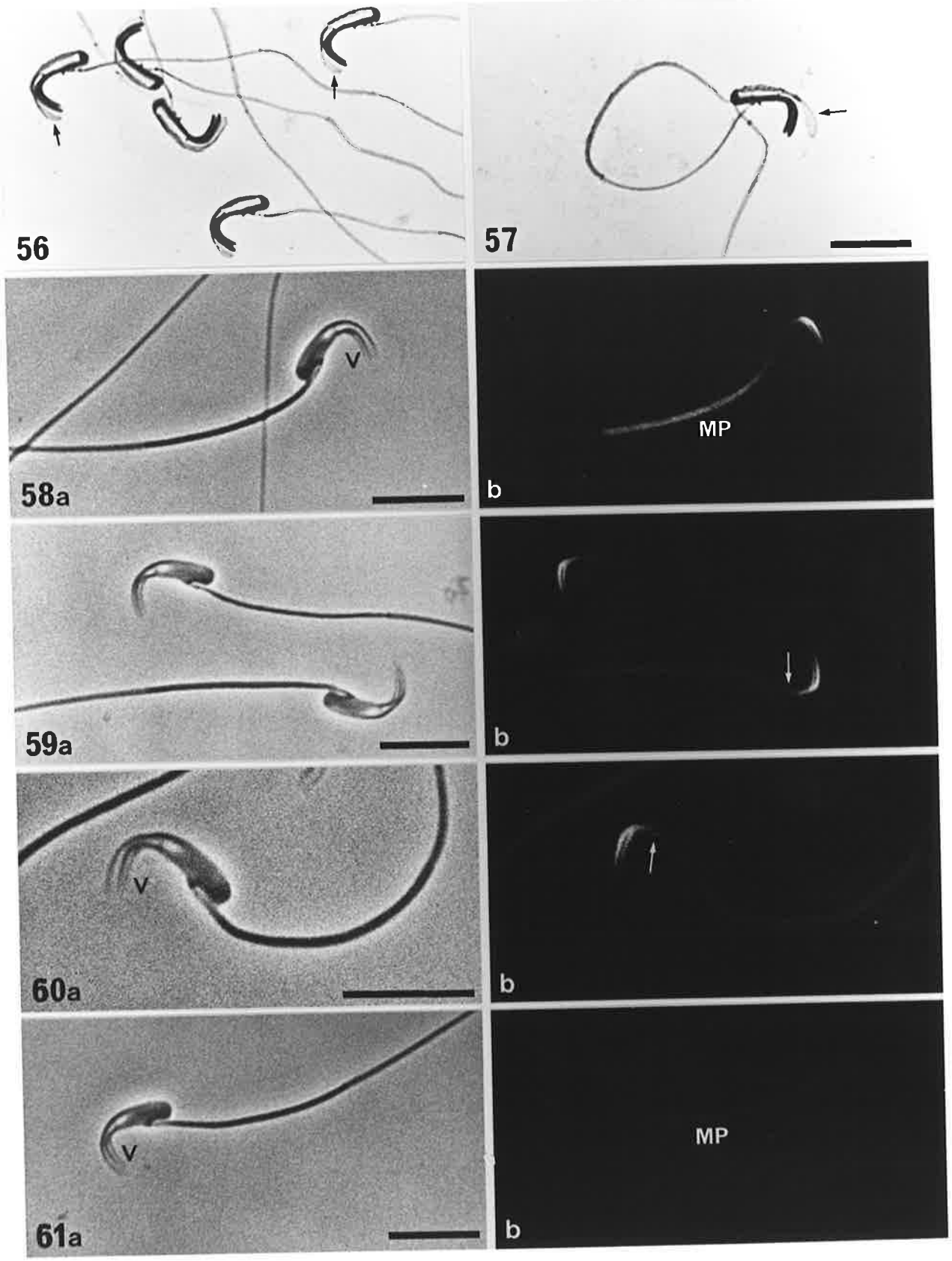
56
57
V
58a
MP
b
59a
b
V
60a
b
V
61a
MP
b

PLATE 14

Figs. 62-66. Thick plastic sections of testis stained with toluidine blue, showing stages I to V in the cycle of the seminiferous epithelium.
Bar = 20 µm. x 776

Fig. 62. Stage I. Intermediate spermatogonia (I) and zygotene primary spermatocytes (z) occupy the basal layer of the epithelium, whilst step 1 round spermatids (RSt) and step 11 maturing spermatids (St) are found in the middle and luminal portions.

Fig. 63. Stage II. Same cell types present as in stage I, but an acrosomal vesicle is present on step 2 round spermatids (arrow), and step 12 spermatids are located further adluminally.

Fig. 64. Stage III. Type B spermatogonia (B) and pachytene primary spermatocytes (Pc) line the base of the tubule. Step 3 round spermatids (RSt), with a large acrosomal vesicle, occupy much of the epithelium, and step 13 spermatids (St) are only found near the lumen.

Fig. 65. Stage IV. Mature spermatozoa (Sz) are being released. Type A spermatogonia (A), resting (R) and pachytene (Pc) primary spermatocytes occupy the basal portion of the epithelium. The anterior surface of step 4 round spermatids (RSt) is capped by the acrosome.

Fig. 66. Stage V. Type A spermatogonia, leptotene (L) and pachytene (Pc) primary spermatocytes are found in the basal compartment, whilst the anterior margin of step 5 spermatids (St) is becoming angular.

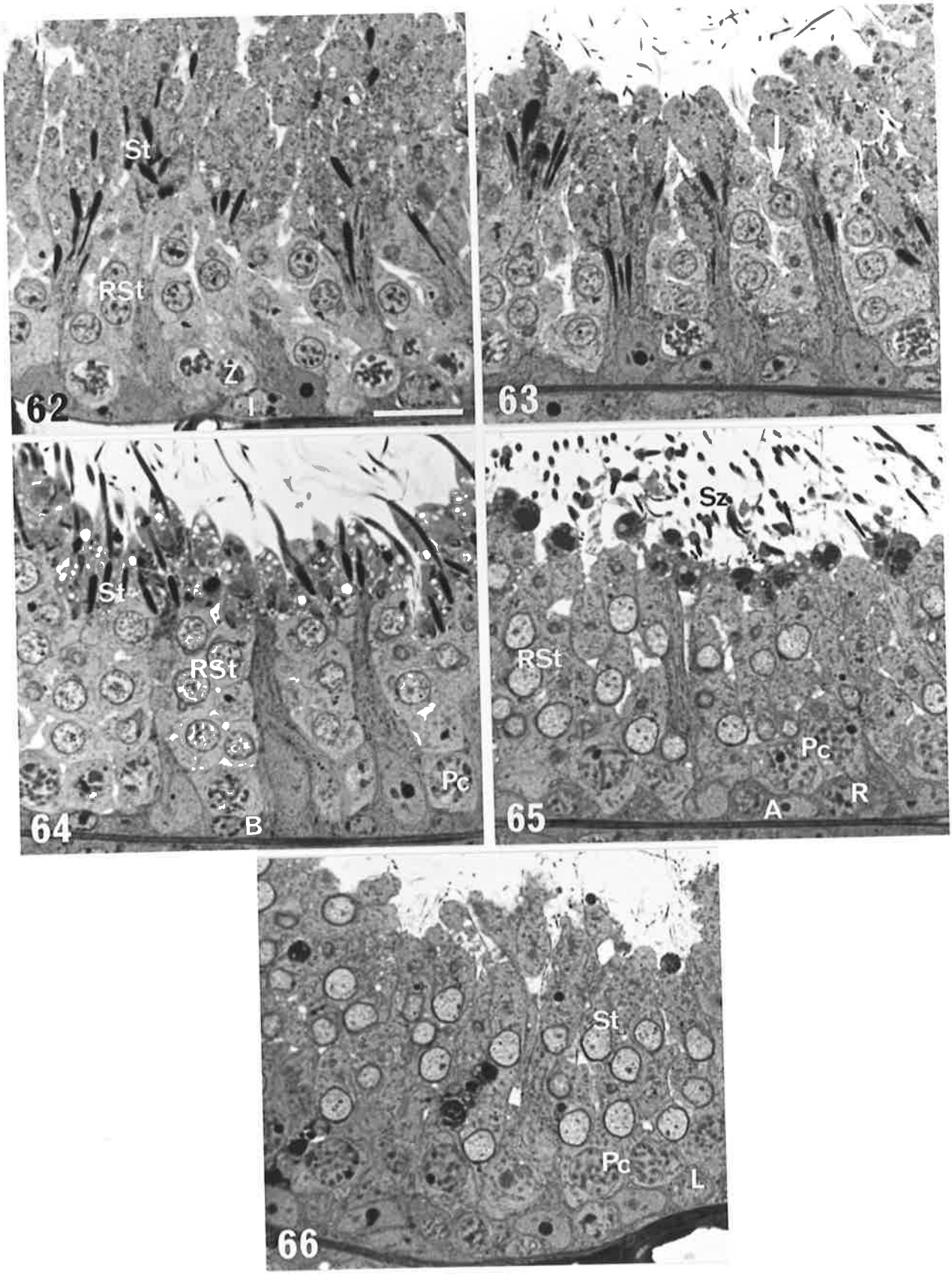
St
RSt
Z
I
62
63
St
RSt
Pc
B
64
Sz
RSt
Pc
A
R
65
St
Pc
L
66

PLATE 15

Figs. 67-71. Thick plastic sections of testis stained with toluidine blue, showing stages VI to X in the cycle of the seminiferous epithelium.
Bar = 20 µm. x 776

Fig. 67. Stage VI. The same cell types are present as in stage V, but nuclear elongation is underway in step 6 spermatids (St).

Fig. 68. Stage VII. Type A spermatogonia (A), zygotene (z) and pachytene (Pc) primary spermatocytes are present in the basal half, and maturing step 7 spermatids (St) are becoming clustered in the luminal compartment.

Fig. 69. Stage VIII. In this stage, nuclear condensation is underway in step 8 spermatids (St), which are oriented towards the basement membrane.

Fig. 70. Stage IX. Type A and intermediate (I) spermatogonia are found in this stage. Zygotene (z) and pachytene (Pc) primary spermatocytes are also present, and nuclear condensation has reached an advanced stage in the step 9 spermatids (St).

Fig. 71. Stage X. Intermediate spermatogonia (I) and zygotene primary spermatocytes (z) occupy the basal compartment. Spermatocytes at metaphase of the first meiotic division (M) are present, as well as secondary spermatocytes (S). Nuclear condensation is virtually complete in step 10 spermatids (St).

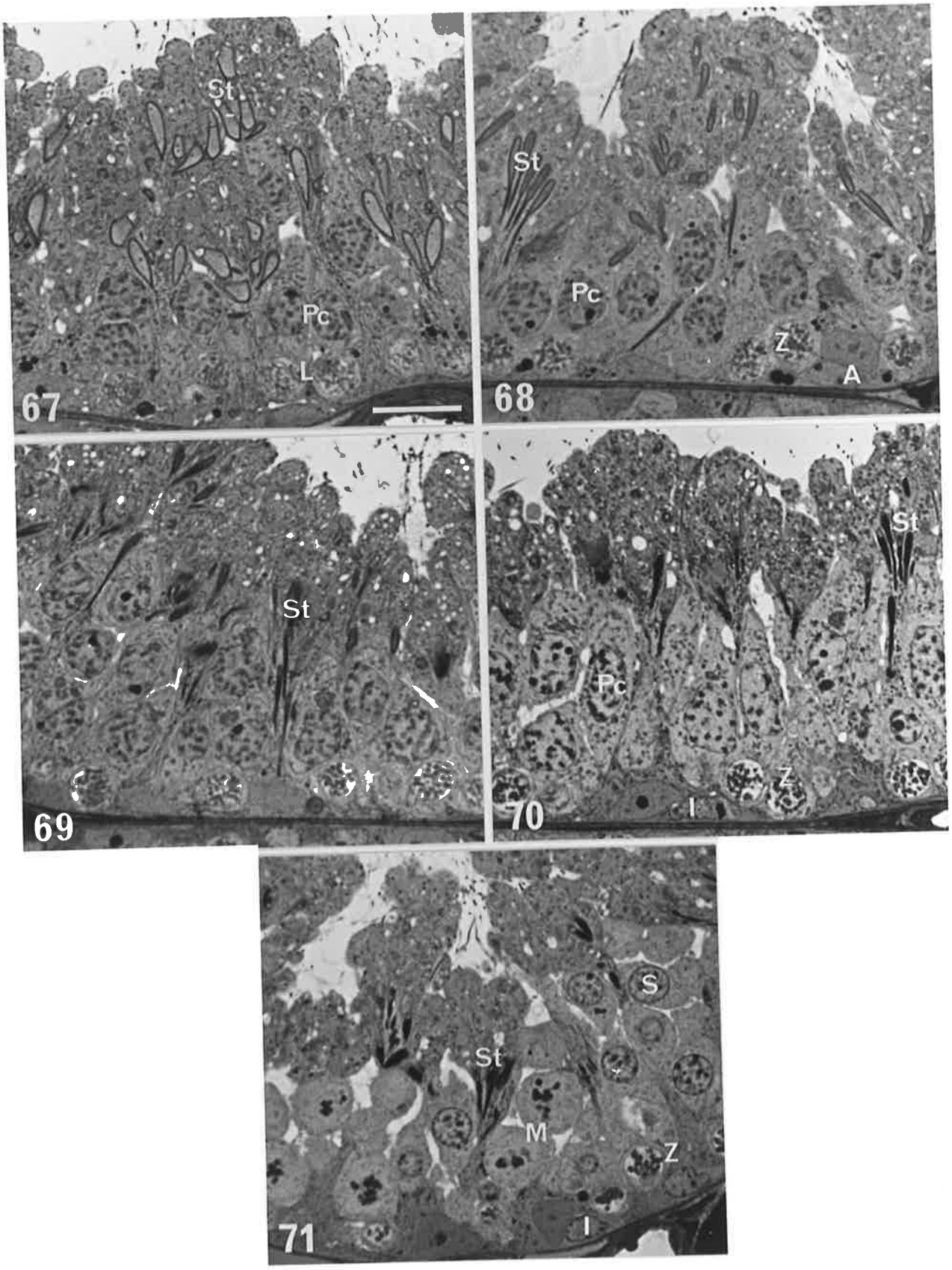
St
Pc
L
67
St
Pc
Z
A
68
St
69
St
Pc
Z
I
70
S
St
M
Z
I
71

PLATE 16

Figs. 72-75. Step 7 spermatids.

Fig. 72. The nucleus (N) has a fine, granular texture, with areas of aggregation present (arrow). The acrosome (Ac) caps the rounded dorsal margin of the sperm head.
Bar = 1 µm. x 11,230

Figs. 73-75. The dorsal hook is bilaterally flattened, and roughly pear-shaped. There is a double nuclear envelope (NE), and a narrow sub-acrosomal space (SAS) which contains some flocculent material. A plate of nuclear envelope extends ventrally from the nucleus, and rows of 15 nm filaments (arrow) line the sub-acrosomal space in this region. The apical segment (AS) of the acrosome extends beyond the tip of the nucleus (Fig. 73), and has a dense core (C) and clear lateral zones. Sertoli cell ectoplasmic specializations (EPS) closely surround the dorsal hook.
Bar = 1 µm. x 22,600 (73)
0.5 µm. x 28,000 (74)
0.2 µm. x 80,900 (75)

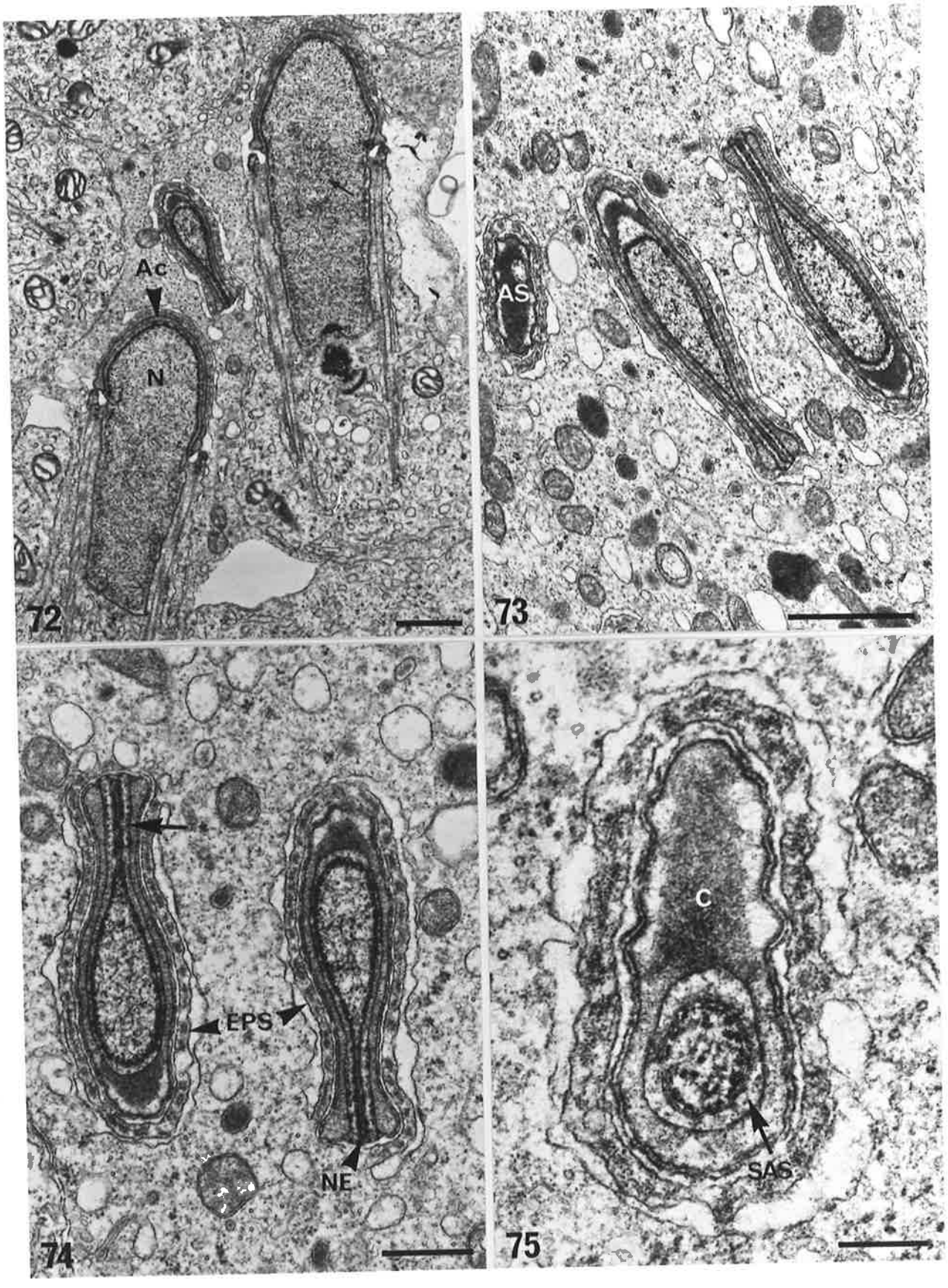
Ac
N
72
AS
73
EPS
NE
74
C
SAS
75

PLATE 17

Fig. 76-79. Step 8 spermatids.

Fig. 76. The sperm head is becoming bilaterally flattened, and nuclear condensation is underway. The chromatin is coarse and granular.
Bar = 1 µm. x 14,100

igs. 77-79. The dorsal hook is highly flattened, and the size of the nucleus (N) is reduced. The plate of nuclear envelope (NE) is extensive, as is the acrosomal zonule (AZ) adjacent to the inner acrosomal membrane. On the ventral margin of the hook a dense lamina (DL) forms in close association with the plasma membrane. At the tip of the nucleus, an expansion of the sub-acrosomal space (SAS) forms between the nucleus and apical segment (AS) of the acrosome (Fig. 79). The smooth endoplasmic reticulum (SER) in the ectoplasmic specialization is often distended.
Bar = 0.5 µm. x 49,160 (77)
0.2 µm. x 60,250 (78)
0.2 µm. x 66,100 (79)


76

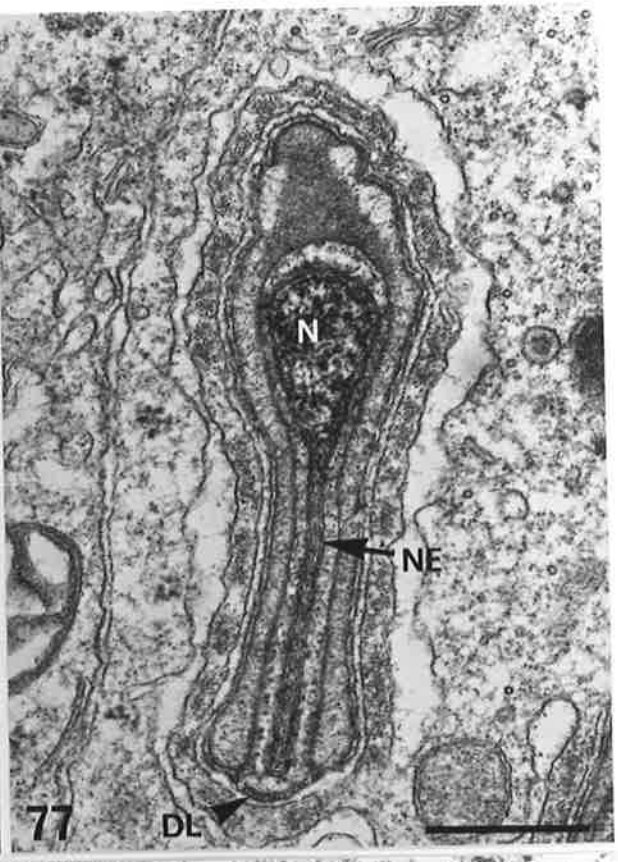
N
NE
DL
77

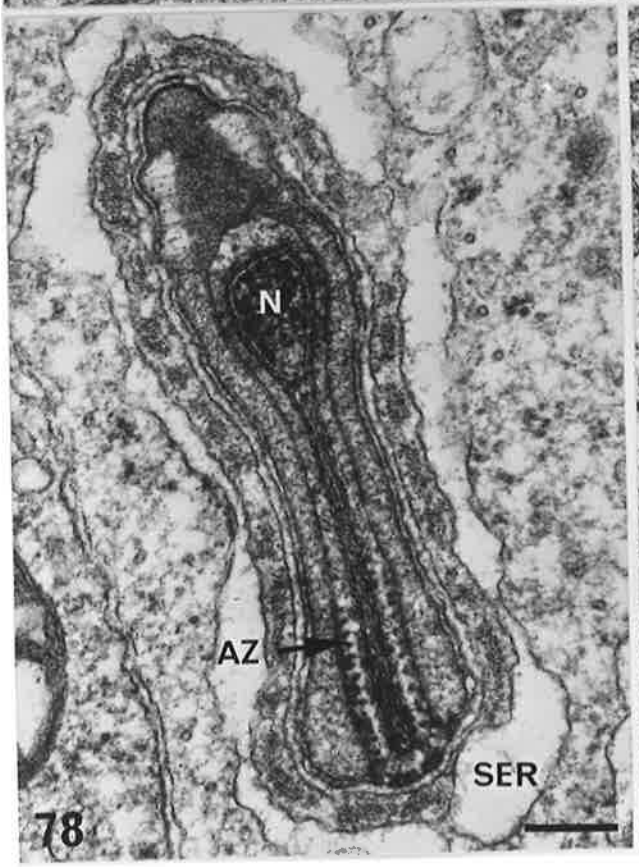
N
AZ
SER
78

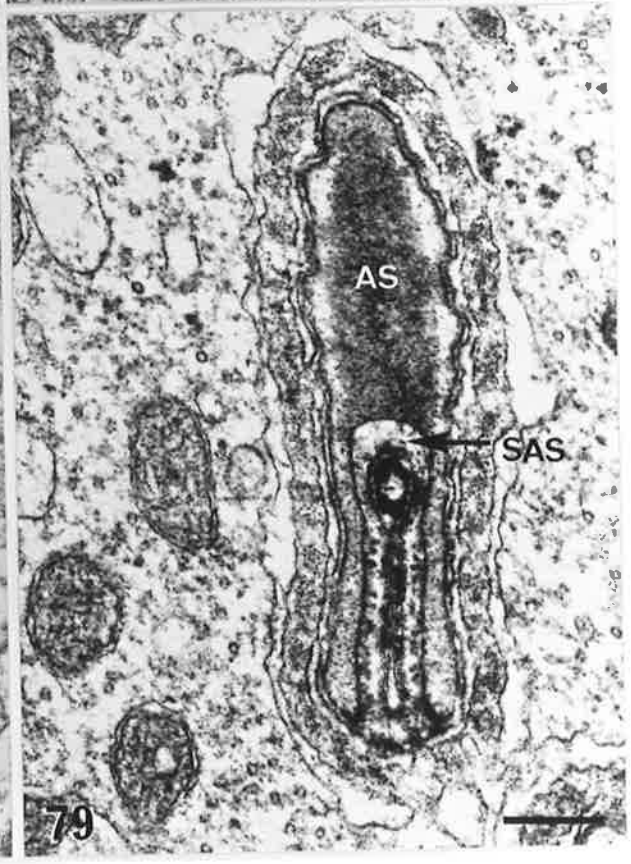
AS
SAS
79

PLATE 18

Figs. 80-83. Step 9 spermatids.

Condensation of the nucleus (N) is almost complete in the dorsal hook and anterior part of the sperm head, whilst posteriorly, the chromatin is clumped. On the ventral margin of the dorsal hook, the sub-acrosomal space (SAS) sometimes bulges out, capped by the post-acrosomal dense lamina (DL). Fig. 82 shows the structure of the dense lamina, as well as the acrosomal zonule (AZ) and the plate of nuclear envelope (NE). In the apical regions of the dorsal hook, the apical segment becomes tilted to one side, and the acrosome extends further ventrally on one side (arrows). The apical segment does not cap the tip of the hook (arrow-head).

Bar = 0.5 µm. x 24,630 (80)
0.5 µm. x 47,960 (81)
0.2 µm. x 165,500 (82)
1 µm. x 16,800 (83)

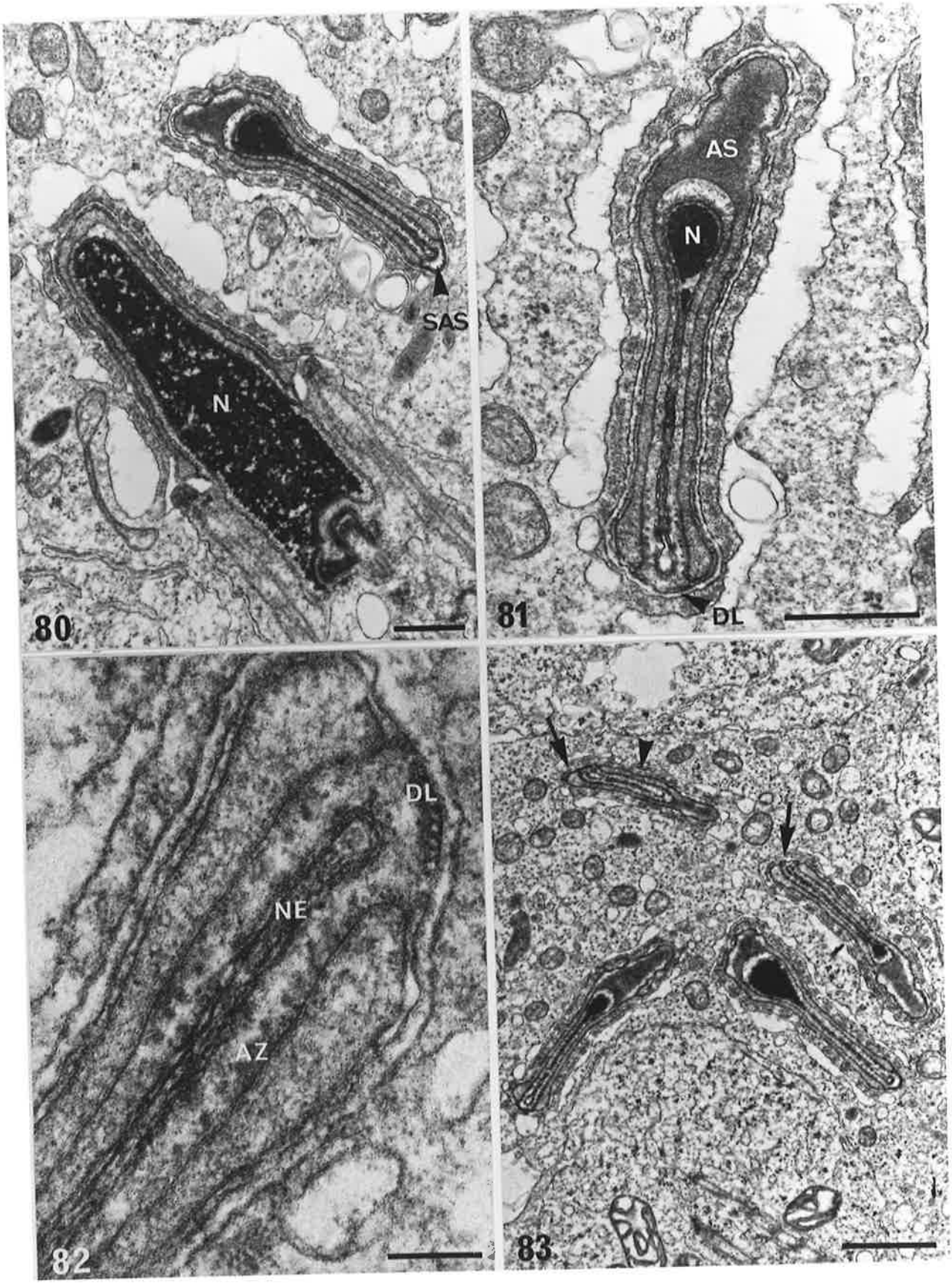
SAS
N
80
AS
N
DL
81
DL
NE
AZ
82
83

PLATE 19

Figs. 84-89. Step 11 spermatids.

Fig. 84. Nuclear condensation is almost complete, but numerous vacuoles (NV) are present throughout the nucleus. The acrosome can be divided into three segments: apical (AS), principal (PS) and equatorial (ES) segments. The post-acrosomal region (PAR) has formed on the ventral and caudal margins of the sperm head, and there is an accumulation of sub-acrosomal material on the dorsal margin (arrow).
Bar = 1 µm. x 17,440

Figs. 85-87. Basal region of the dorsal hook. The apical segment (As) is reduced in size and positioned on one side of the hook. The dense lamina (DL) is well developed, and the acrosomal zonule (AZ) underlies the entire acrosome except for the apical segment.
Bar = 0.2 µm. x 60,600 (85)
x 51,040 (86)
x 41,100 (87)

Figs. 88, 89. Apical region of the dorsal hook. It is bilaterally flattened, but asymmetrical due to formation of a separate plate of acrosome on one side (VAP). The apical segment is absent. The acrosomal zonule (AZ) and nuclear envelope (NE) are prominent in the sub-acrosomal space, which is devoid of other contents.
Bar = 0.5 µm. x 32,790 (88)
0.2 µm. x 50,670 (89)

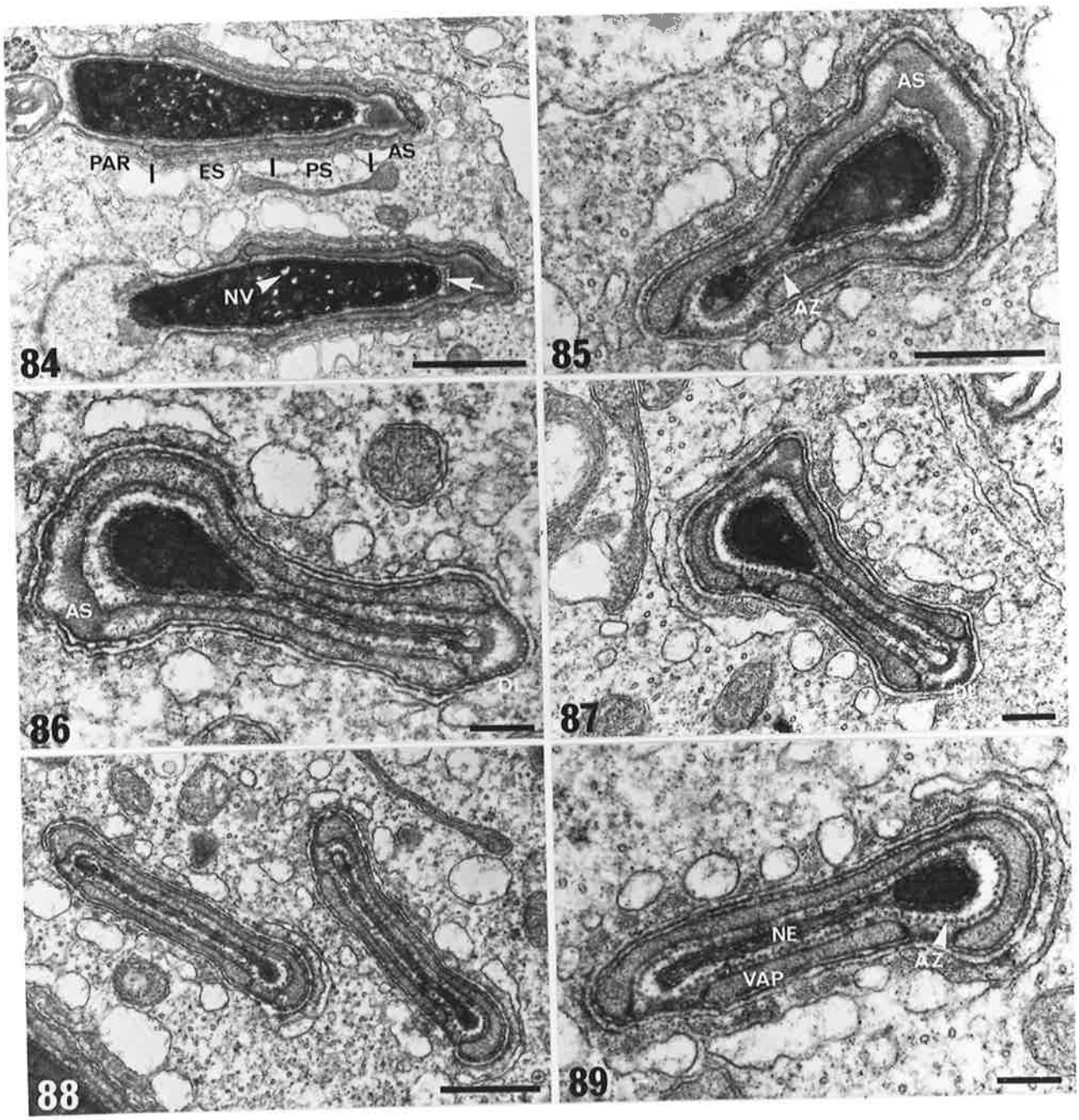
PAR
ES
PS
AS
NV
84
AS
AZ
85
AS
86
87
88
NE
VAP
AZ
89

PLATE 20

Figs. 90-93. Step 12 spermatids.

Fig. 90. The nucleus (N) is nearly fully condensed, and the contents of the acrosome have also condensed, especially in the apical segment (AS). The equatorial segment (ES) is separated from the principal segment (PS) by an abrupt decrease in thickness. The sub-acrosomal space (SAS) contains some flocculent material.
Bar = 0.5 µm. x 34,260

Fig. 91. The sub-acrosomal space, capped by the dense lamina, bulges out on the ventral surface of the dorsal hook, and the dorsal surface at the base of the ventral hook (arrows). The two acrosomal projections (AP) have formed.
Bar = 0.5 µm. x 28,120

Figs. 92, 93. The dorsal hook is asymmetrical in shape, with the acrosomal plate (VAP) located on its ventral border. The excess nuclear envelope is absent, and the sub-acrosomal space only contains the acrosomal zonule (AZ). The hook becomes roughly semi-circular in its apical regions (Fig. 93).
Bar = 0.5 µm. x 28,120 (92)
0.2 µm. x 92,700 (93)

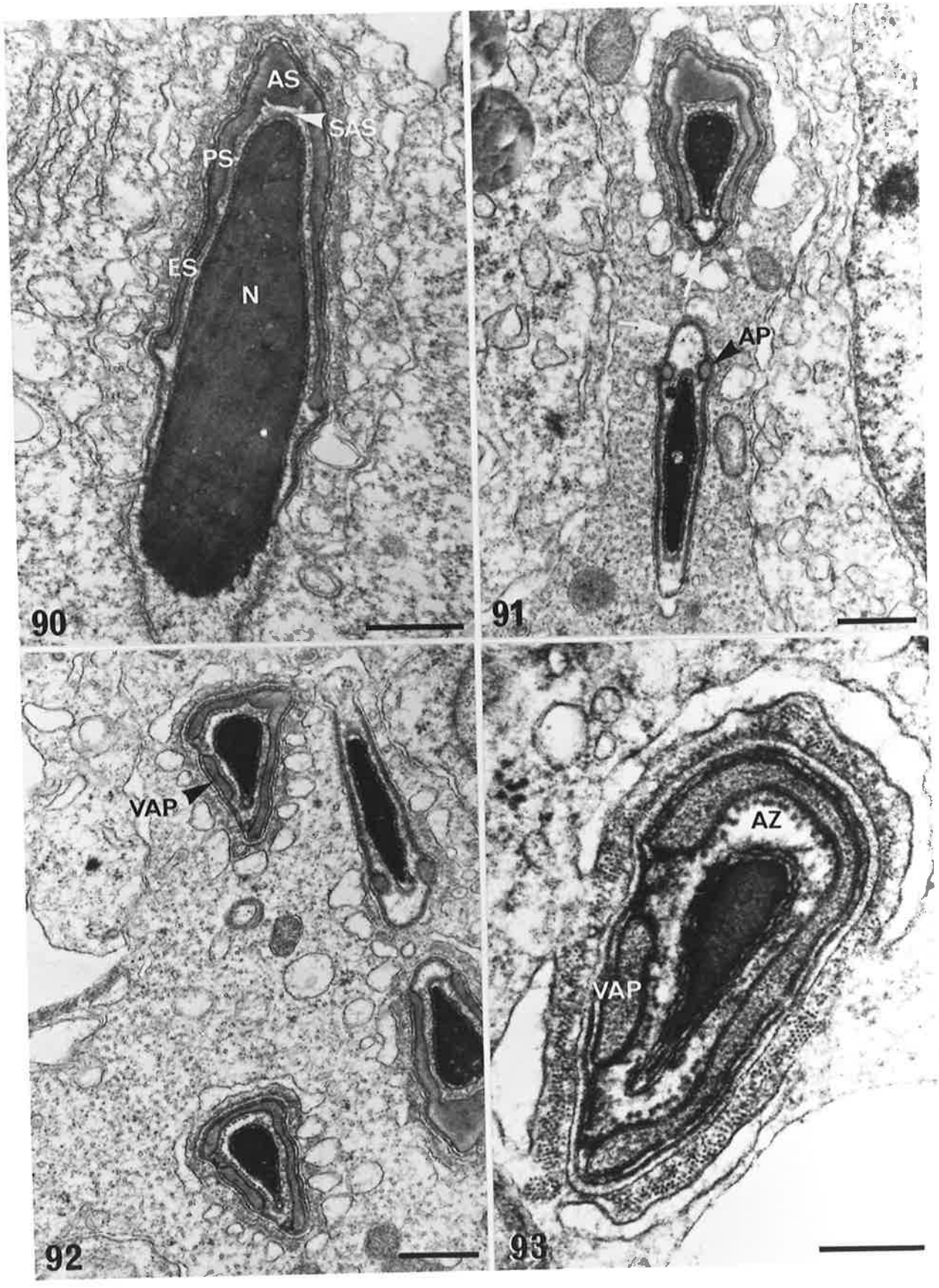
AS
SAS
PS
ES
N
90
AP
91
VAP
92
AZ
VAP
93

PLATE 21

Figs. 94-98. Step 12 spermatids.

Figs. 94. Sagittal section of the sperm head showing an expanded region of the sub-acrosomal space (SAS) at the base of the ventral hooks.
Bar = 0.5 µm. x 34,260

Fig. 95. Longitudinal section of the ventral margin of the sperm head. The expanded region often contains membrane whorls (MW), and is bounded by an extension of the post-acrosomal dense lamina (DL). The Sertoli cell ectoplasmic specializations are absent from this region.
Bar = 0.2 µm. x 57,100

Fig. 96. Higher magnification of the base of the ventral hook, showing the membrane whorl (MW), and the projections (Pr) which link the dense lamina and the plasma membrane (PM).
Bar = 0.2 µm. x 77,800

Fig. 97. At its initial formation, the ventral hook is completely enclosed at its base by the dense lamina, and only contains small amounts of flocculent material (arrow).
Bar = 0.5 µm. x 30,230

Fig. 98. In this spermatid, a second ventral hook is beginning to form. It is not capped by the post-acrosomal dense lamina (arrow). In the dorsal hook, a membrane whorl (MW) is located in the sub-acrosomal space. Part of a tubulobulbar complex (TBC) is located in the Sertoli cell cytoplasm between the dorsal and ventral hooks.
Bar = 0.5 µm. x 30,230

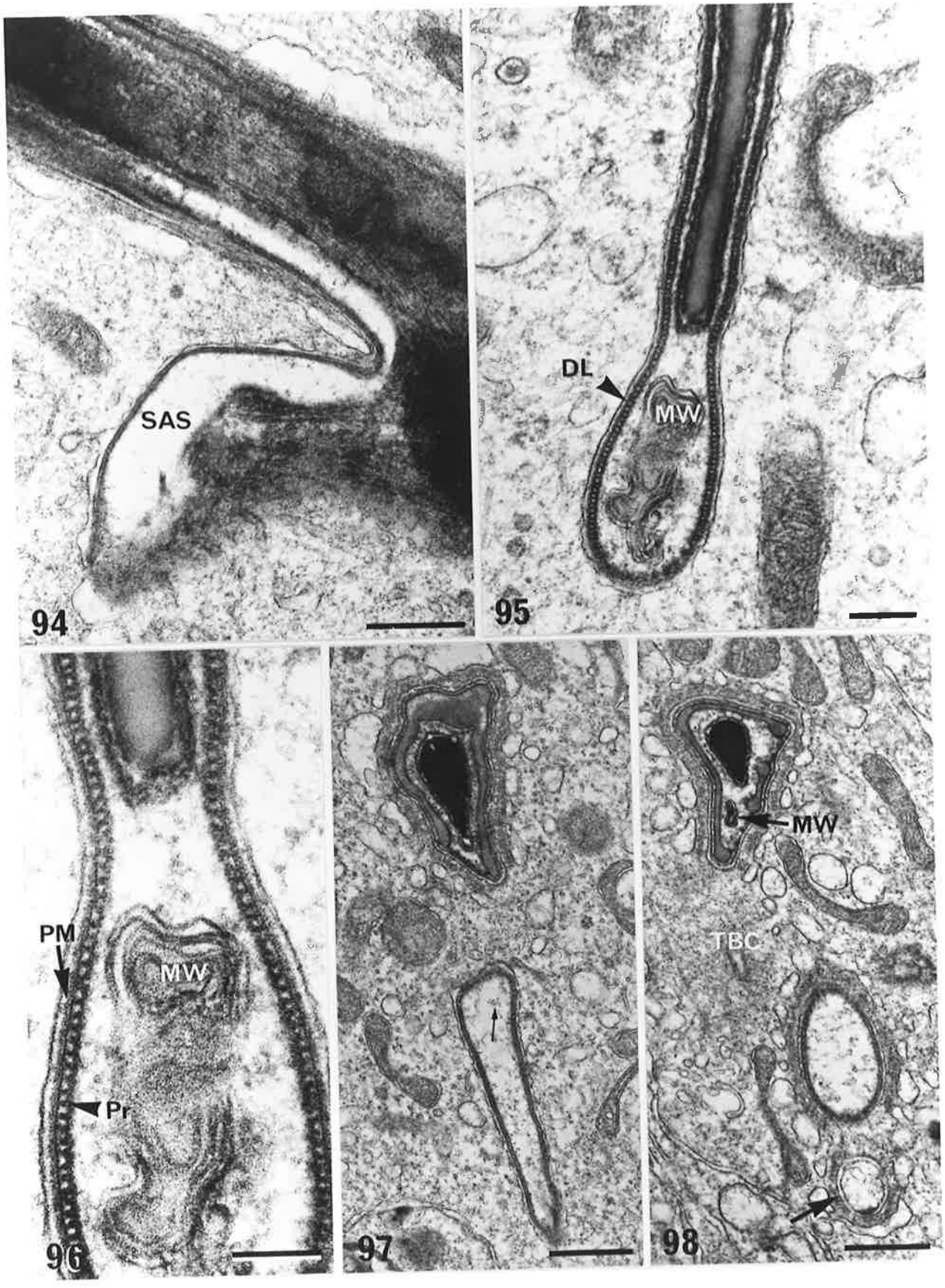
SAS
94
DL
MW
95
PM
MW
Pr
96
97
MW
TBC
98

PLATE 22

Figs. 99-104. Step 13a spermatids.

Fig. 99. In this stage, the nucleus (N) is condensed, and the apical segment (AS) forms a narrow ridge on the dorsal margin of the sperm head. The sub-acrosomal space (SAS) is expanded, but is largely devoid of contents. The entire sperm head is enclosed by the ectoplasmic specializations (EPS).
Bar = 0.5 µm. x 25,850

Fig. 100. The ventral hooks extend ventrally (arrow) from their base, and the acrosomal projections (AP) are present.
Bar = 1 µm. x 16,420

Figs. 101-104. The ventral hooks form as round, membrane-bound structures, and only contain membrane whorls (MW). The post-acrosomal dense lamina (DL) forms in close proximity to the plasma membrane. It forms initially as discrete subunits, which coalesce to produce a continuous lamina. The middle hook develops before the ventral hook. The dense lamina forms on the dorsal margin of each hook prior to capping the ventral margin. Each hook is enclosed by the Sertoli cell ectoplasmic specialization (EPS).
Bar = 0.2 µm. x 47,770 (101,102)
x 86,150 (103)

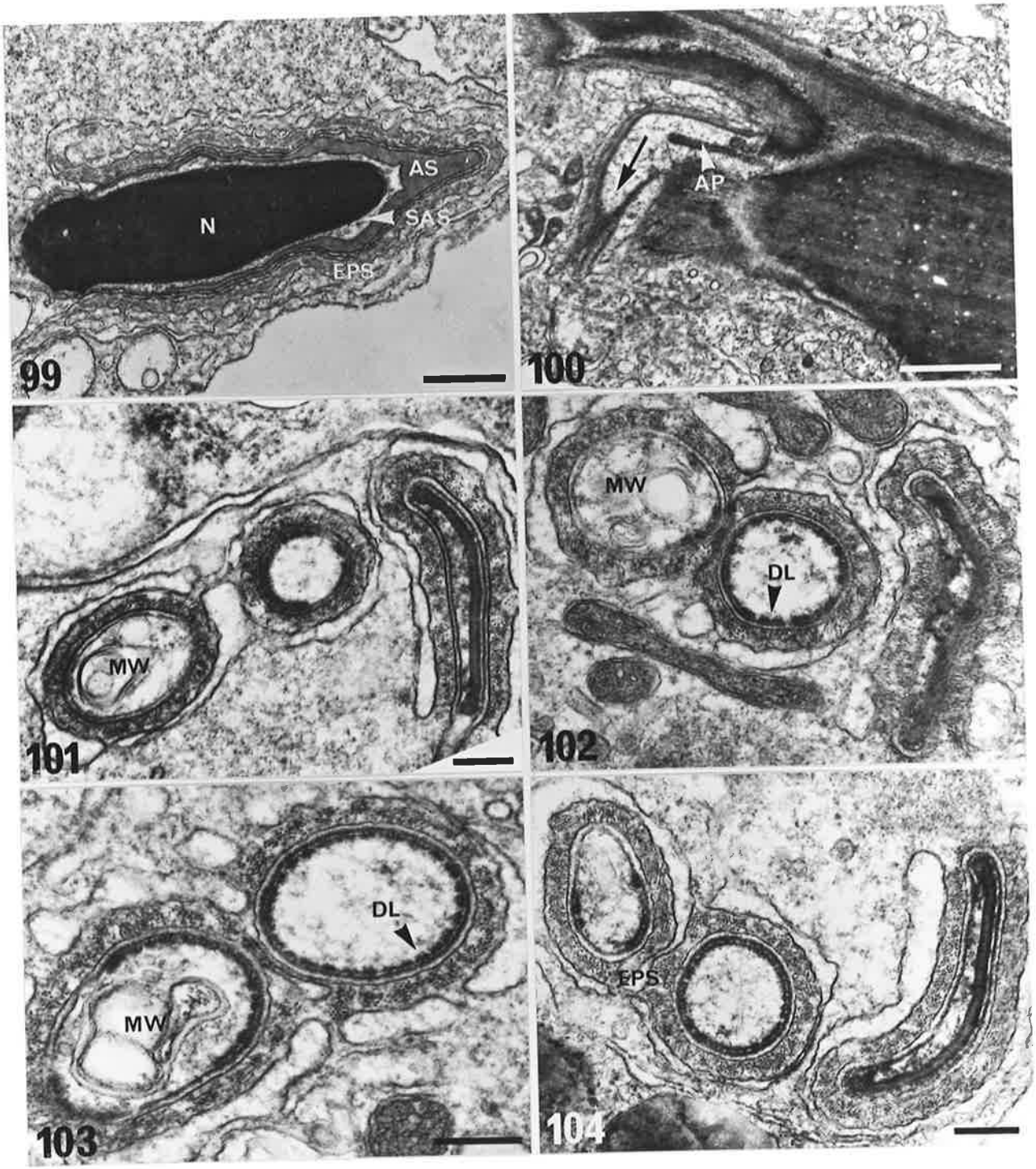
AS
N
SAS
EPS
99
AP
100
MW
101
MW
DL
102
DL
MW
103
EPS
104

PLATE 23

Figs. 105-109. Stepm 13a spermatids.

Fig. 105. Higher magnification of developing ventral hooks, showing the discrete lamina sub-units (arrow), and areas with a complete lamina (DL). A dense accumulation of material is located on the ventral border of the ventral hook (arrowhead).
Bar = 0.2 µm. x 71,160

Figs. 106, 107. Upon completion of their elongation, the ventral hooks are round or ovoid in shape, and contain some clumped, electron-dense material (arrows). The dense lamina (DL) is continuous around the periphery. The dorsal hook (D) has attained its final shape. The sub-acrosomal space (SAS) also contains small amounts of electron-dense material. There is a short segment of dense lamina (DL) on either side of the ventral acrosomal plate (VAP).
Bar = 0.2 µm. x 63,600

Figs. 108, 109. Sections cut through the post-acrosomal region on the caudal (Fig. 108) and ventral (Fig. 109) margins of the sperm head, revealing the regularly arranged projections which link the lamina and plasma membrane. The sub-acrosomal space (SAS) is largely devoid of contents.
Bar = 0.1 µm. x 116,220

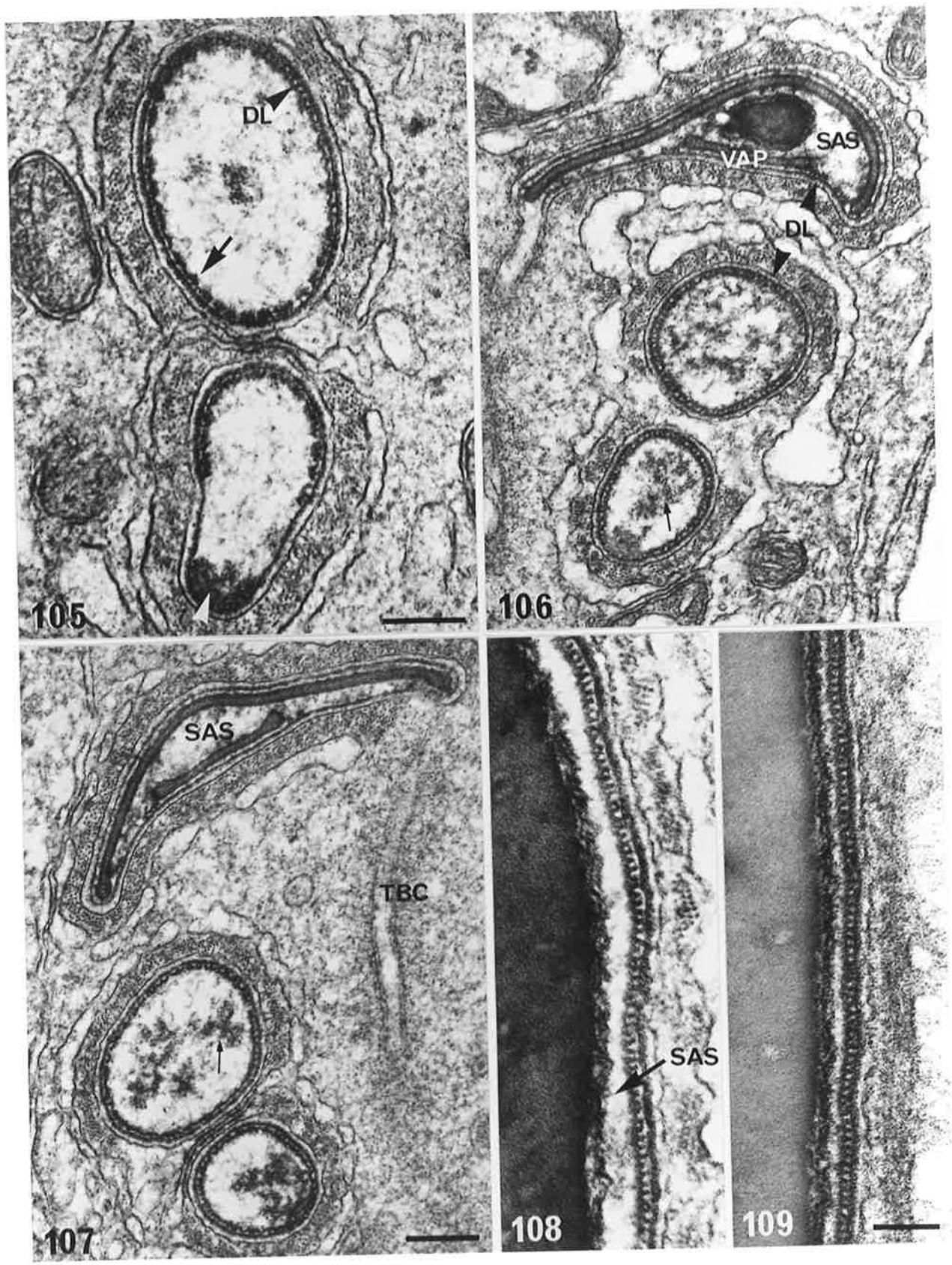
DL
105
VAP
SAS
DL
106
SAS
TBC
107
SAS
108
109

PLATE 24

Figs. 110-115. Step 13b spermatids.

Fig. 110, 111. The nucleus (N) is homogeneously electron-dense, and the acrosomal contents are fully condensed. The apical segment (AS) is often extensive, but narrow. The subacrosomal space (SAS) is narrow, and only contains some flocculent material, but the dorsal ridges (DR) have formed. A tubulobulbar complex (TBC) is present in Fig. 111.
Bar = 0.5 µm. x 33,150

Figs. 112-115. Bundles of 5-7 nm diameter microfilaments (Mf) appear in the dorsal and ventral margins of the two ventral hooks. The hooks become bilaterally flattened, and there is an increase in the amount of electron-dense material in the core of the ventral hooks (arrow), and in the subacrosomal space (SAS) in the dorsal hook. The ventral hooks come to reside in a single recess in the Sertoli cell, surrounded by the ectoplasmic specializations (EPS) (Fig. 115).
Bar = 0.5 µm. x 42,280 (112-114)
0.2 µm. x 50,310 (115)

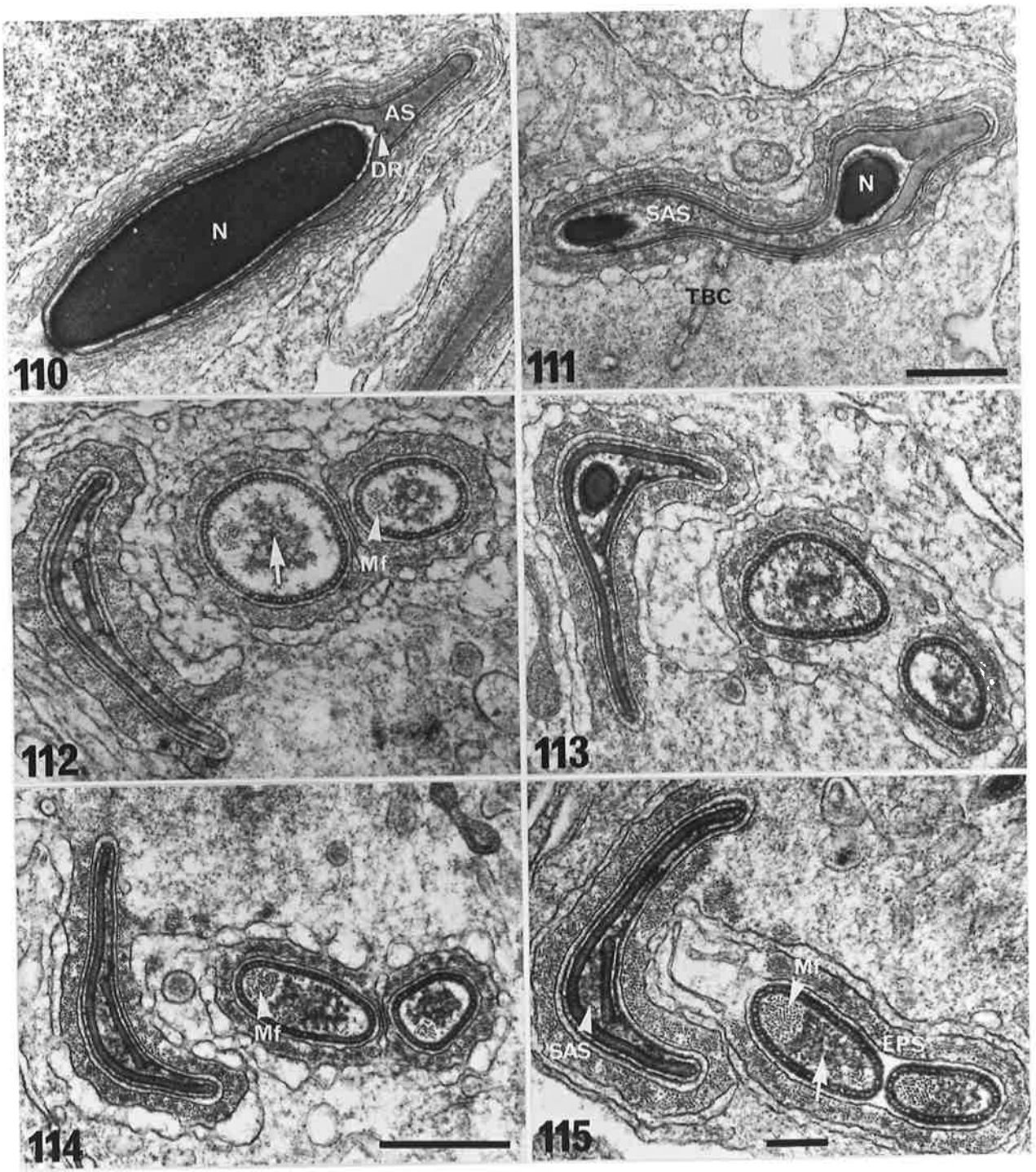
AS
DR
N
110
N
SAS
TBC
111
Mf
112
113
Mf
114
Mf
SAS
EPS
115

PLATE 25

Figs. 116-121. Step 13b spermatids.

Fig. 116. High magnification of part of the ventral hook. The filaments are 5-7 nm in diameter, with a centre-centre spacing of about 12 nm.
Bar = 0.05 µm. x 278,370

Fig. 117. Transverse section of the ventral hook, showing the hexagonal packing of the microfilaments (Mf), the electron-dense core material (arrow), and the projections (Pr) of the dense lamina.
Bar = 0.05 µm. x 196,500

Fig. 118. This longtudinal section cut through the ventral hooks demonstrates the filamentous nature of the bundles, and possible attachment sites to the dense lamina or clumped core material (arrow). Clumps of granular material occupy the basal regions of the hook (arrowhead).
Bar = 0.5 µm. x 41,960

Fig. 119. Clumps of moderately electron-dense core material are present in the basal regions of the ventral hooks.
Bar = 0.2 µm. x 56,970

Fig. 120. High magnification of a section cut near the tip of the ventral hooks, showing the close association of the projections (Pr) with the plasma membrane (PM), microfilaments (Mf), and bundles of microfilaments in the ectoplasmic specializations (arrow).
Bar = 0.1 µm. x 154,590

Fig. 121. In oblique sections cut through the hooks, the projections represent parallel ridges (arrow).
Bar = 0.1 µm. x 99,780

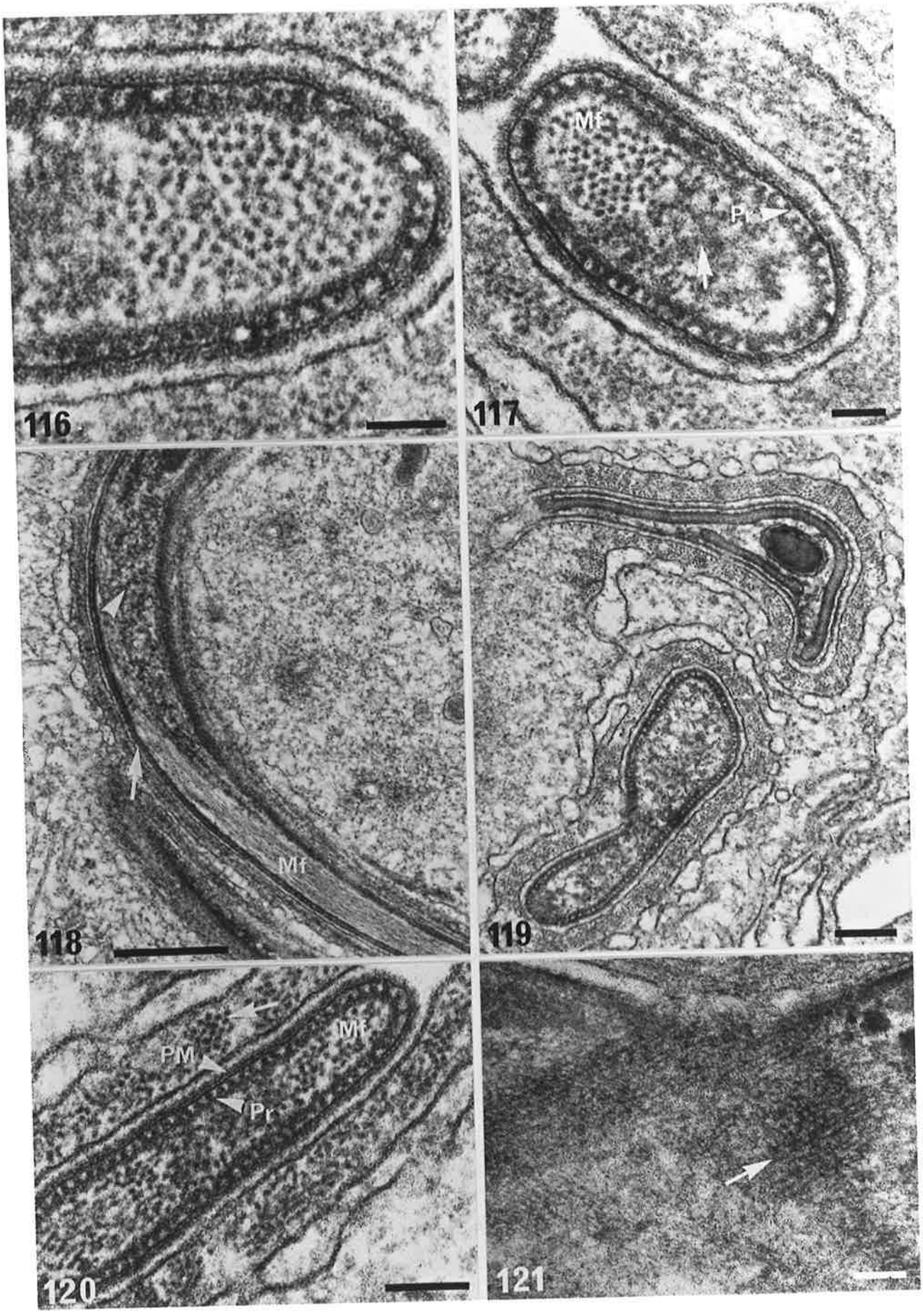
116
117
Mf
Pr
118
Mf
119
120
Mf
PM
Pr
121

PLATE 26

Figs. 122-125. Step 13b spermatids.

Fig. 122. Transverse section cut through the three hooks, showing the bilateral flattening of the ventral hooks, and tilting of the dorsal hook to one side. The cisternae of smooth endoplasmic reticulum around the hooks are inter-connected. A portion of a tubulobular complex (TBC) is indicated.
Bar = 0.5 µm. x 50,710

Fig. 123. Near the tip of the hooks, the dorsal hook is crescent-shaped, and capped on its dorsal surface by the equatorial segment (ES). The ventral hooks are flattened, there is very little electron-dense core material present, and the microfilaments (Mf) do not occur in bundles.
Bar = 0.5 µm. x 50,710

Figs. 124, 125. After formation of the bundles of microfilaments, the dorsal and sometimes ventral margins of the two ventral hooks become constricted and flattened (arrows). Portions of the post-acrosomal dense lamina (DL) are located on the ventral margin of the dorsal hook.
Bar = 0.5 µm. x 50,710

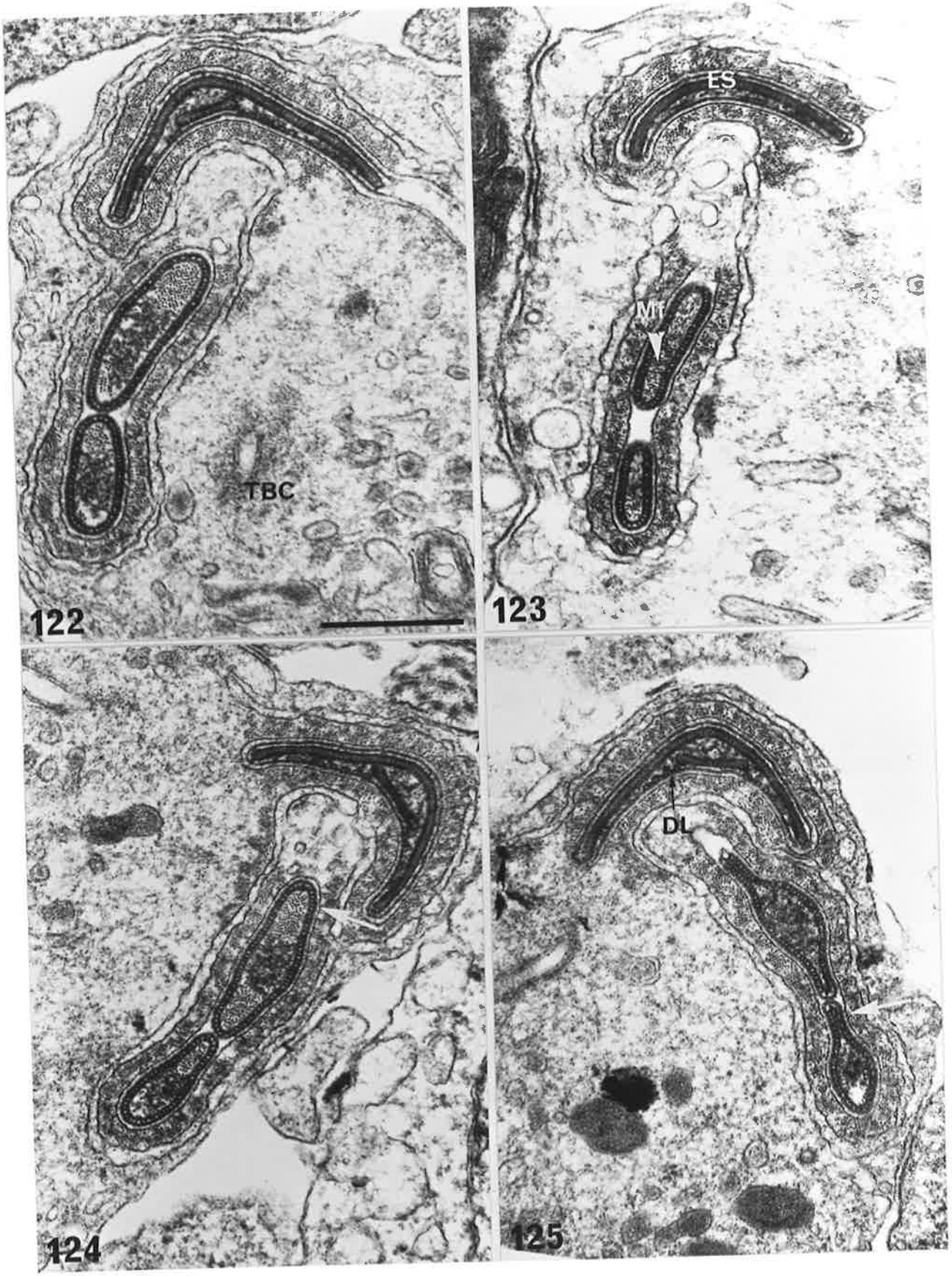
TBC
122
ES
Mt
123
124
DL
125

PLATE 27

Figs. 126-130. Step 13c spermatids.

Fig. 126. The sperm head remains unchanged from step 13b, except that electron-dense sub-acrosomal material has formed in the sub-acrosomal space, especially on the dorsal margin (arrow).
Bar = 0.5 µm. x 38,620

Figs. 127-130. Electron-dense sub-acrosomal material (SAM) condenses concurrently in the dorsal hook and ventral hooks. In the ventral hooks, it is formed from the core towards the dense lamina (DL), and eventually obscures the bundles of microfilaments (Mf).
Bar = 0.2 µm. x 67,400 (127)
0.2 µm. x 63,680 (128)
0.2 µm. x 69,870 (129)
0.1 µm. x 101,620 (130)

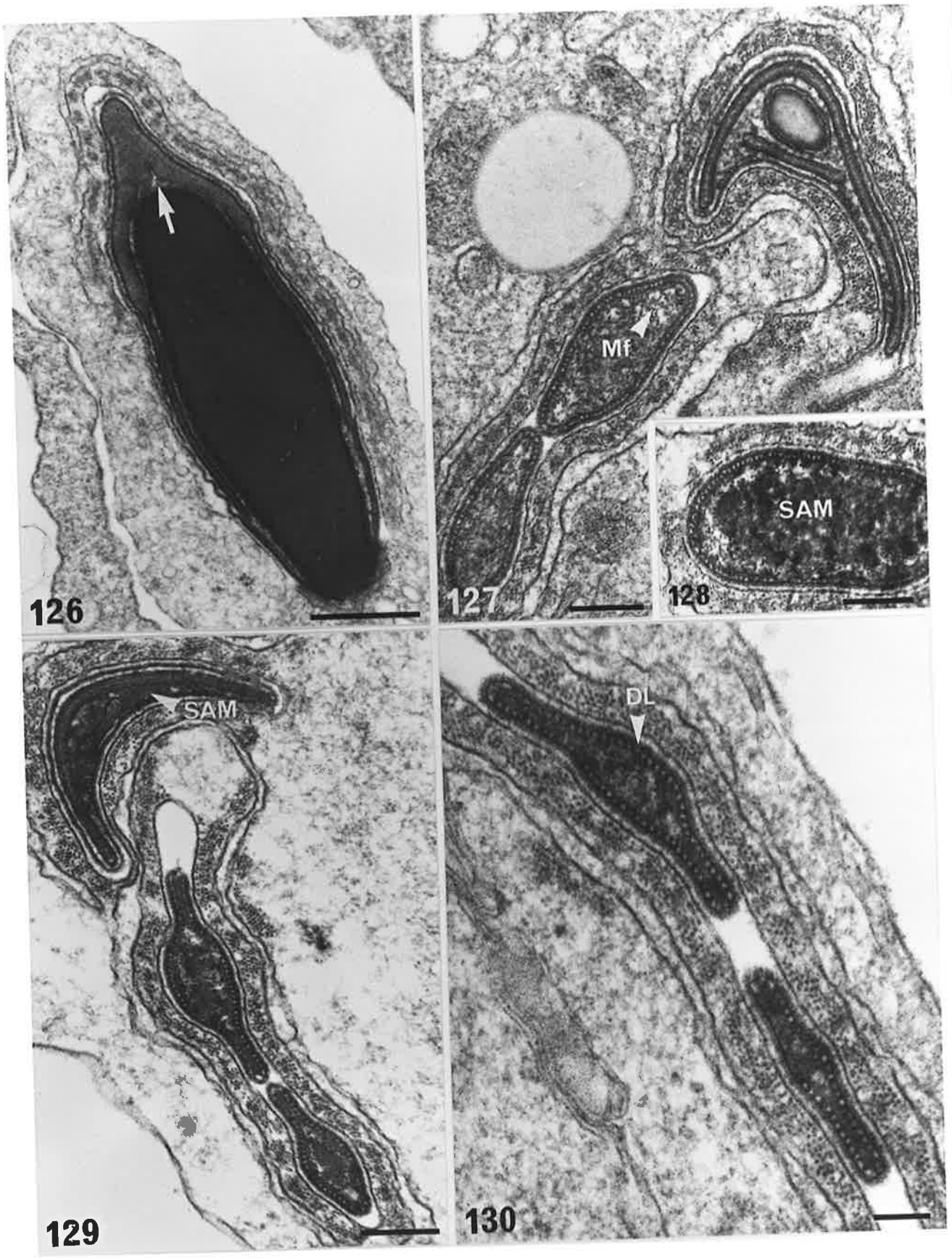
126
Mf
127
SAM
128
SAM
129
DL
130

PLATE 28

Figs. 131-133. Step 13c spermatids.

Fig. 131. High magnification of a transverse section cut through the ventral hooks. This reveals the regular spacing of the projections (Pr), the thickened inner leaflet of the plasma membrane, (PM), the glycocalyx (Gx), and the hexagonally arranged microfilaments in the Sertoli cell ectoplasmic specializations.
Bar = 0.05 µm. x 261,680

Fig. 132. As sub-acrosomal material (SAM) condenses in the core of the ventral hooks, the inner aspect of the dense-lamina (DL) becomes thickened.
Bar = 0.1 µm. x 156,590

Fig. 133. High magnification of the dense lamina, showing the shape of the projections (Pr), and their attachment to the plasma membrane (PM).
Bar = 0.05 µm. x 479,320

Figs. 134,135. Released testicular spermatozoa. The sperm head exhibits the same ultrastructural features as in step 13c spermatids. The plasma membrane (PM) is smooth, though slightly ruffled over the equatorial segment (ES). The ventral hooks are filled with moderately electron-dense material, and the junction between the core and peripheral layers is marked by a less homogeneous area (arrows).
Bar = 0.5 µm. x 39,740 (134)
0.1 µm. x 146,670 (135)

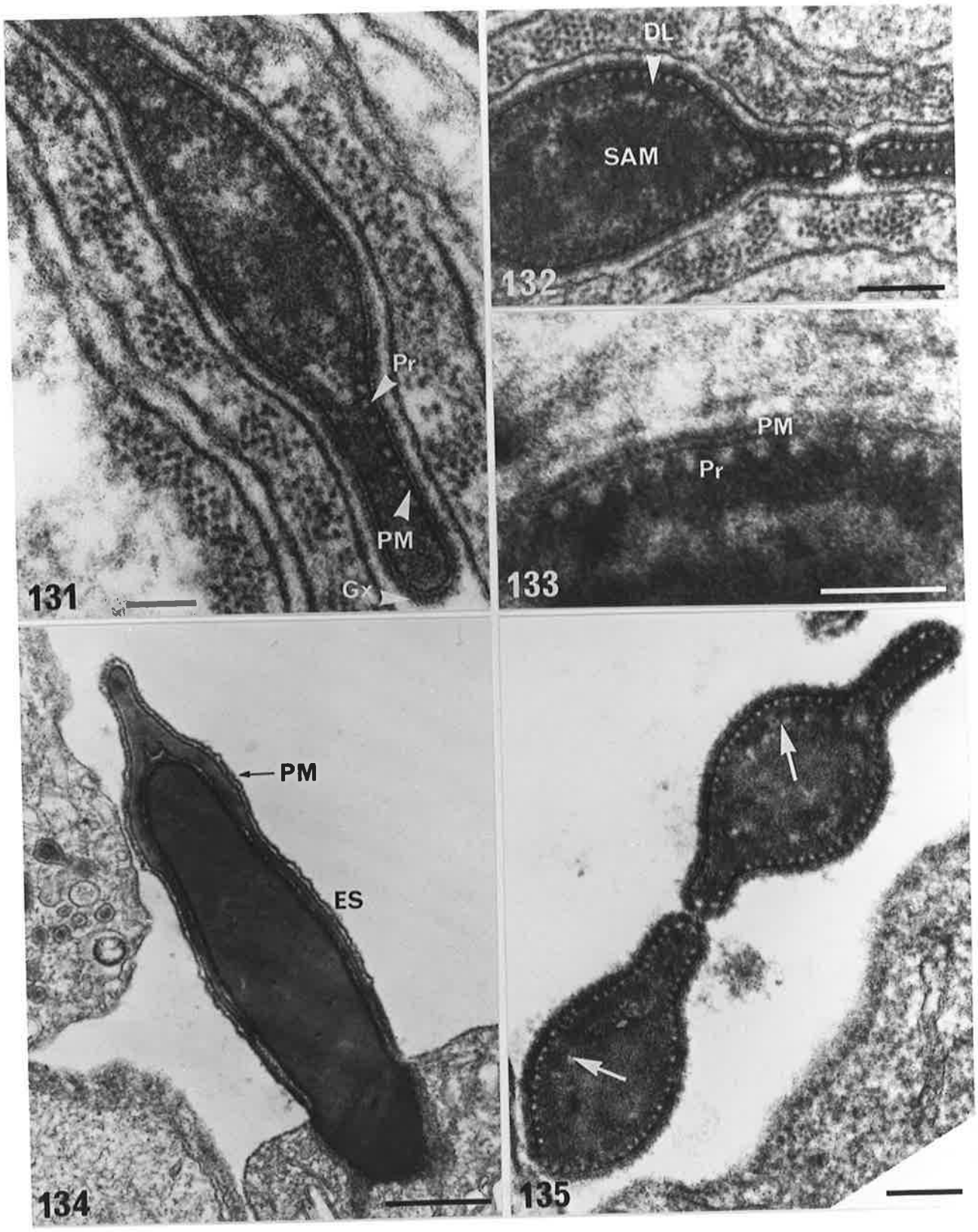
131
Pr
PM
Gx
132
DL
SAM
133
PM
Pr
134
PM
ES
135

PLATE 29

Figs. 136-142. Isolated spermatids stained with silver nitrate. Bar = 10 µm. x 1,650

Fig. 136. Step 7/8 spermatid. An argyrophilic band extends along the ventro-lateral aspect of the sperm head (arrow).

Fig. 137. Step 11 spermatid. The nucleus (N) has become considerably reduced in size, and stains weakly. The ventral and caudal margin of the sperm head stains intensely. This extends along the dorsal hook, where two bands are present (arrow).

Figs. 138-140. Step 12 spermatids. There is a broad argyrophilic band on the caudal and ventral margins of the sperm head (PAR). Two thin bands extend along the dorsal hook (D). An expanded area is located at the base of the ventral hooks, and often a single hook extends ventrally from this area (arrows).

Figs. 141,142. Step 13 spermatids. The extent of staining is reduced on the ventral and caudal margins, and the two ventral hooks exhibit an identical pattern of staining to the PAR (arrow).

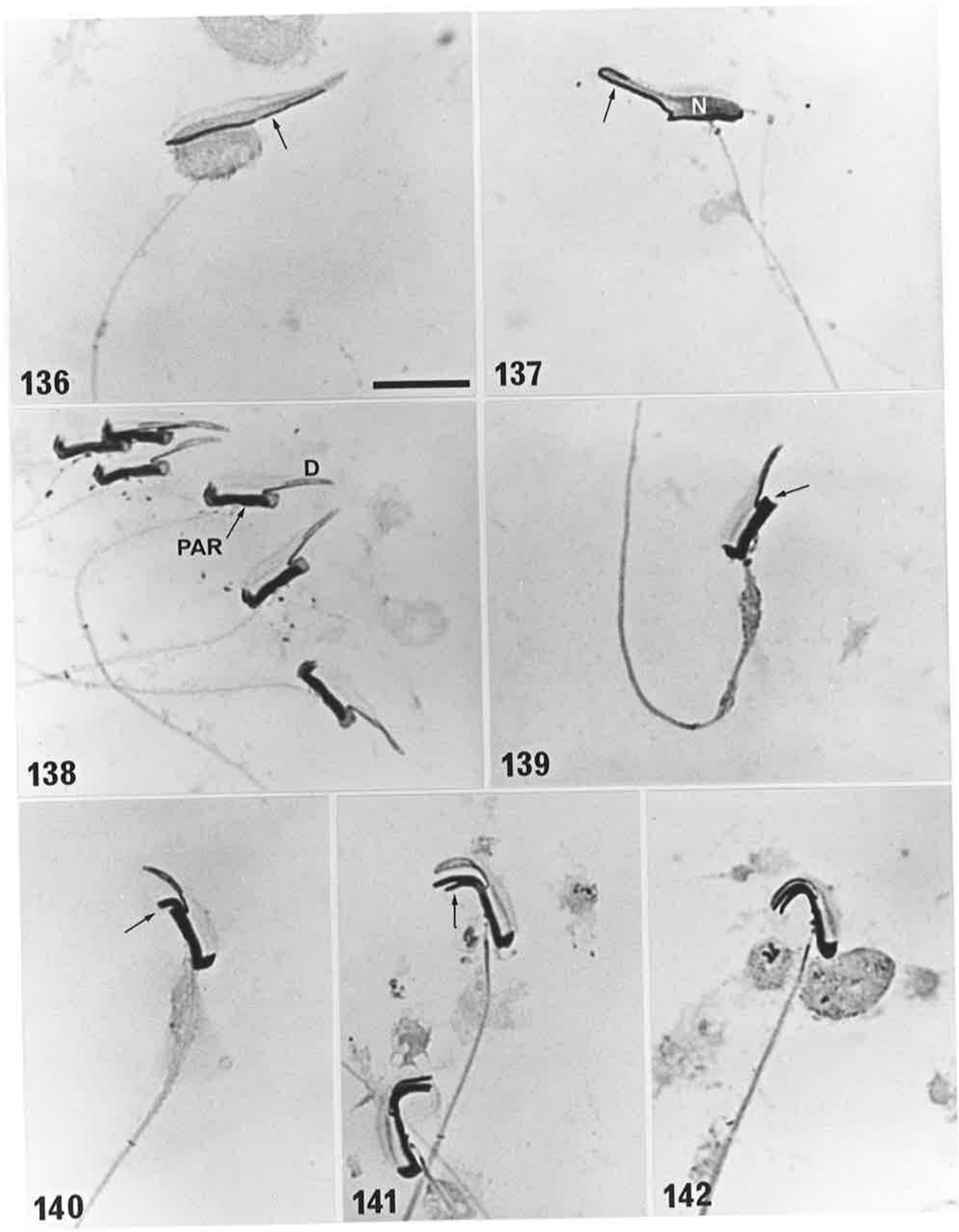
136
137
N
138
D
PAR
139
140
141
142

PLATE 30

Figs. 143-148. Paired phase contrast (a) and fluorescence (b) micrographs of mechanically isolated spermatids stained with NBD-phallacidin.
Bar = 10 µm. x 1,650

Figs. 143-145. Step 7-11 spermatids. A band of intense fluorescence is located over the acrosomal region (Ac). The post-acrosomal region (PAR) is almost completely non-fluorescent.

Figs. 146-148. Step 12/13a spermatids. During their initial formation, the region of the ventral hooks (V) is non-fluorescent (Fig. 146). As the hooks elongate, they become fluorescent, and the intensity increases till it matches (Fig. 147) or exceeds (Fig. 148) the fluorescence on the remainder of the sperm head. This is associated with curvature of the dorsal hook (D), and the entire sperm head region exhibits a moderate degree of fluorescence (Fig. 148). Ventrally-oriented bands of intense fluorescence are found in the concave region ventral to the dorsal hook (arrow).

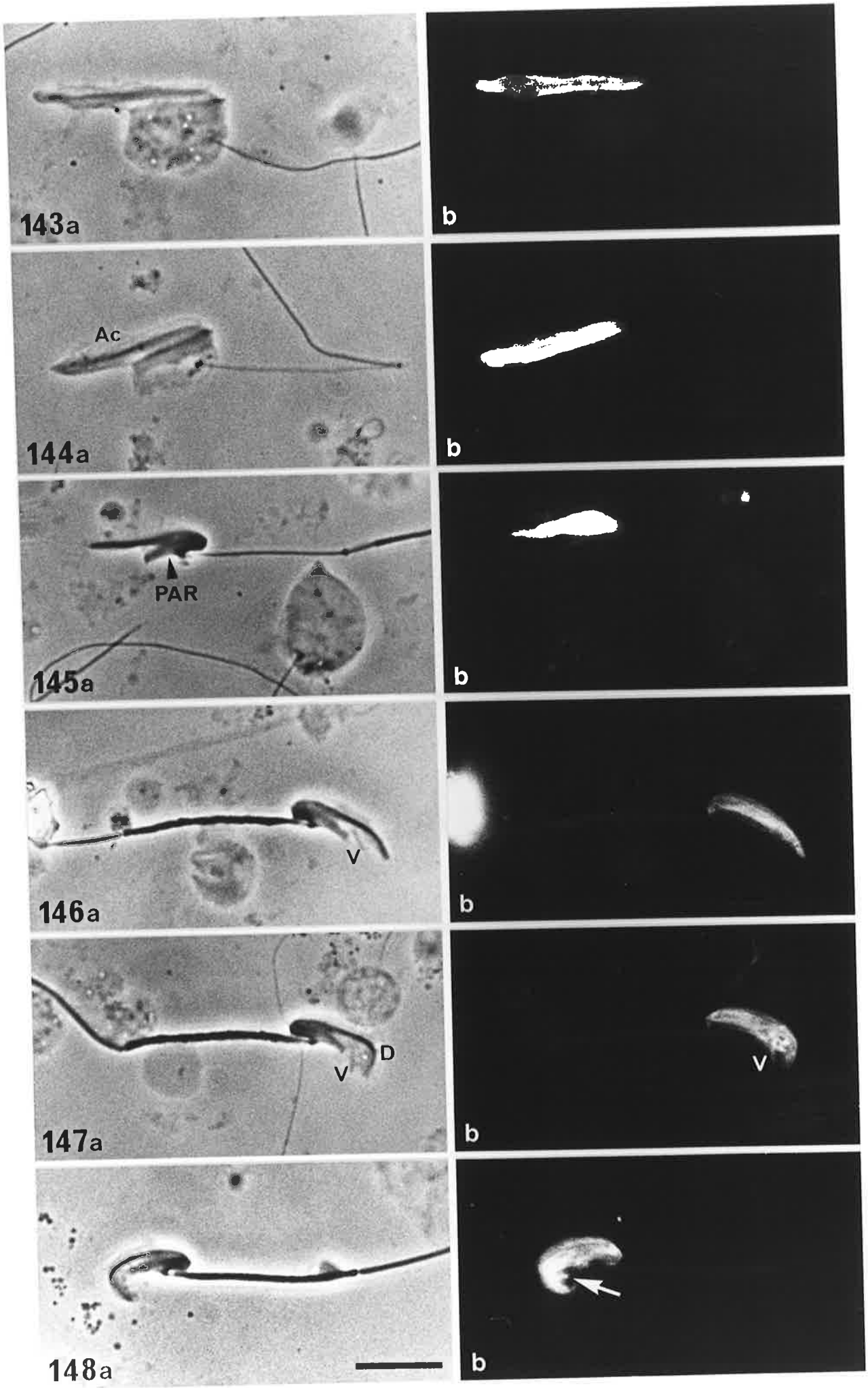
143a
b
Ac
144a
b
PAR
145a
b
V
146a
b
D
V
147a
V
b
148a
b

PLATE 31

Figs. 149-151. Paired phase contrast (a) and fluorescence (b) micrographs of mechanically isolated spermatids and spermatozoa stained with NBD-phallacidin.
Bar = 10 µm. x 1,650

Figs. 149,150. Step 13b spermatids. The ventral hook region fluoresces intensely. In Fig. 150, the ectoplasmic specializations (EPS) have become dislodged, revealing directly that the fluorescence emantes from the two ventral hooks (V).

Fig. 151. In testicular spermatozoa, intense fluorescence originates from the two ventral hooks (V). The middle piece (MP) is weakly fluorescent.

Figs. 152,153. Control preparations. Weak fluorescence is sometimes found in the posterior regions of the sperm head, but areas of intense fluorescence are not present. The middle piece (MP) exhibits weak fluorescence in late spermatids (Fig. 153).
Bar = 10 µm. x 1,650

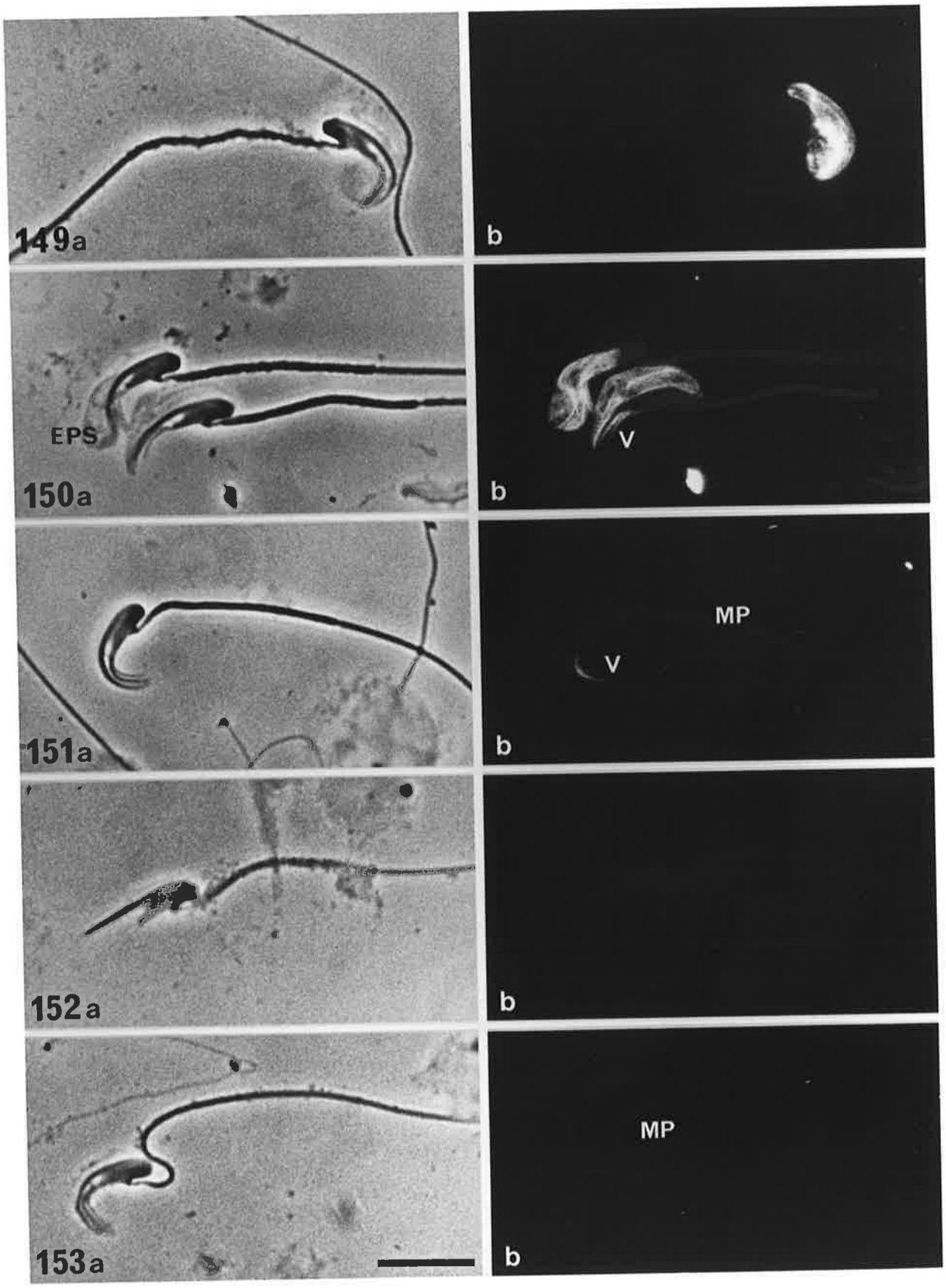
149a
b
EPS
150a
V
b
151a
MP
V
b
152a
b
153a
MP
b

PLATE 32

Figs. 154-156. Paired phase contrast (a) and fluorescence (b) micrographs of enzymatically isolated spermtids stained with NBD-phallacidin.
Bar = 10 µm. x 1,650

Figs. 154,155. Step 13b spermatids. The ventral hooks (V) are the only fluorescent region in the sperm head. The pseudoperforatorium (Pp) is completely negative. The middle piece (MP) exhibits weak fluorescence.

Fig. 156. Testicular spermatozoon. The ventral hooks (V) exhibit intense fluorescence, and two bands of fluorescence originate from the base of the hooks. The middle piece (MP) is weakly fluorescent.

Figs. 157,158. Control preparations. There is no fluorescence in the region of the ventral hooks (V), although the sperm head and middle piece (MP) sometimes exhibit weak autofluorescence.
Bar = 10 µm. x 1,650

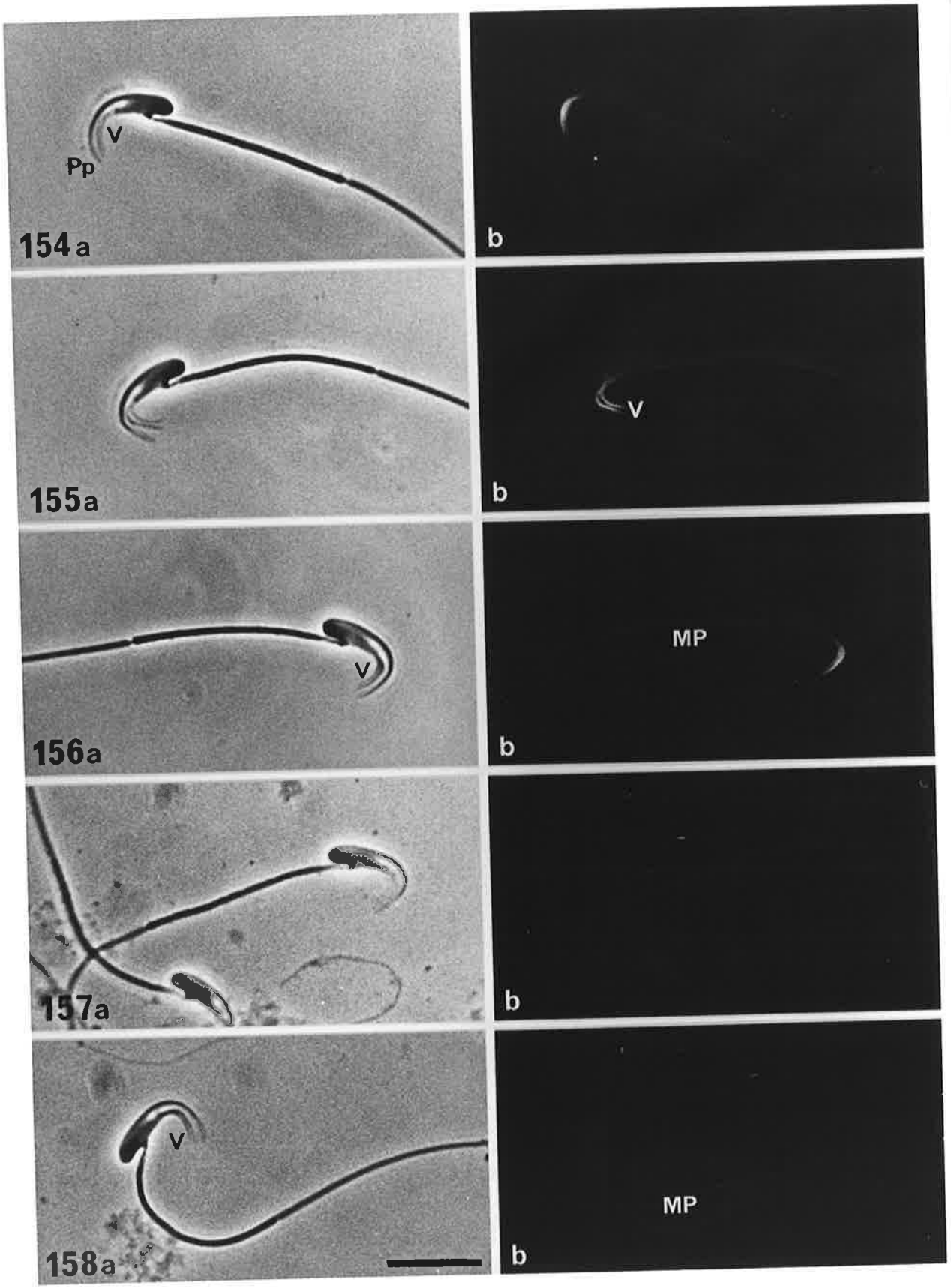
V
Pp
154a
b
155a
V
b
156a
V
MP
b
157a
b
158a
V
MP
b

PLATE 33

Figs. 159-163. Treatment of cauda epididymal sperm with trypsin to cleave the sperm heads from tails.

Fig. 159. Phase contrast micrograph showing >97% cleavage.
Bar = 100 µm. x 109

Figs. 160-162. Effect of trypsin on sperm head ultrastructure. There is a variable degree of swelling of the principal segment (PS) and loss of the plasma membrane (PM). The sub-acrosomal material (SAM) remains intact. The basal plate (BP) is firmly attached to the nucleus (Fig. 161). The ventral hooks appear unaffected by this treatment, except that the plasma membrane becomes loosened (arrow). The sub-acrosomal material (SAM) in the dorsal hook remains intact, but the plasma membrane is damaged, and the contents of the equatorial segment (ES) have dispersed.
Bar = 0.5 µm. x 46,770 (160)
x 32,950 (161,162)

Fig. 163. Effect of trypsin on sperm tail ultrastructure. The plasma membrane has been removed, and there is swelling and loss of the matrix in some mitochondria (Mc). The organization of the axoneme (Ax) has been disrupted, though this is more pronounced in the middle piece.
Bar = 1 µm. x 12,120


159

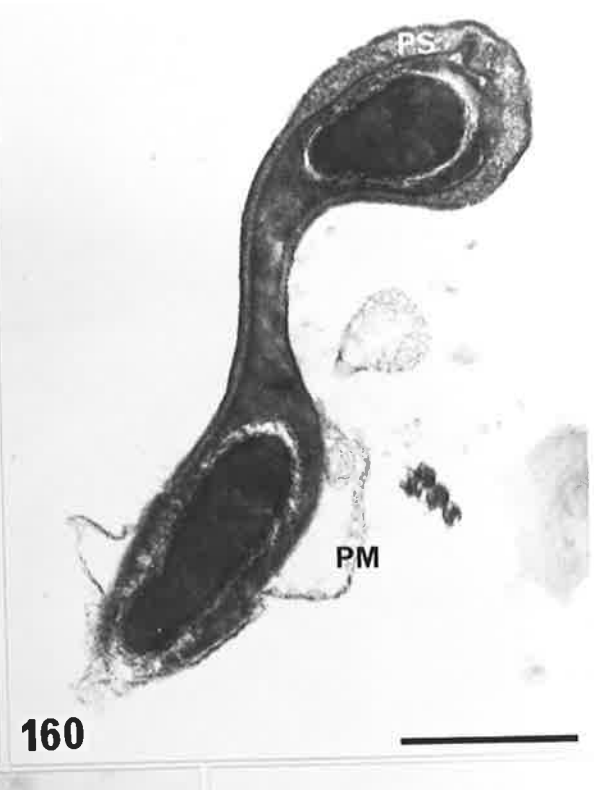

160

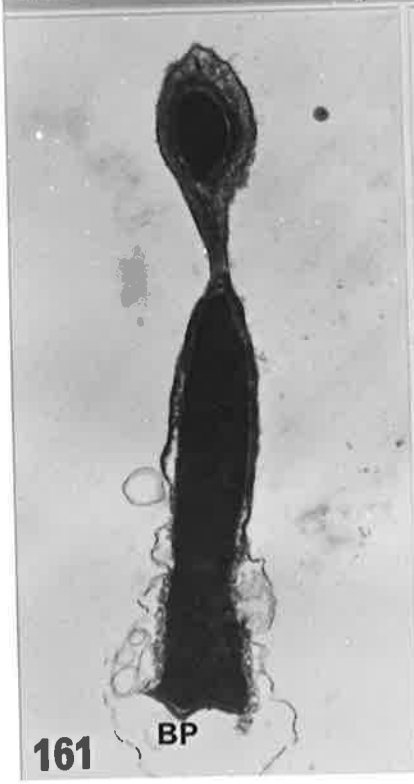

161

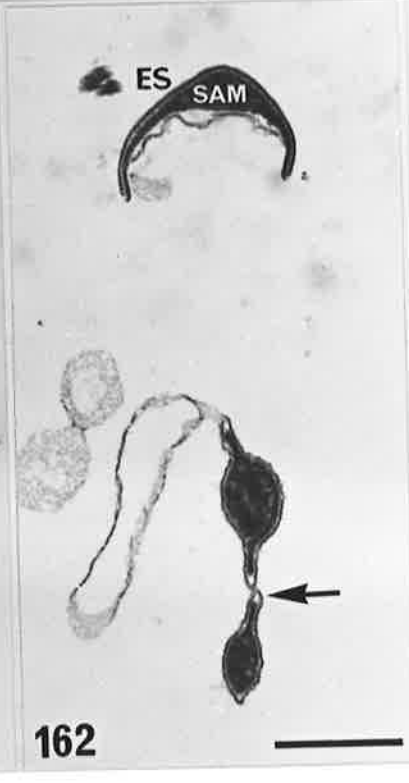

162

163

PLATE 34

Figs. 164-170. Isolated sperm heads and tails after discontinuous sucrose gradient centrifugation.

Fig. 164. Phase contrast micrograph of isolated tails, showing >98% purity. Some tails are coiled.
Bar = 100 µm. x 116

Fig. 165. Phase contrast micrograph of isolated heads. The purity of this fraction is >95%.
Bar = 100 µm. x 116

Fig. 166. The sperm head appears unaffected by this procedure, although the ventral hooks are sometimes spread apart (arrow).
Bar = 5 µm. x 2,285

Figs. 167,168. The acrosome in the principal (PS) and equatorial (ES) segments is disrupted, with partial dispersion of its contents. The plasma membrane is absent. The sub-acrosomal material (SAM) in the dorsal and ventral hooks is unaffected. The post-acrosomal dense lamina (DL) is also intact.
Bar = 0.5 µm. x 39,530

Fig. 169. Phase contrast micrograph of isolated tails. The mitochondrial sheath is eroded (arrow), and the tails are often coiled or broken at the annulus.
Bar = 50 µm. x 390

Fig. 170. In the middle piece and principal piece, the organization of the axoneme (Ax) is severly disrupted, the plasma membrane is absent, and in the middle piece, the mitochondria (Mc) are swollen.
Bar = 0.5 µm. x 39,530

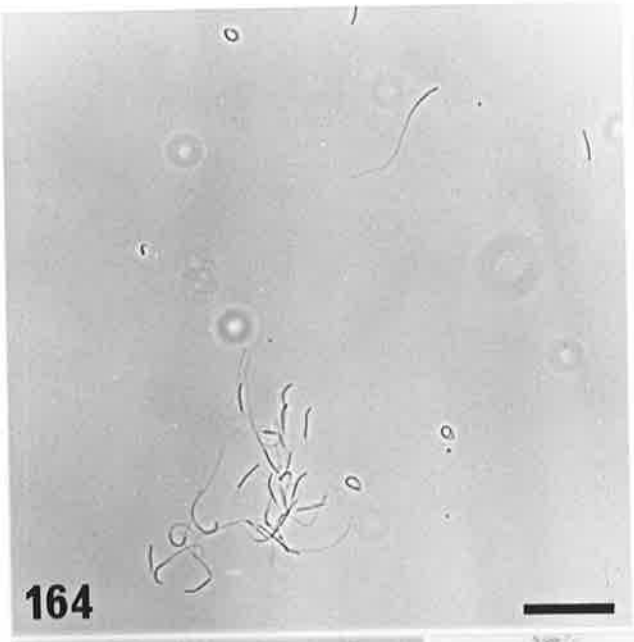
164

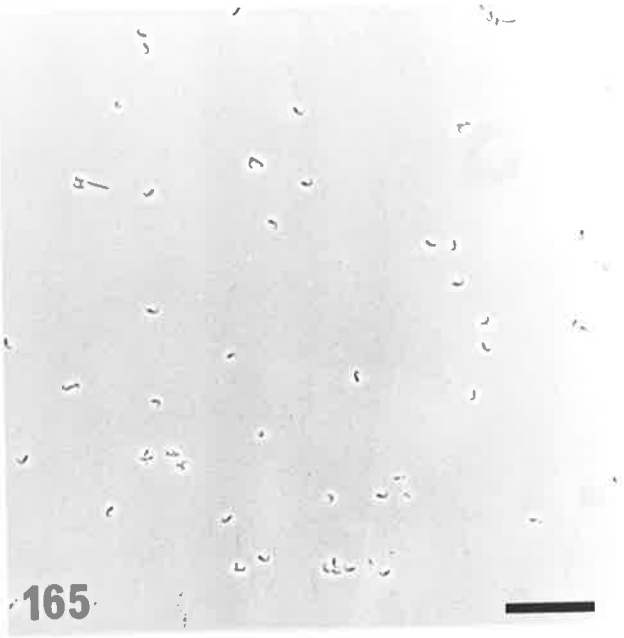
165


166

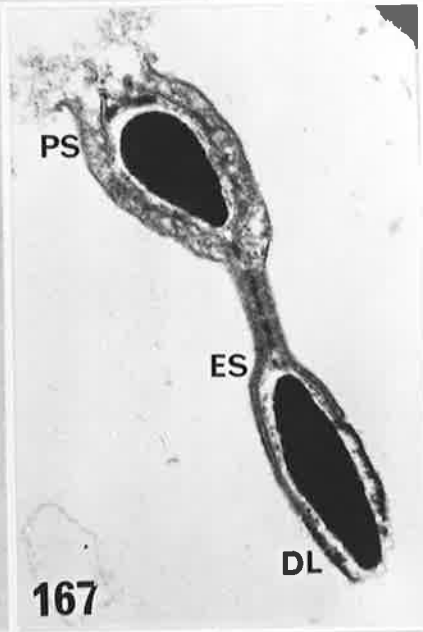
PS
ES
DL
167

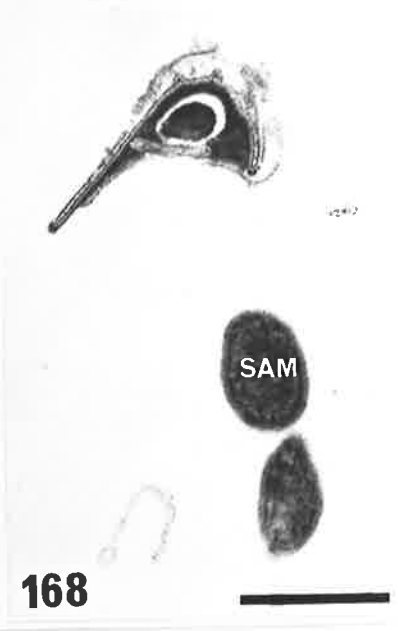
SAM
168

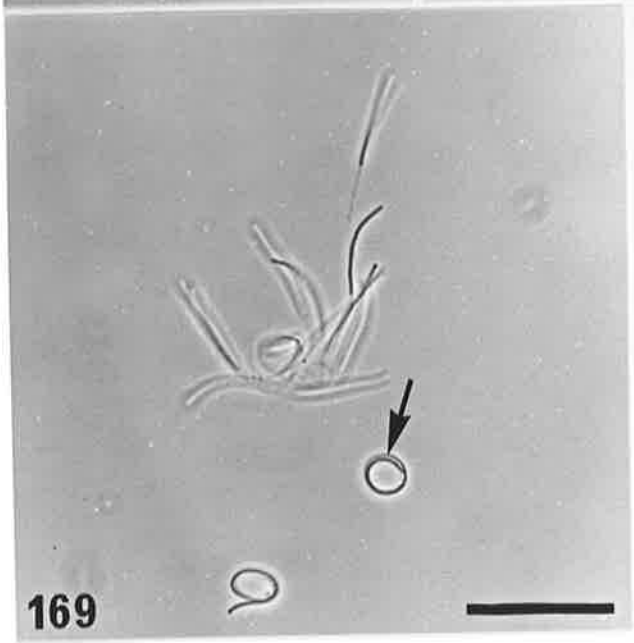
169

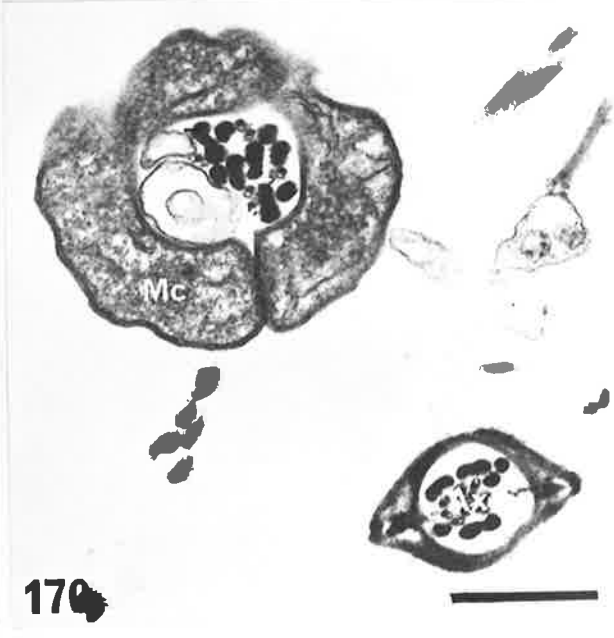
Mc
170

PLATE 35

Figs. 171-175. Treatment of sperm heads and tails with TX100 or SB_{16} for 2 hours.

Fig. 171. TX-100. The acrosome is almost completely solubilized, except for some remnants in the equatorial segment (ES). The ventral hooks are intact, although most of the plasma membrane has been solubilized (arrow).
Bar = 0.2 µm. x 56,280

Figs. 172-174. Treatment of sperm head with SB_{16}. The acrosome (Ac) has been solubilized, and only a few remnants remain. The nucleus (N), sub-acrosomal material (SAM), dorsal ridges (DR), and post-acrosomal dense lamina (DL) appear to be unaffected. In Fig. 174, the projections (Pr) are clearly evident, although there are remnants of the plasma membrane (arrows).
Bar = 0.2 µm. x 56,280 (172,173)
0.1 µm. x 66,770 (174)

Fig. 175. Treatment of tails with SB_{16} has removed the remaining plasma membrane, and largely solubilized the mitochondria, except for the outer mitochondrial membrane (OMM).
Bar = 0.5 µm. x 32,010

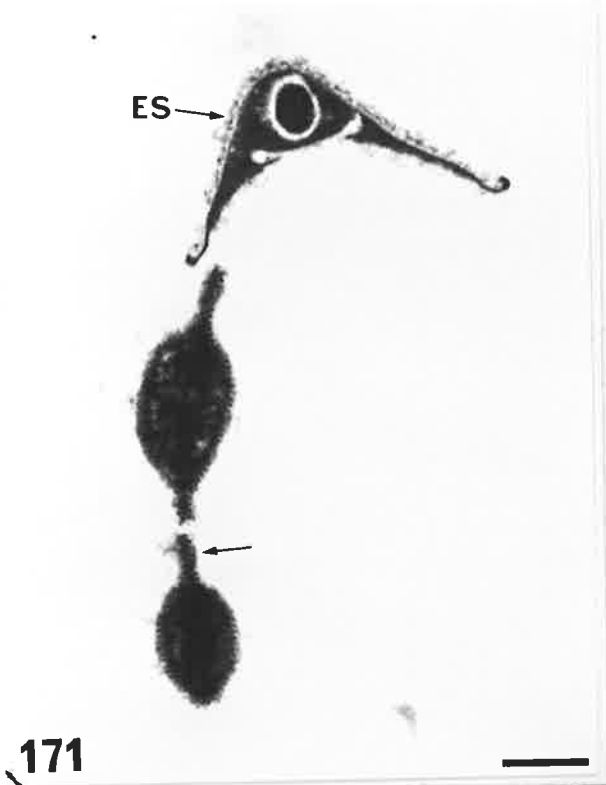

171

172

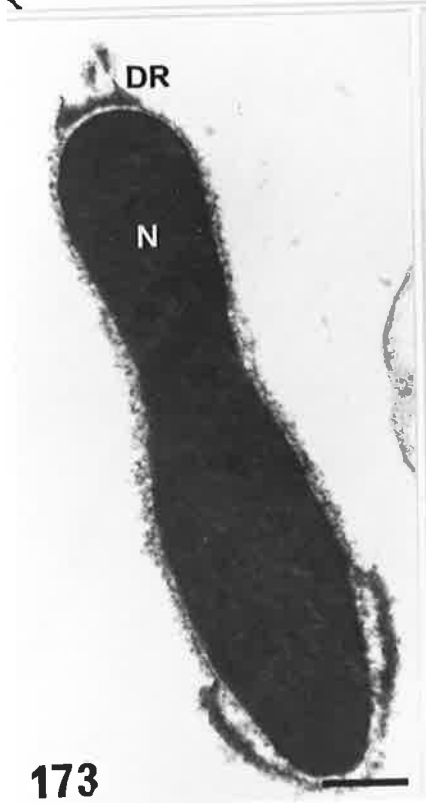

173

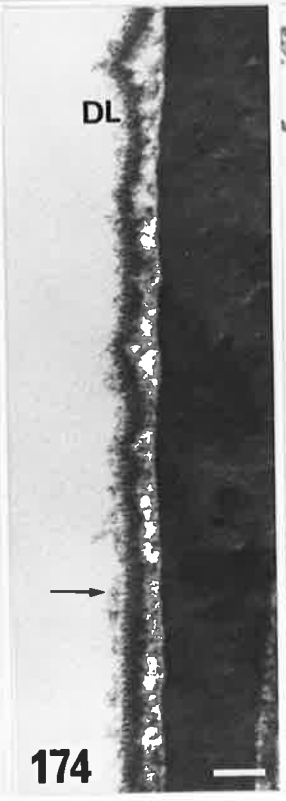

174

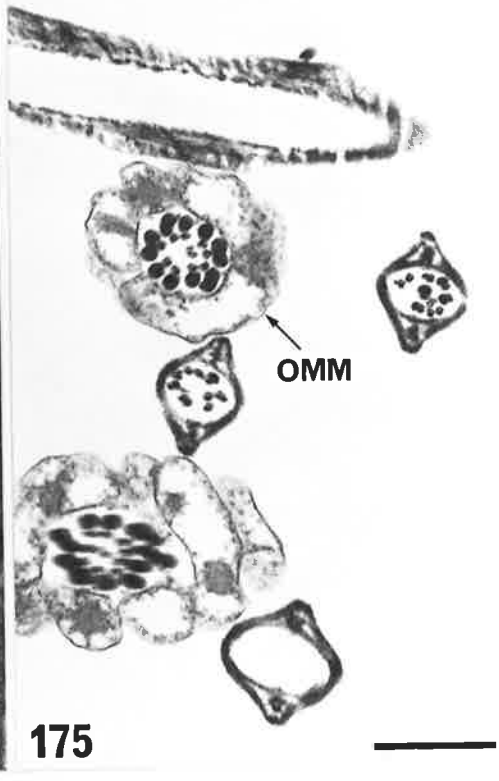

175

PLATE 36

Figs. 176-179. Treatment of sperm heads and tails with SDS for 4 hours.

Fig. 176. Phase contrast micrograph showing that the ventral hooks (V) and pseudoperforatorium (Pp) have become swollen and elongated.
Bar = 10 µm. x 1,880

Figs. 177,178. The sub-acrosomal material (SAM) in the dorsal and ventral hooks is granular, but incompletely solubilized (Fig. 177). The nucleus (N) is largely unaffected, but the basal plate and post-acrosomal dense lamina are solubilized (Fig. 178).
Bar = 0.2 µm. x 55,030 (177)
0.5 µm. x 34,050 (178)

Fig. 179. SDS appears to have solubilized all sperm tail components except the outer mitochondrial membrane (OMM), dense fibres (ODF) and fibrous sheath (FS).
Bar = 0.5 µm. x 41,510

Figs. 180,181. Treatment of sperm heads with SDS and DTT for 10-20 minutes.

Fig. 180. The sperm head is partially decondensed, though to a lesser degree in the dorsal hook (D), and the ventral hooks and pseudoperforatorium have been solubilized.
Bar = 10 µm. x 1,880

Fig. 181. The nuclear material (N) in the dorsal hook is still compact, but the sub-acrosomal material and ventral hooks are absent.
Bar = 0.5 µm. x 30,930

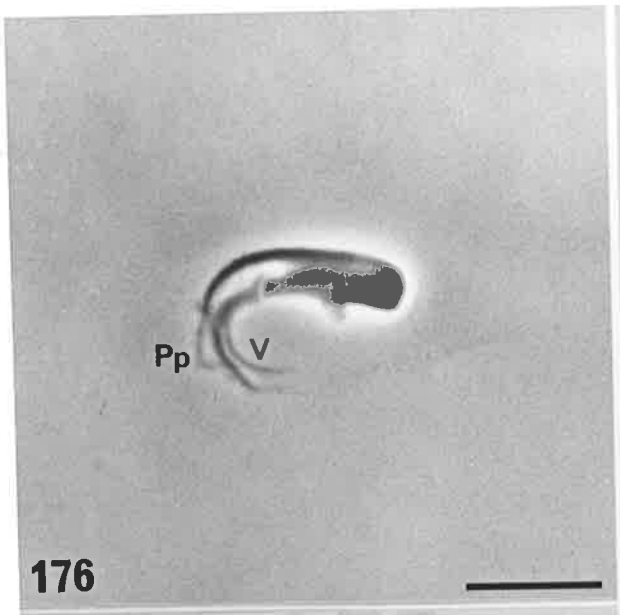
Pp
V
176

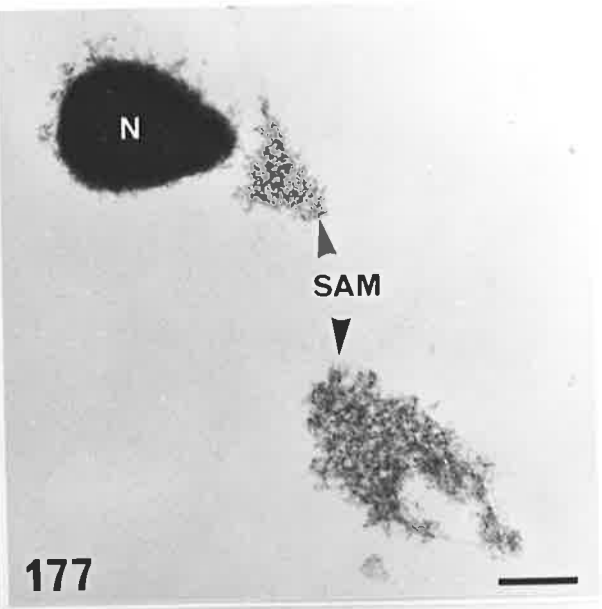
N
SAM
177

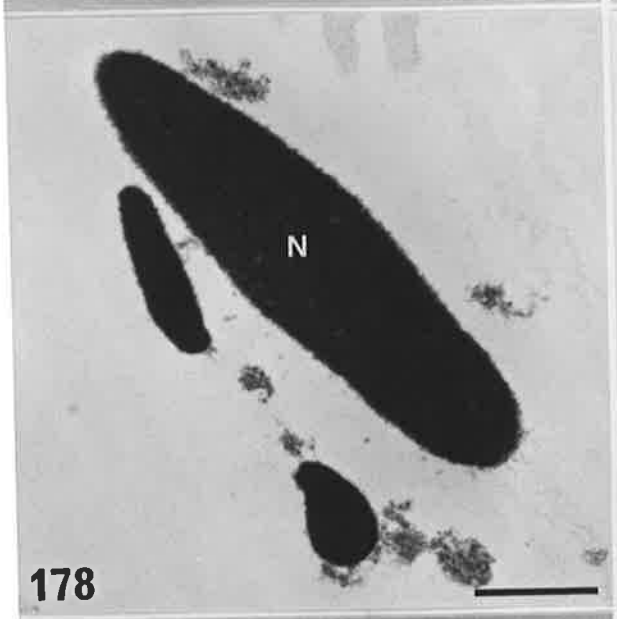
N
178

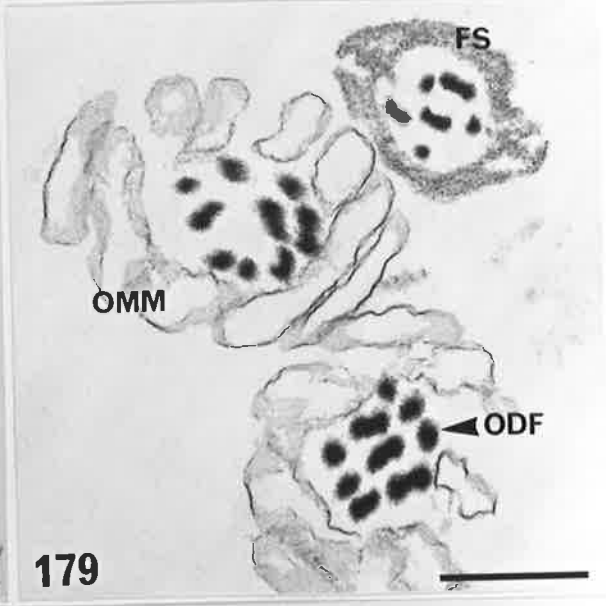
FS
OMM
ODF
179

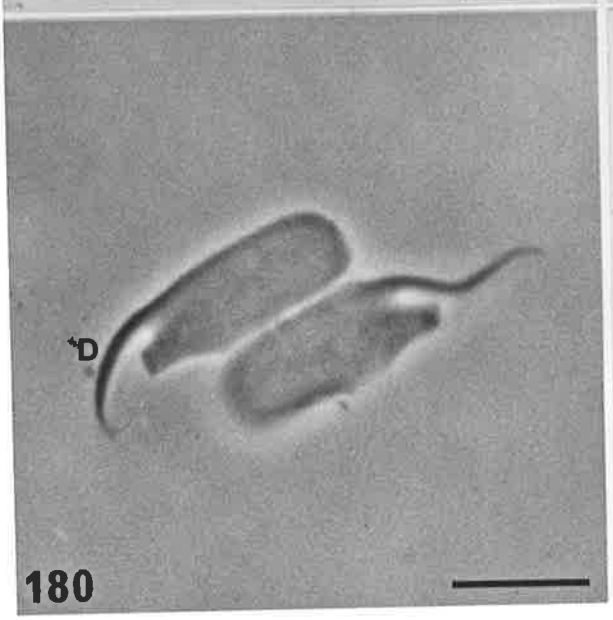
D
180

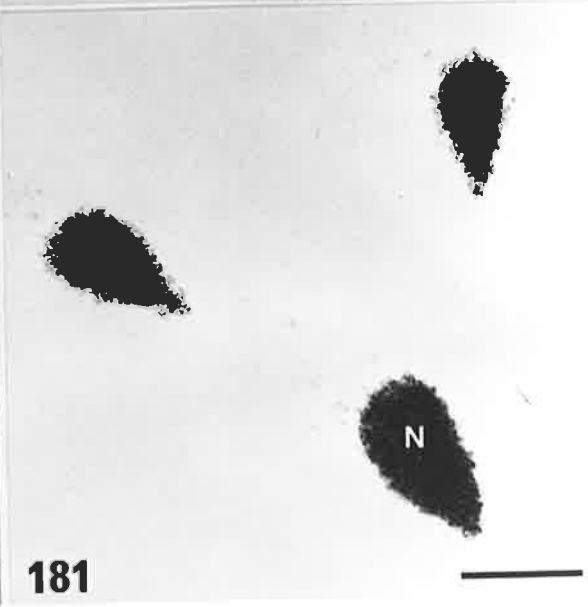
N
181

PLATE 37

Figs. 182,183. Treatment of sperm heads and tails with SDS and DTT for 10-20 minutes.

Fig. 182. The nucleus (N) is partially decondensed, and represents the only remaining sperm head structure.
Bar = 0.5 µm. x 33,950

Fig. 183. The fibrous sheath (FS) has been partially solubilized, the outer mitochondrial membrane is absent, but the dense fibres (ODF) are intact, although the cortical zone is wispy. The connecting piece (CP) is unaffected.
Bar = 0.5 µm. x 35,660

Fig. 184-187. Treatment of sperm heads and tails with sarkosyl and DIT for 20-30 minutes.

Fig. 184. Phase contrast micrograph showing that the nucleus has decondensed, leaving intact the ventral hooks (V) and pseudoperforatorium (Pp). Several prongs extend caudally from these structures (arrows).
Bar = 5 µm. x 2,190

Fig. 185. The core and peripheral layers of the ventral hooks (V), and the sub-acrosomal material in the dorsal hook (D) appears to be unaffected. Chromatin fibrils adhere to the hooks (arrow).
Bar = 0.2 µm. x 42,720

Fig. 186. The mitochondrial sheath in the middle piece has been extracted, and the dense fibres (ODF) tend to splay out. The connecting piece (CP) is intact.
Bar = 10 µm. x 970

Fig. 187. The dense fibres (ODF) and fibrous sheath remain largely intact.
Bar = 0.2 µm. x 58,200

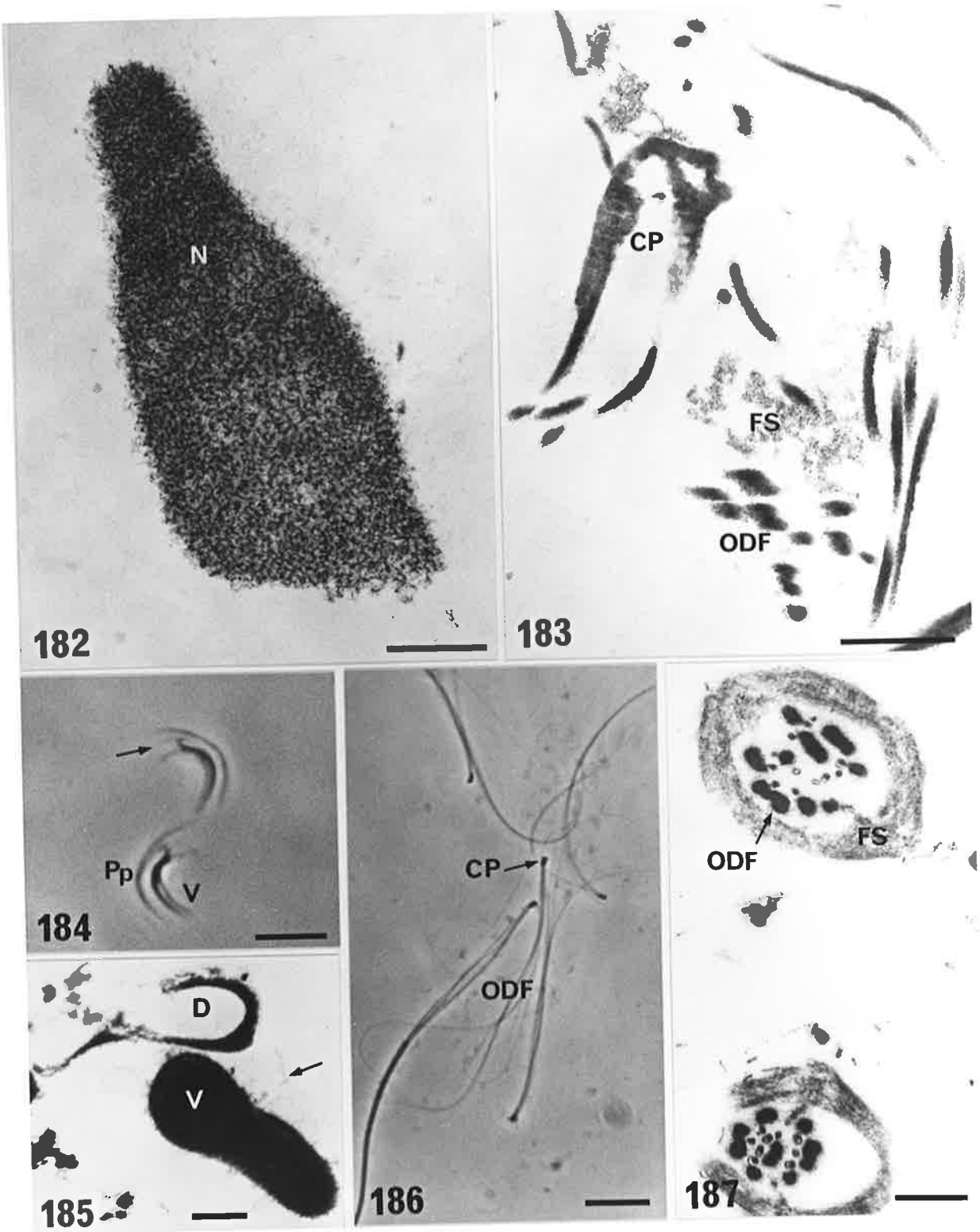
N
182
CP
FS
ODF
183
Pp
V
184
D
V
185
CP
ODF
186
ODF
FS
187

PLATE 38

Figs. 188-190. Electrophoretic analysis of proteins solubilized from sperm heads (H), tails (T) or intact sperm (I). Other lanes contain molecular weight markers (M) and rabbit skeletal muscle actin (A).

Fig. 188. Extraction with SDS (lanes 2-4) or SDS and DTT (lanes 6-8) after pretreatment with SB_{16}. In the head fraction (H), the three major polypeptide bands are at 14-16 (S_1), 41-42 (S_2) and 44 (S_3) kd. Minor bands which are not present in the tail fraction occur at 12.5 (S_4), 46 (S_5), 86.5 (S_6) and 90 (S_7) kd. The majority of bands in the intact sperm fractions (I) also occur in the tail fractions (T). The predominant tail bands are at 19,25,29,31,32,34,48,52 and 66 kd (lanes 3,7).

Fig. 189. Sarkosyl and DTT. Loading of gels with low amounts of extracted protein reveals that the major band (S_1) in the head fraction (H) has a molecular weight of 15 kd.

Fig. 190. Extraction of proteins with either SDS (lanes 2-4) or SDS and DTT (lanes 6-8) after preincubation in SB_{16}, or sarkosyl and DTT (lanes 10-12). The same three major bands (15,42 and 44 kd) and four minor bands (12.5,46,86.5 and 90 kd) occur in each head fraction. S_6 and S_7 are not apparent in the SDS and DTT fraction (lane 6) (See Fig. 188 - lane 6).

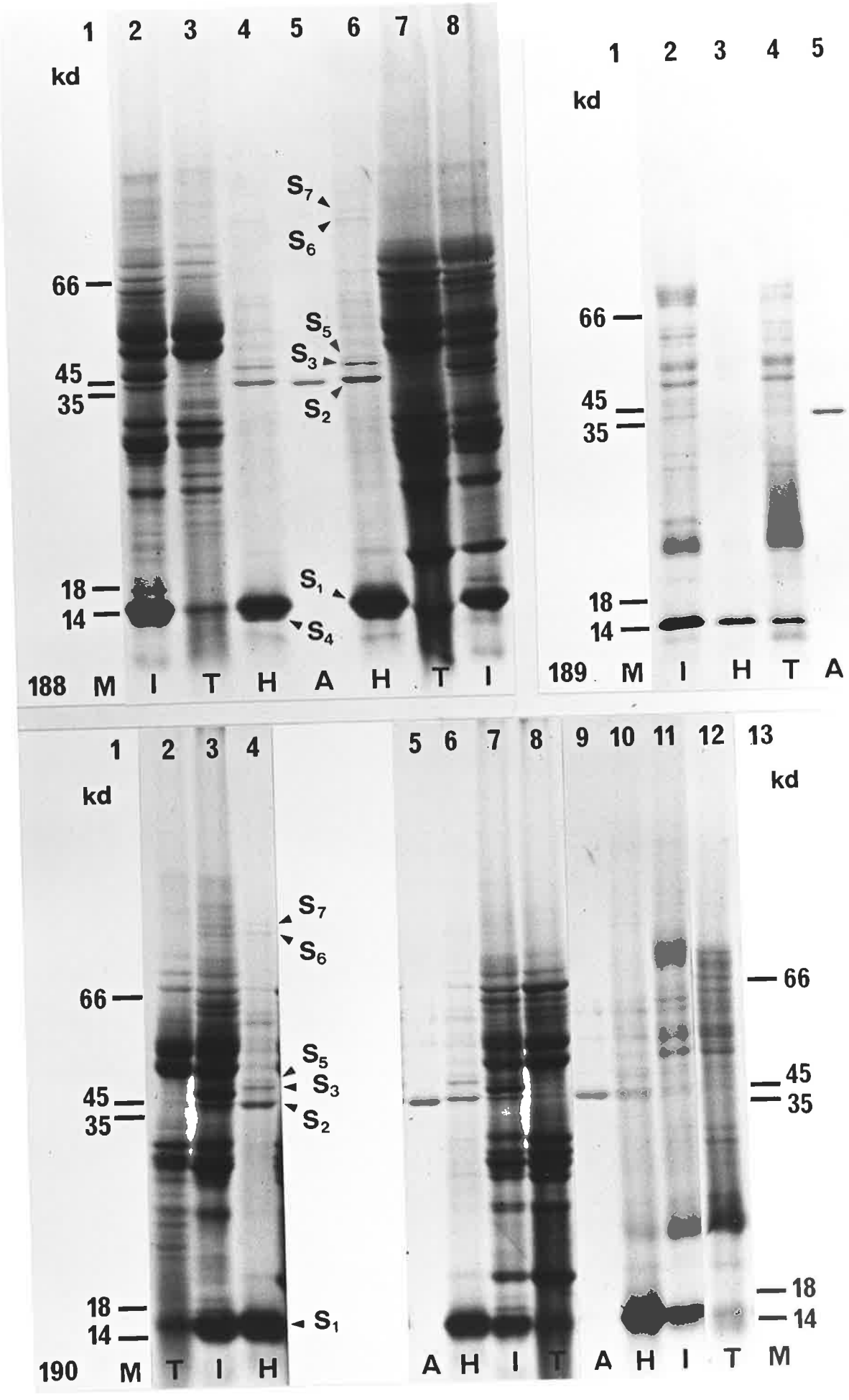
1 2 3 4 5 6 7 8
kd
66
45
35
18
14
S7
S6
S5
S3
S2
S1
S4
188 M I T H A H T I
1 2 3 4 5
kd
66
45
35
18
14
189 M I H T A
1 2 3 4
kd
66
45
35
18
14
S7
S6
S5
S3
S2
S1
190 M T I H
5 6 7 8 9 10 11 12 13
kd
66
45
35
18
14
A H I T A H I T M

PLATE 39

Fig. 191. The epididymis has been divided into seven segments. These include the proximal caput (P.CT), distal caput (D.CT), proximal corpus (P.CT), mid corpus (M.CP), distal corpus (D.CP), proximal cauda (P.CD), and distal cauda (D.CD). The proximal end of the vas deferens (V) is also shown (arrow). Bar = 2 mm x 6.2

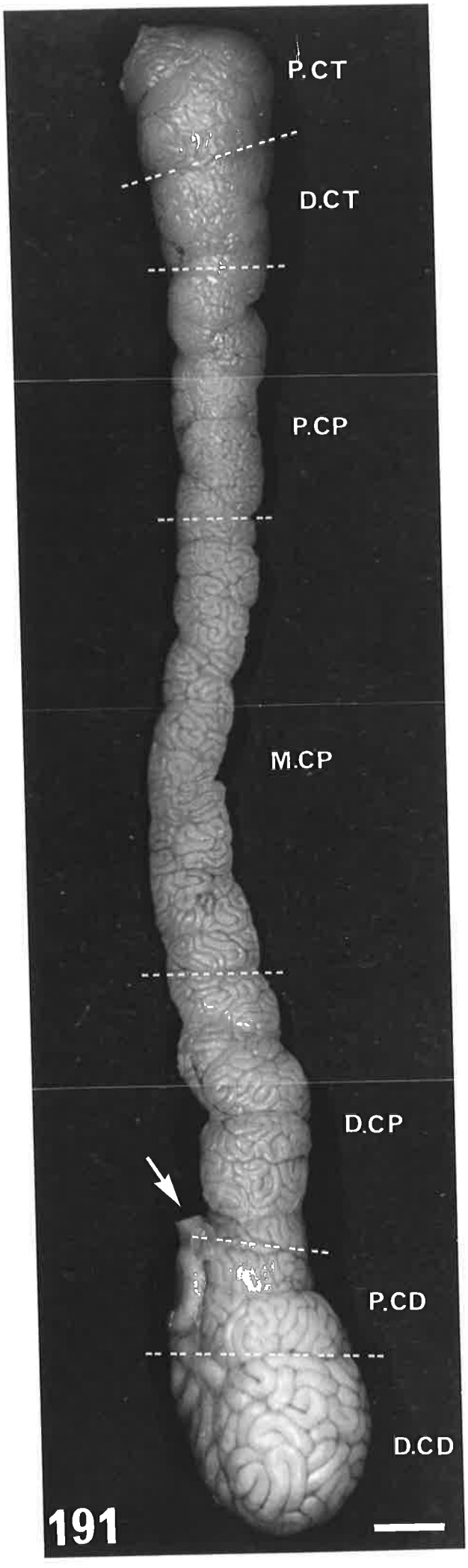
P.CT
D.CT
P.CP
M.CP
D.CP
P.CD
D.CD
191

PLATE 40

Figs. 192-198. Phase contrast micrographs of spermatozoa from the testis and different segments of the epididymis. The three hooks are closely apposed. The distal border of the middle piece is marked (--).
Bar = 20 µm. x 880

Figs. 192,193. Testis. The cytoplasmic droplet (CPD) is usually located in the neck region, but occurs in the proximal third of the middle piece in some sperm (arrows).

Fig. 194. Proximal caput. The CPD is often situated in the middle third of the middle piece (arrow).

Figs. 195,196. Distal caput. The CPD is located in either the middle or distal third of the middle piece, and the tail is bent sharply at that point (arrows).

Fig. 197. Proximal corpus. The droplet is predominantly located in the distal third of the middle piece (arrow).

Fig. 198. Distal cauda. In about 23-28% of sperm, the CPD has been shed.

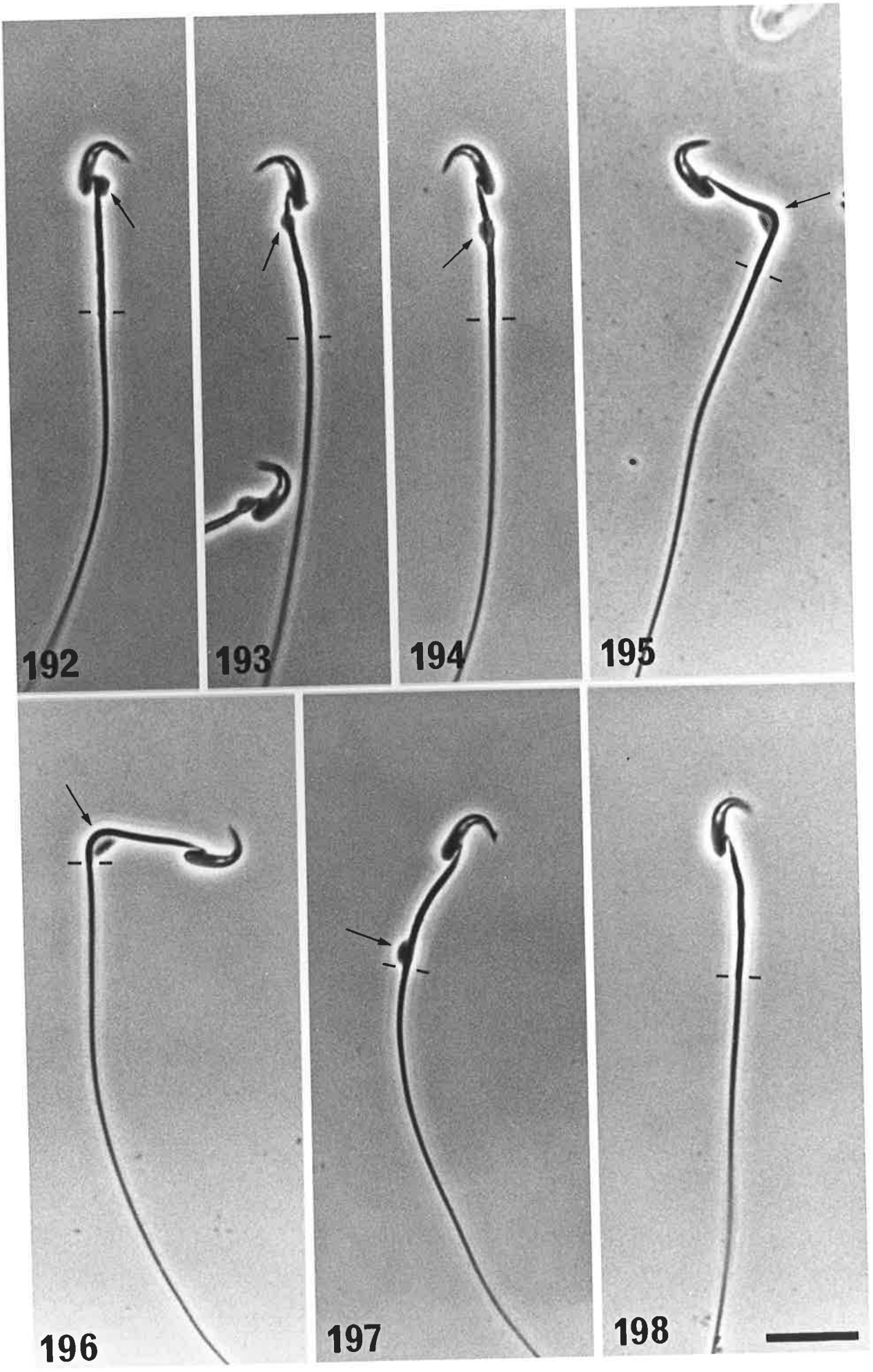
192
193
194
195
196
197
198

PLATE 41

Fig. 199. Proximal caput. The plasma membrane (PM) is closely applied to the acrosome, and is only slightly ruffled over the equatorial segment (ES). The apical segment (AS) projects from the dorsal margin as a narrow ridge. Electron-dense material is present in the peri-acrosomal space (arrows).
Bar = 0.5 µm. x 51,300

Fig. 200. Proximal caput. In the equatorial segment, a dense band of material lies in close proximity to the inner and outer acrosomal membranes, giving them a pentalaminar appearance (arrows).
Bar = 0.1 µm. x 146,840

Fig. 201. Distal caput. The plasma membrane (PM) is smooth and closely associated with the acrosome. The size of the apical segment (AS) has become considerably reduced.
Bar = 0.5 µm. x 51,300

Fig. 202. Distal caput. Higher magnification of the dorsal margin of the sperm head shown in Fig. 201. There is an accumulation of sub-acrosomal material (SAM), and less electron-dense zones near the outer acrosomal membrane in the principal segment (arrows).
Bar = 0.1 µm. x 146,840

Fig. 203. Distal caput. Higher magnification of the equatorial segment, showing the pentalaminar appearance of the acrosomal membranes (arrows).
Bar = 0.5 µm. x 223,100

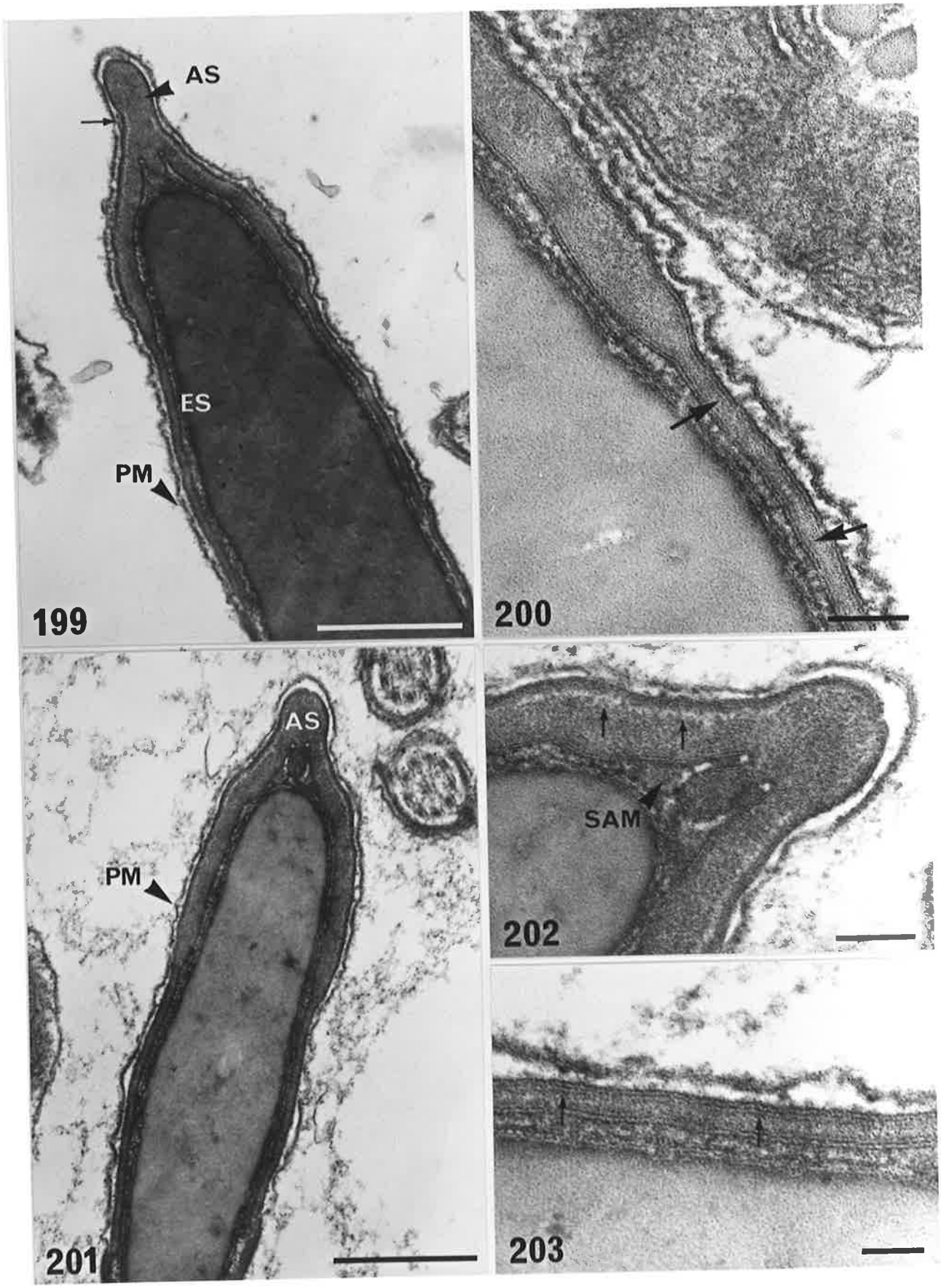
AS
ES
PM
199
200
AS
PM
201
SAM
202
203

PLATE 42

Fig. 204. Proximal corpus. The projections (Pr) to the plasma membrane in the ventral hooks are readily visualized.
Bar = 0.1 µm. x 240,230

Fig. 205. Mid corpus. The apical segment of the acrosome (Ac) is virtually non-existent. The plasma membrane (PM) has become more ruffled in the equatorial segment.
Bar = 0.5 µm. x 39,740

Fig. 206. Mid corpus. Higher magnification of the dorsal margin of the sperm head. There is little or no electron-dense material in the peri-acrosomal space (arrows), and the heterogeneous zones in the acrosome are less evident (arrowheads).
Bar = 0.2 µm. x 99,030

Fig. 207. Distal corpus. Transverse section of the ventral hooks, showing that the projections (Pr) are difficult to visualize.
Bar = 0.1 µm. x 160,680

Fig. 208. Distal cauda. The plasma membrane (PM) is smooth in contour, and closely applied to the principal segment of the acrosome, but is ruffled over the equatorial segment (ES).
Bar = 0.5 µm. x 58,860

Fig. 209. Distal cauda. Variable glycocalyx material (VGM) is attached to the ventral surface of the dorsal hook, but doesn't bind to the ventral hooks (V). It contains areas of increased density (arrows) and small electron-dense granules (arrowheads). Tubular structures (TS) are found in the dorsal hook concavity.
Bar = 0.5 µm. x 48,600

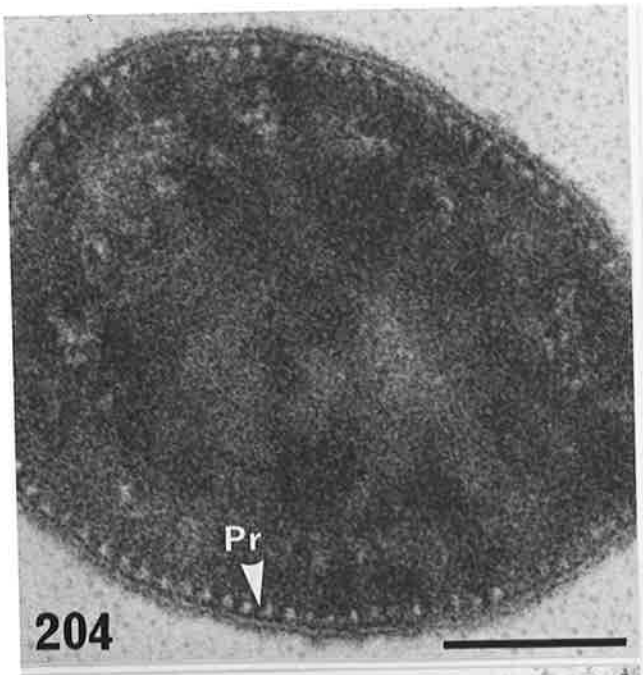
Pr
204

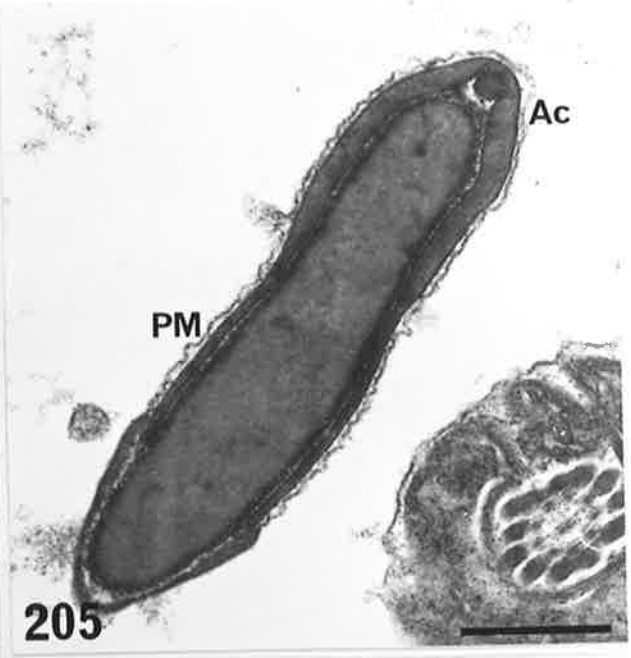
Ac
PM
205

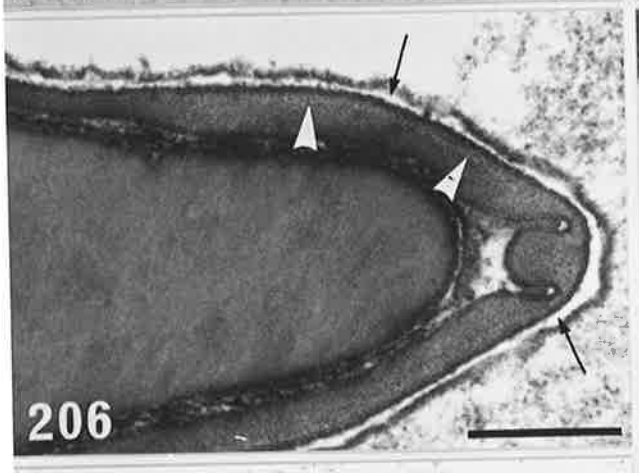
206

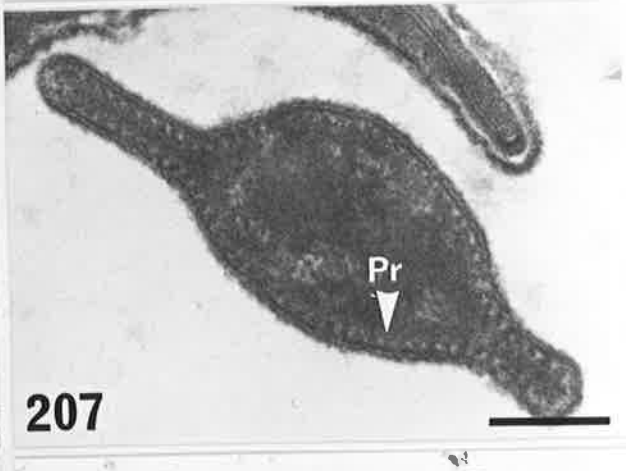
Pr
207

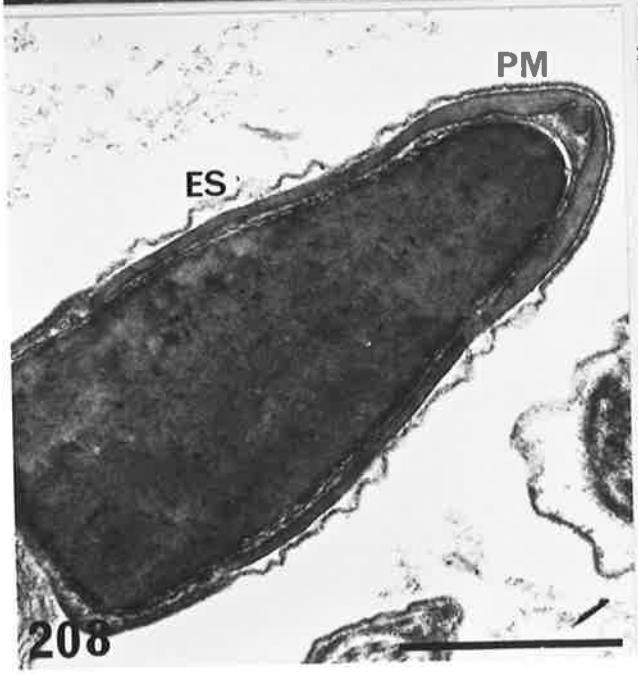
PM
ES
208

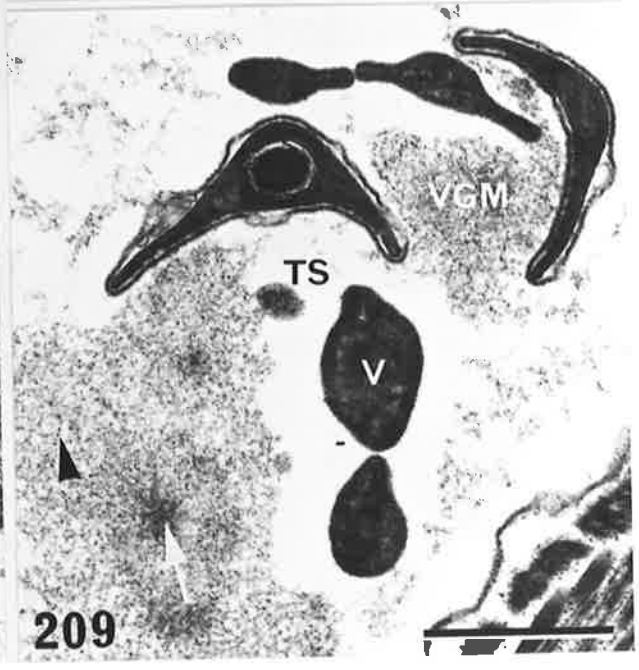
VGM
TS
V
209

PLATE 43

Figs. 210,211. Phase contrast micrographs of plains mouse cumulus clots. Oocytes (O) are distributed throughout the clots.
Bar = 0.5 mm. x 56

Fig. 212. Thick plastic section stained with toluidine blue. The cumulus cells are evenly distributed throughout the complex. Areas of increased cell density (asterisk), and clusters of cumulus cells (arrowhead) are also apparent.
Bar = 100 µm. x 180

Fig. 213. Thick plastic section stained with toluidine blue. A distinct corona radiata is not evident.
Bar = 50 µm. x 365

Fig. 214. Phase contrast micrograph of a cumulus-free plains mouse oocyte. The zona pellucida (ZP) is about 6 µm thick, and separated from the vitellus (Vi) by a narrow perivitelline space (PVS). The second meiotic spindle (Sp) is shown.
Bar = 50 µm. x 365

Figs. 215,216. Phase contrast micrographs of oocytes stained with lacmoid. The zona pellucida has been solubilized during staining. In most oocytes, the spindle (Sp) is situated in a slightly expanded region, which is devoid of organelles. The chromosomes are regularly arranged (Fig. 215). In some oocytes, the chromosomes tend to be spread out and the spindle is disorganized (Fig. 216).
Bar = 50 µm. x 365

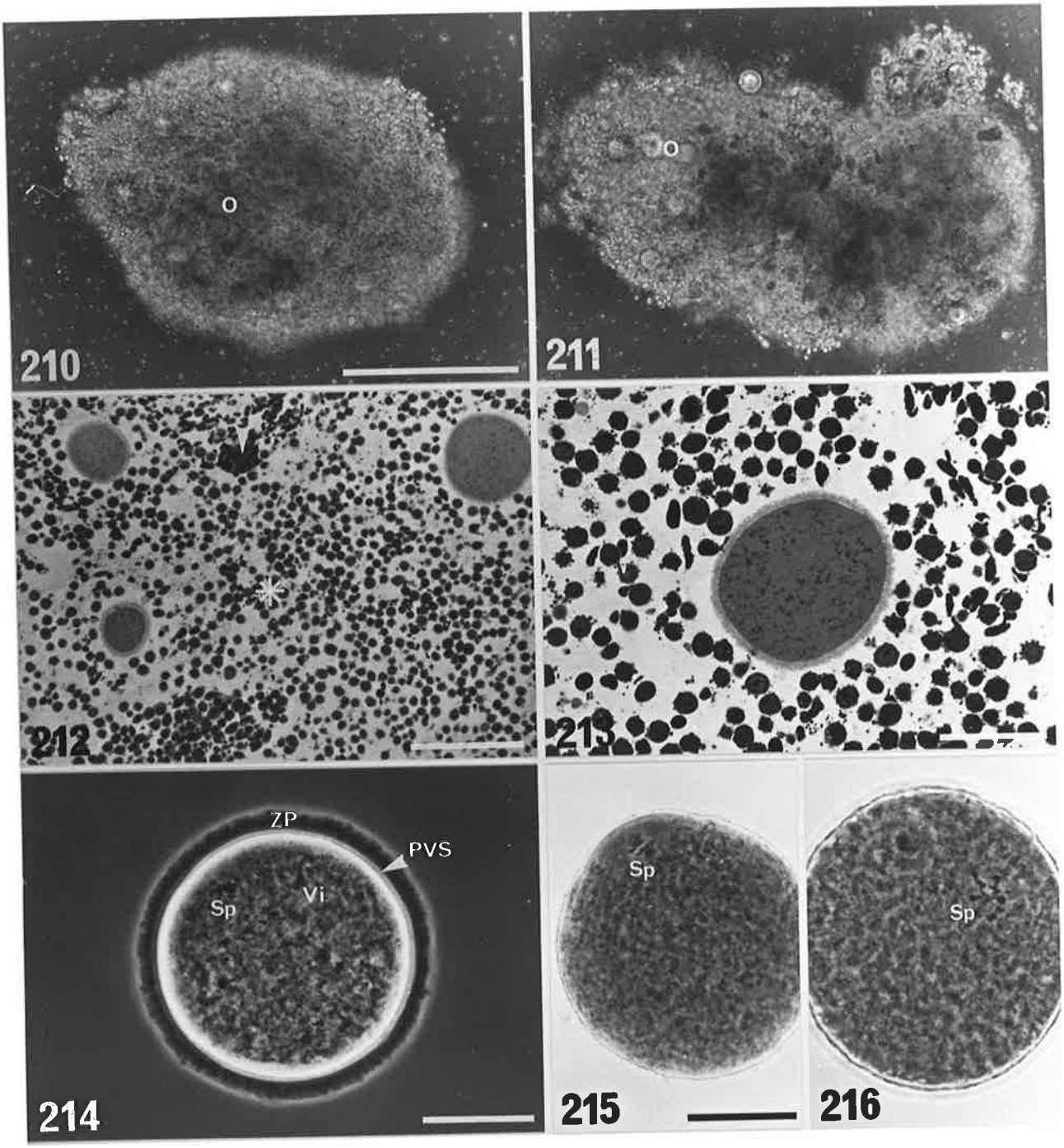
O
210
O
211
212
213
ZP
PVS
Vi
Sp
214
Sp
215
Sp
216

PLATE 44

Figs. 217,218. Mitochondria (Mc) often occur in stacked arrays or clusters throughout the vitellus. They have transverse cristae, and an electron-dense matrix. Cisternae of smooth endoplasmic reticulum (SER) are abundant, and contain flocculent material (Fig. 217). Mitochondria (Mc) often occur in close proximity to Golgi complexes (G) (Fig. 218).
Bar = 1 µm. x 23,120

Fig. 219. Golgi complexes (G) occur in the cortex of the oocyte, in association with mitochondria (Mc), and amorphous structures (Am). Cortical granules (CG) are also shown.
Bar = 5 µm. x 6,790

Fig. 220. Higher magnification of the amorphous structures, revealing a membranous or periodic substructure (arrow).
Bar = 1 µm. x 23,120

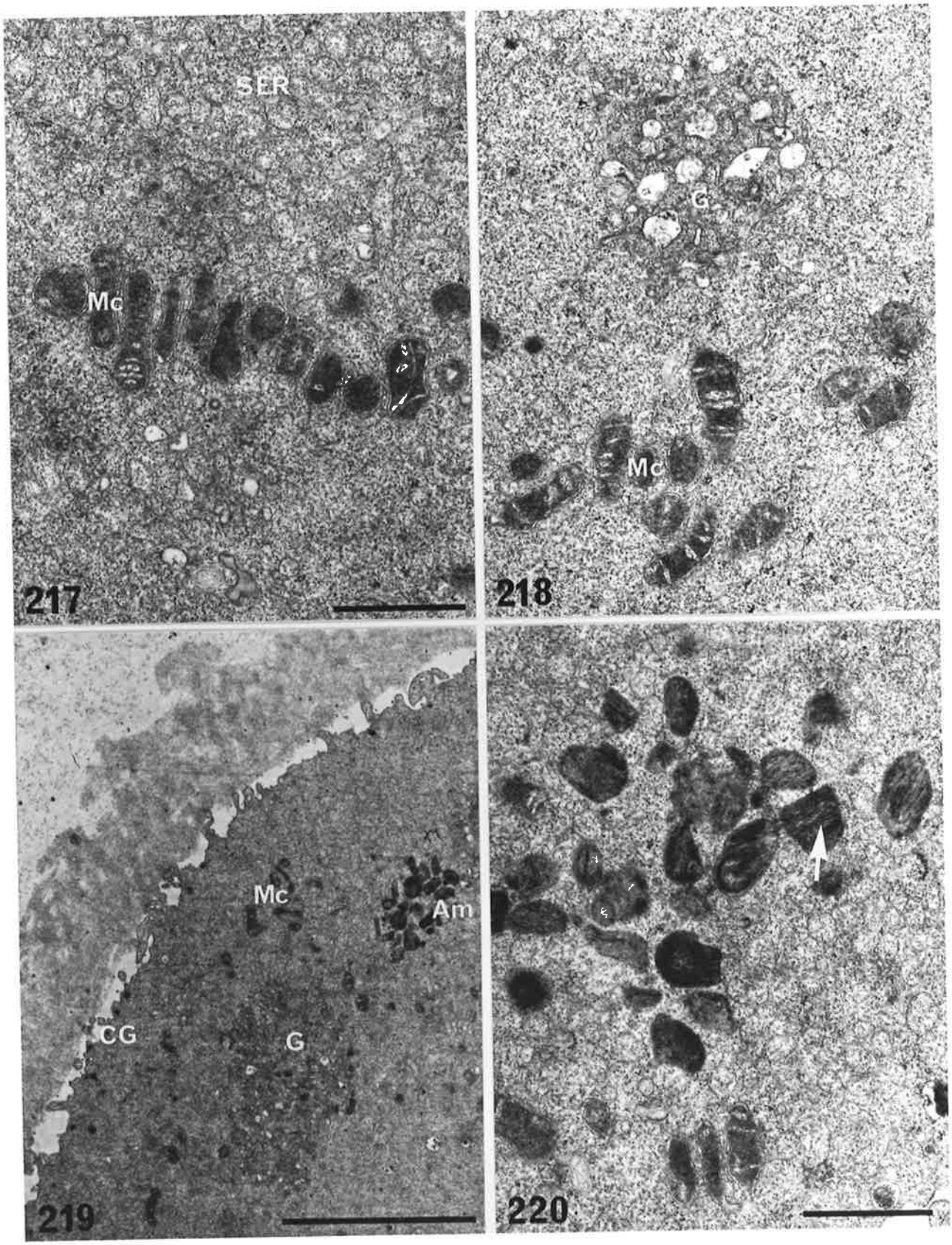
SER
Mc
217
G
Mc
218
Mc
Am
CG
G
219
220

PLATE 45

Figs. 221-225. Cortical Granules.

Figs. 221,222. Cortical granules (CG) are located close to the oolemma. They occur as a monolayer (Fig. 221) or in small clusters (Fig. 222). The number of microvilli (Mv) is variable. The fibrous nature of the zona pellucida (ZP) is also shown.
Bar = 1 µm. x 23,450

Fig. 223. Two types of cortical granules are present, dense (DG) and granular (GG). Both are surrounded by a unit membrane. The dense type (DG) has a homogeneous, electron-dense core, whilst the granular type (GG) are larger, and have a granular core.
Bar = 0.5 µm. x 50,490

Figs. 224,225. The contents of cortical granules, and even intact ones, are sometimes present in the peri-vitelline space (Fig. 224, arrow), or observed in the process of discharging their contents into the space (Fig. 225, arrow).
Bar = 1 µm. x 23,450 (224)
0.5 µm. x 50,490 (225)

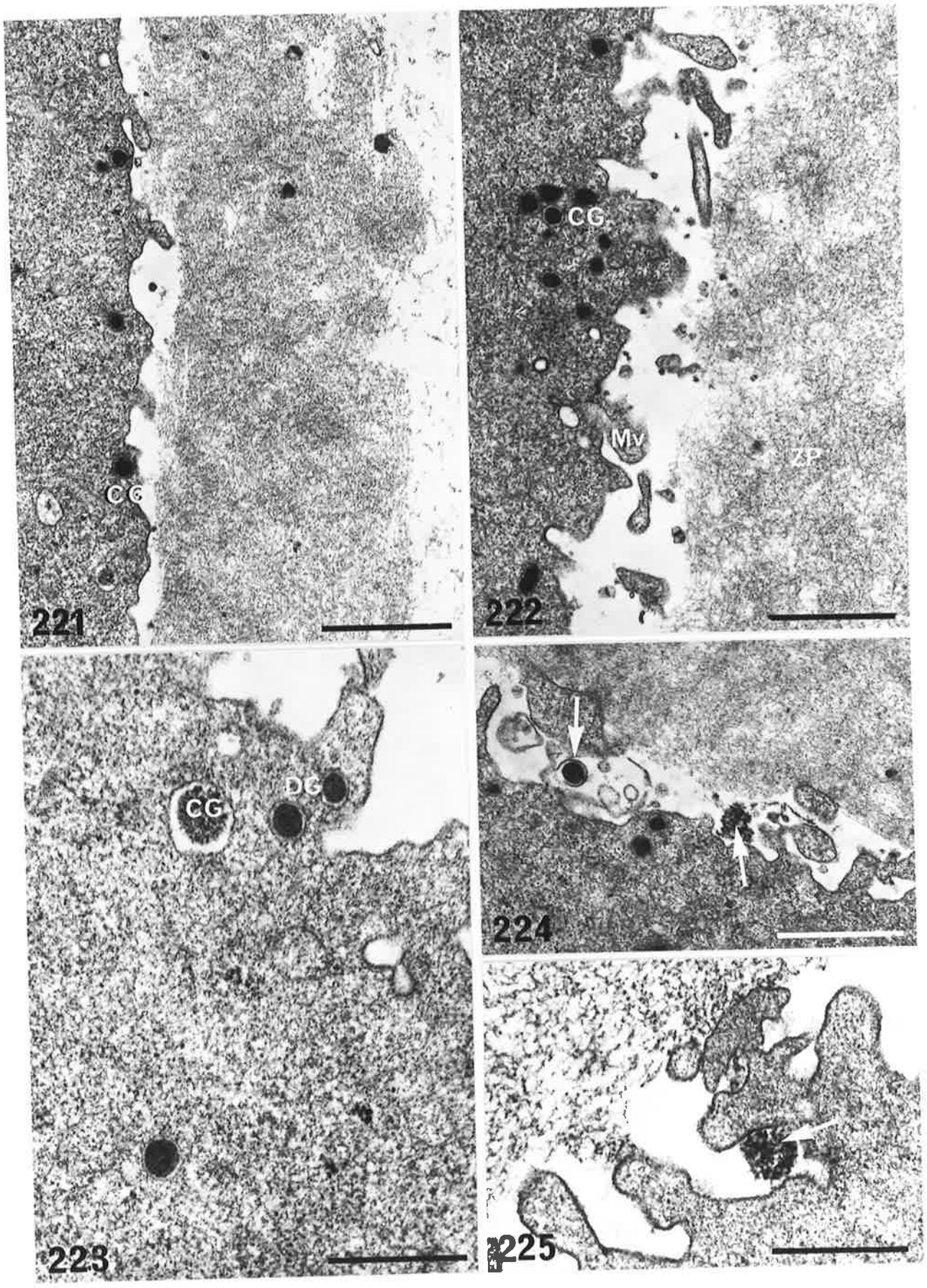
CG
221
CG
Mv
ZP
222
CG
DG
223
224
225

PLATE 46

Figs. 226-232. Peri-vitelline space and polar body.

Fig. 226. The peri-vitelline space contains numerous microvilli (Mv) and membranous elements, some of which appear to bud off from the vitellus (arrows).
Bar = 2 µm. x 7,755

Fig. 227. Double membrane structures sometimes occupy the peri-vitelline space (arrow). Dense cortical granules (DG) are also shown adjacent to the oolemma.
Bar = 0.5 µm. x 23,220

Fig. 228. Small granules are found in the PVS (arrow). They are often enclosed in a vesicle.
Bar = 0.2 µm. x 49,510

Fig. 229. The peri-vitelline granules stain strongly with ruthenium red.
Bar = 0.5 µm. x 39,760

Fig. 230. Phase contrast micrograph showing the first polar body (PB).
Bar = 50 µm. x 446

Fig. 231. The polar body is large and roughly ovoid in shape. The chromosomes are distributed randomly (arrow).
Bar = 20 µm. x 780

Fig. 232. The polar body sometimes breaks down, and appears as a mass of membranous elements, which are ruthenium red-positive.
Bar = 2 µm. x 7,240

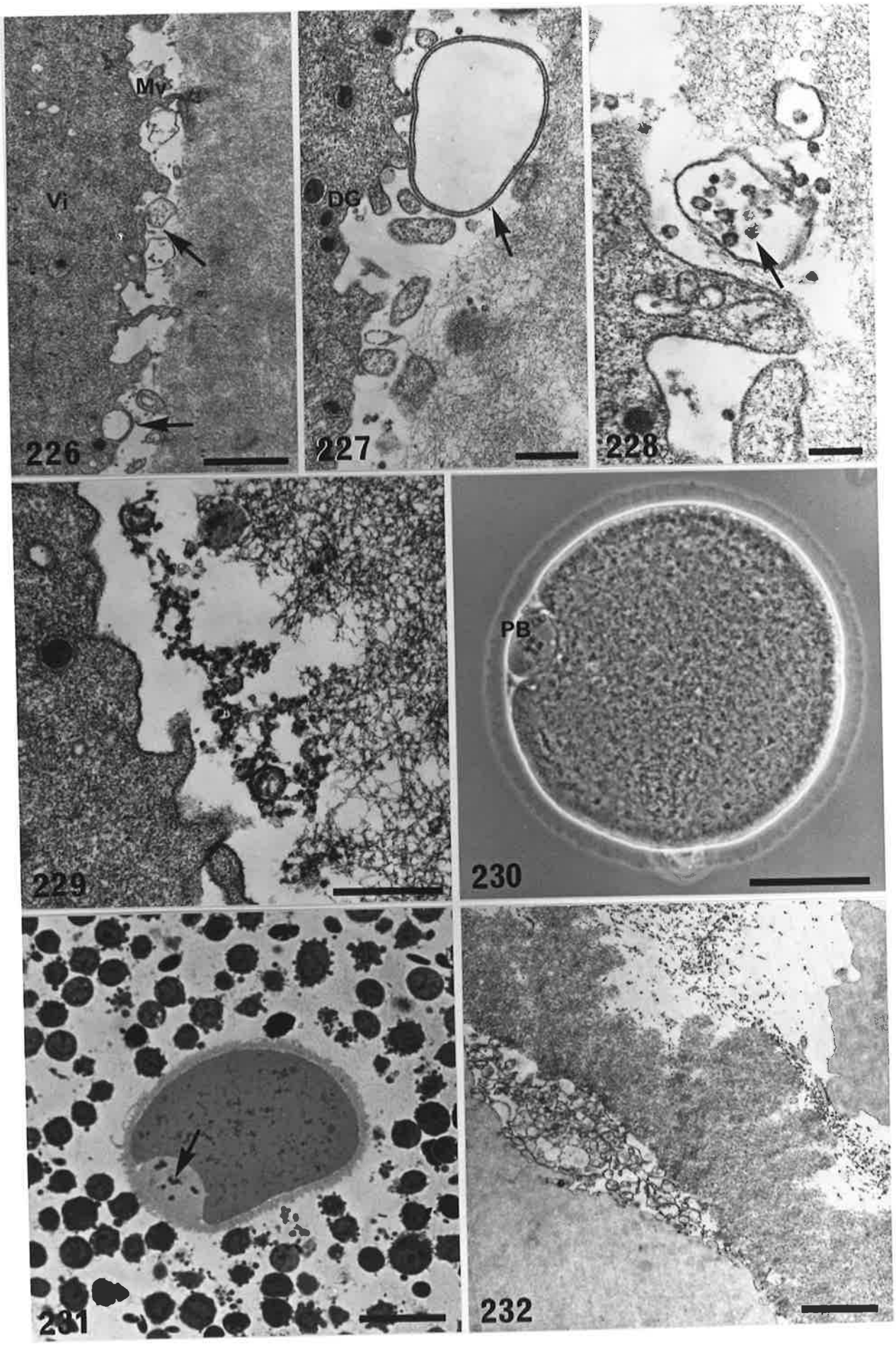
Mv
Vi
226
DG
227
228
229
PB
230
231
232

PLATE 47

Figs. 233-239. Structure of the zona pellucida.

Fig. 233. Scanning electron micrograph showing the porous nature of the outer surface of the zona pellucida.
Bar = 10 µm. x 1,790

Fig. 234. Higher magnification of the area shown in Fig. 232. The zona consists of concentrically arranged pores (Po), bordered by fibrous elements.
Bar = 2 µm. x 4,900

Fig. 235. There is no gradient in the density of the zona substance from the inner to outer surfaces, although the outer surface contains numerous pores (Po), which are less obvious on the inner surface.
Ruthenium Red. Bar = 1 µm. x 18,630

Fig. 236. Oblique section of the zona pellucida, showing its fibrous sub-structure.
Bar = 0.2 µm. x 56,260

Fig. 237. After staining with ruthenium red, the zona consists of an interlocking meshwork of 8 nm diameter fibrils.
Bar = 0.1 µm. x 144,000

Fig. 238. Oblique section through the porous outer zone. Bands of circumferentially oriented fibrils encircle each pore (Po).
Bar = 1 µm. x 24,100

Fig. 239. Peri-vitelline granules (arrow), and possible cortical granules (CG) are also found within the zona.
Bar = 1 µm. x 19,550


233

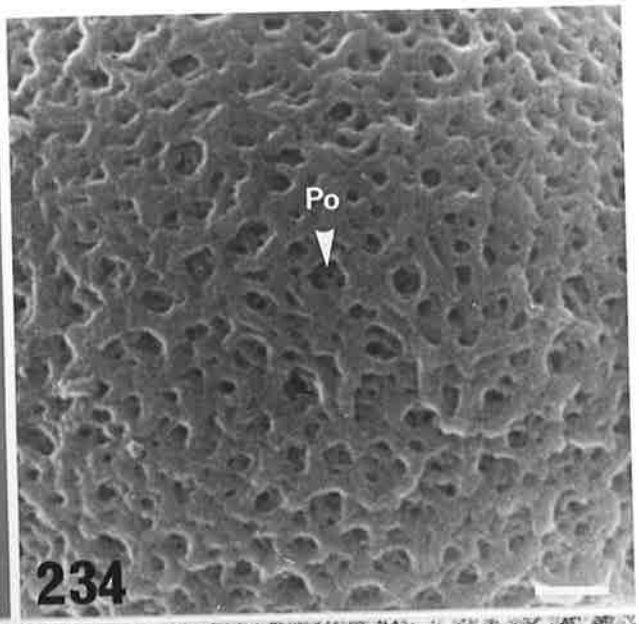
Po
234

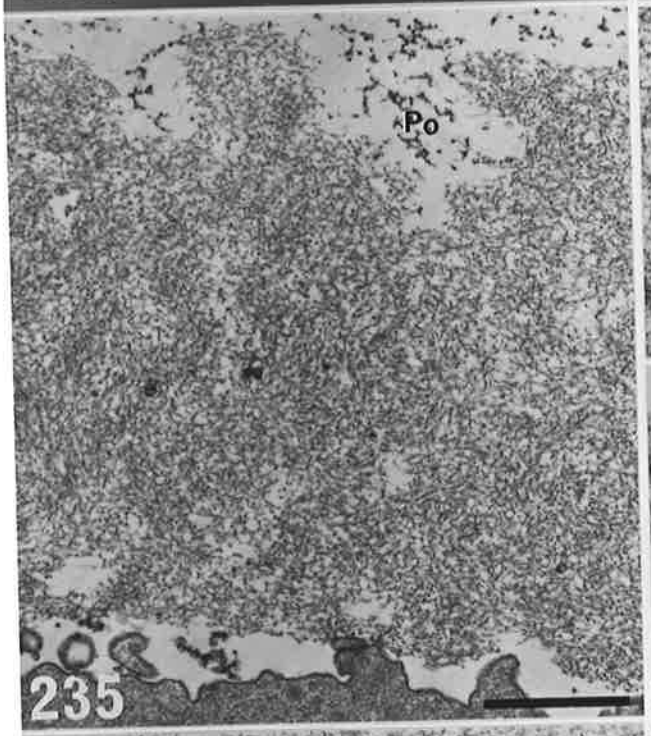
Po
235

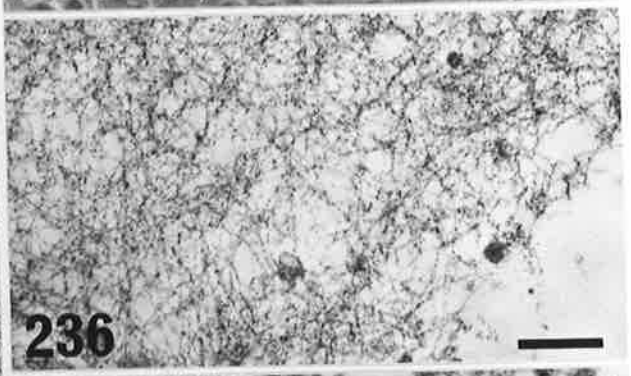
236

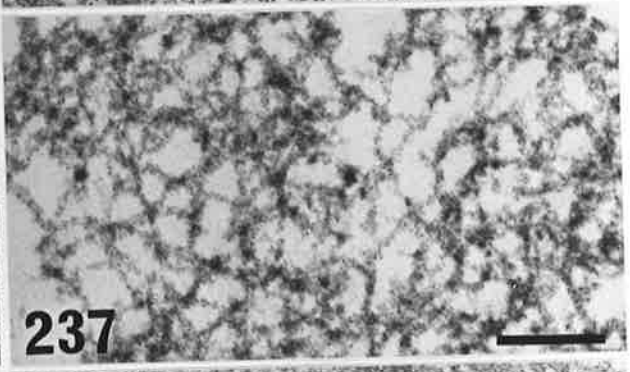
237

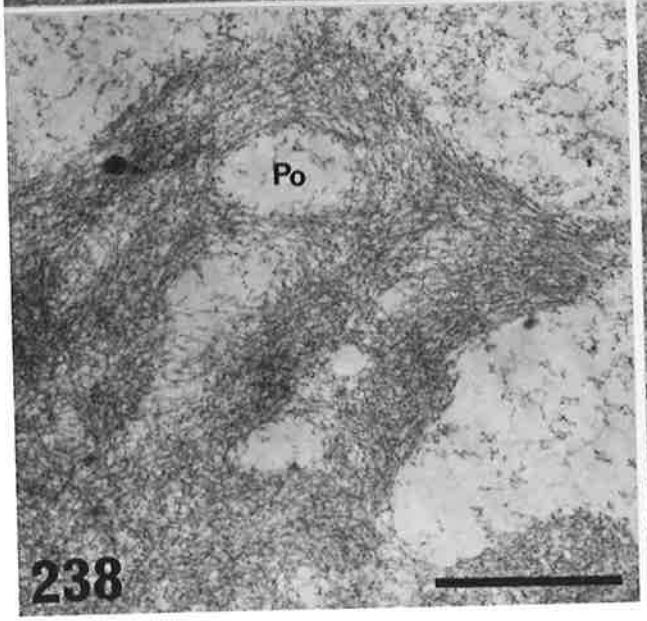
Po
238

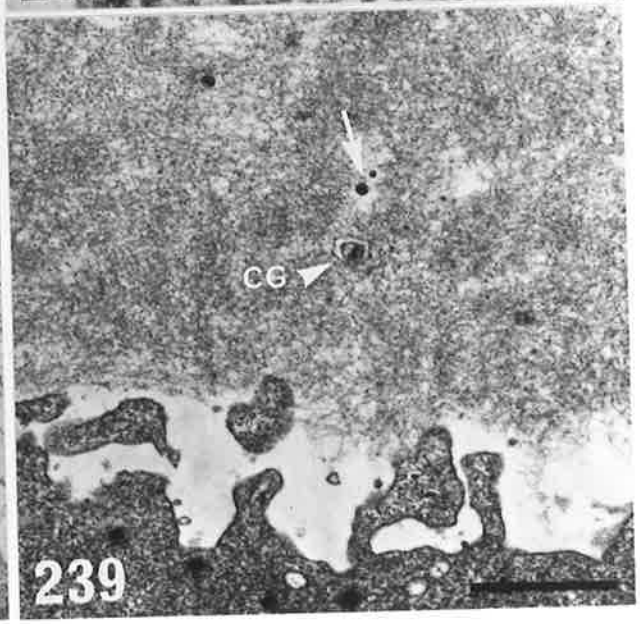
CG
239

PLATE 48

Figs. 240-243. Structure of the cumulus cells.

Fig. 240. Four types of cumulus cells are present in the oocyte-cumulus complex: small, necrotic cells (1), small cells with extensive blebbing (2), large, round cells (3), and large cells with many microvilli (4).
Toluidine blue. Bar = 50 µm. x 570

Fig. 241. Type 2 cumulus cells have many large blebs (Bl) on their surface, which contain various cellular organelles, and are sometimes vacuolated (arrow).
Bar = 2 µm. x 7,060

Figs. 242,243. The organelles present in the cytoplasm of cumulus cells include mitochondria (Mc), rough endoplasmic reticulum (RER), Golgi complexes (G), polyribosomes (Ri), lipid droplets (Li), and membrane whorls (MW).
Bar = 1 µm. x 24,060

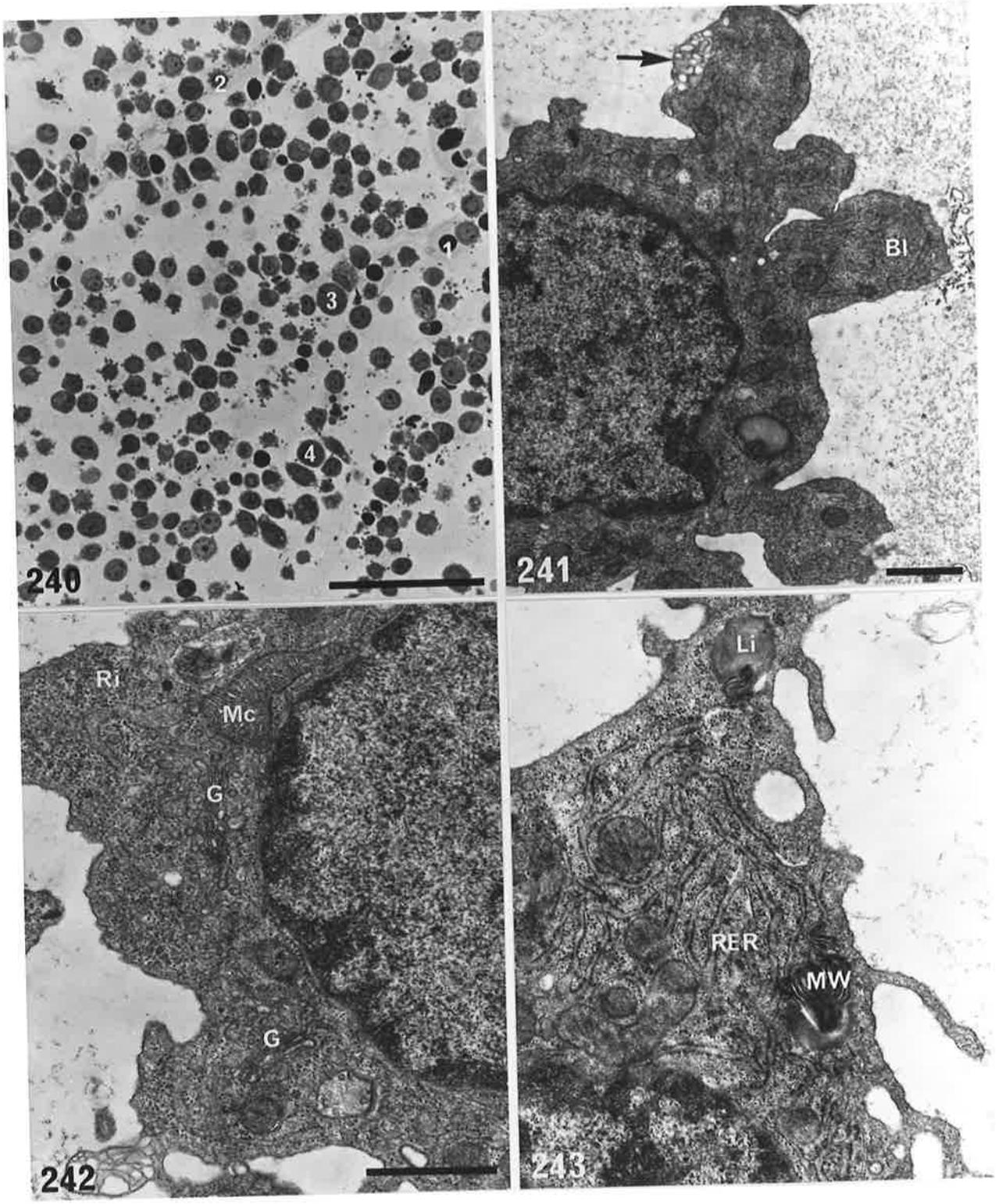
2
3
4
240
Bl
241
Ri
Mc
G
G
242
Li
RER
MW
243

PLATE 49

Figs. 244-246. Oocyte-cumulus complexes fixed in the presence of ruthenium red. Thick plastic sections stained with toluidine blue.
Bar = 50 µm. x 600

Fig. 244. There is usually a homogeneous distribution of the extra-cellular matrix (ECM) around the oocyte (O), but areas of increased density occur near the edge of the complex, and in other regions (arrowheads).

Fig. 245. Homogeneous distribution of the extra-cellular material (ECM).

Fig. 246. In this portion of a complex, there are zones of high density and strands of ECM (arrows).

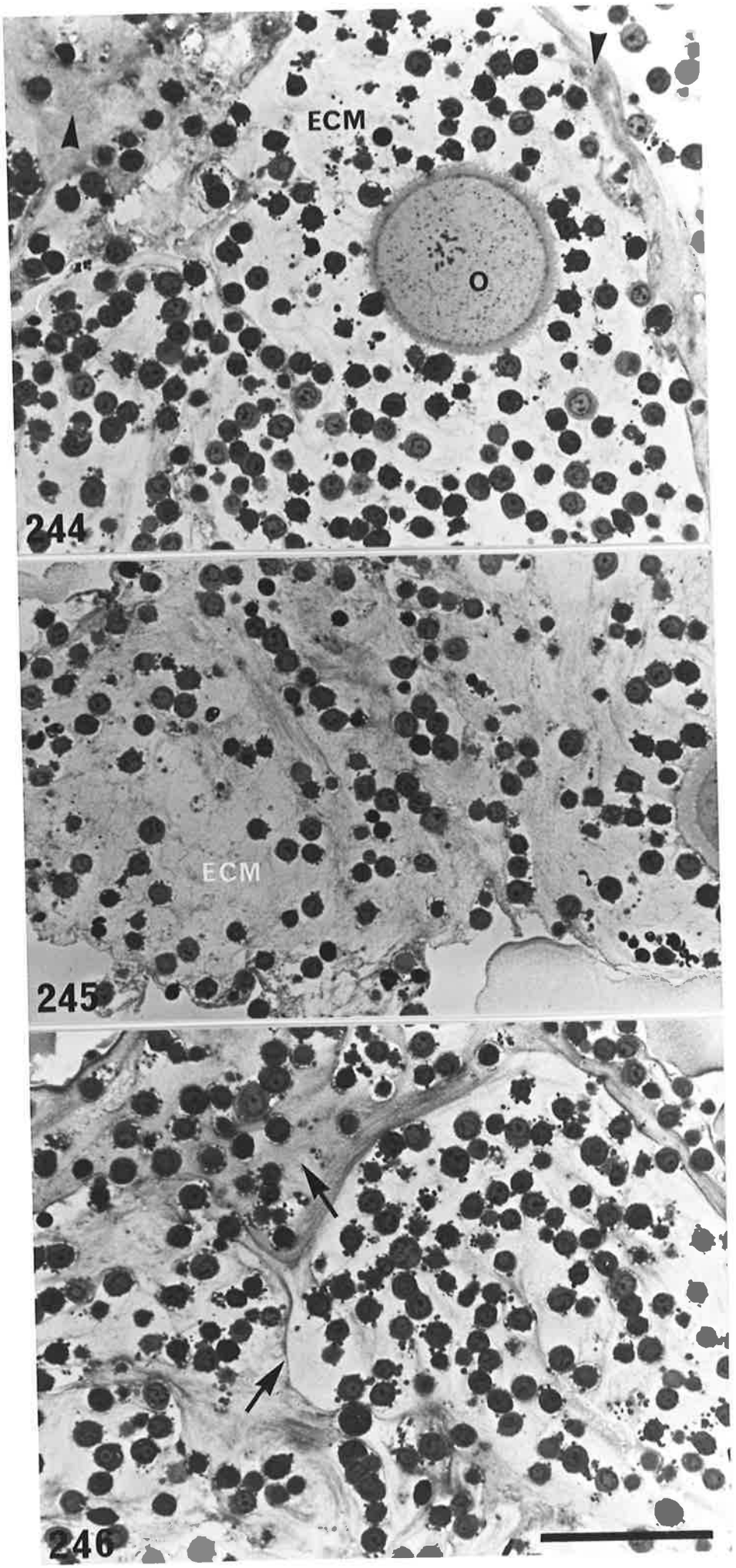
ECM
O
244
ECM
245
246

PLATE 50

Figs. 247-250. Distribution of the ECM granules throughout the oocyte-cumulus complex. Ruthenium red. Unstained sections.

Fig. 247. Dense bands of granules are not usually present on the surface of the zona pellucida (ZP), except near cumulus cells (arrow).
Bar = 5 µm. x 6,040

Fig. 248. A clear space often surrounds cumulus cells (CC). Increased numbers of granules occur between closely apposed cells (arrow).
Bar = 5 µm. x 6,040

Fig. 249. In the outer part of the cumulus oophorus, the distribution and density of the granules is variable. A clear space usually occurs around cumulus cells (CC).
Bar = 10 µm. x 1,930

Fig. 250. The outer edge of the oocyte-cumulus complex consists of a dense band of granules (arrowhead). Strands of granules (Sr) are also frequently found in the outer regions.
Bar = 5 µm. x 6,040

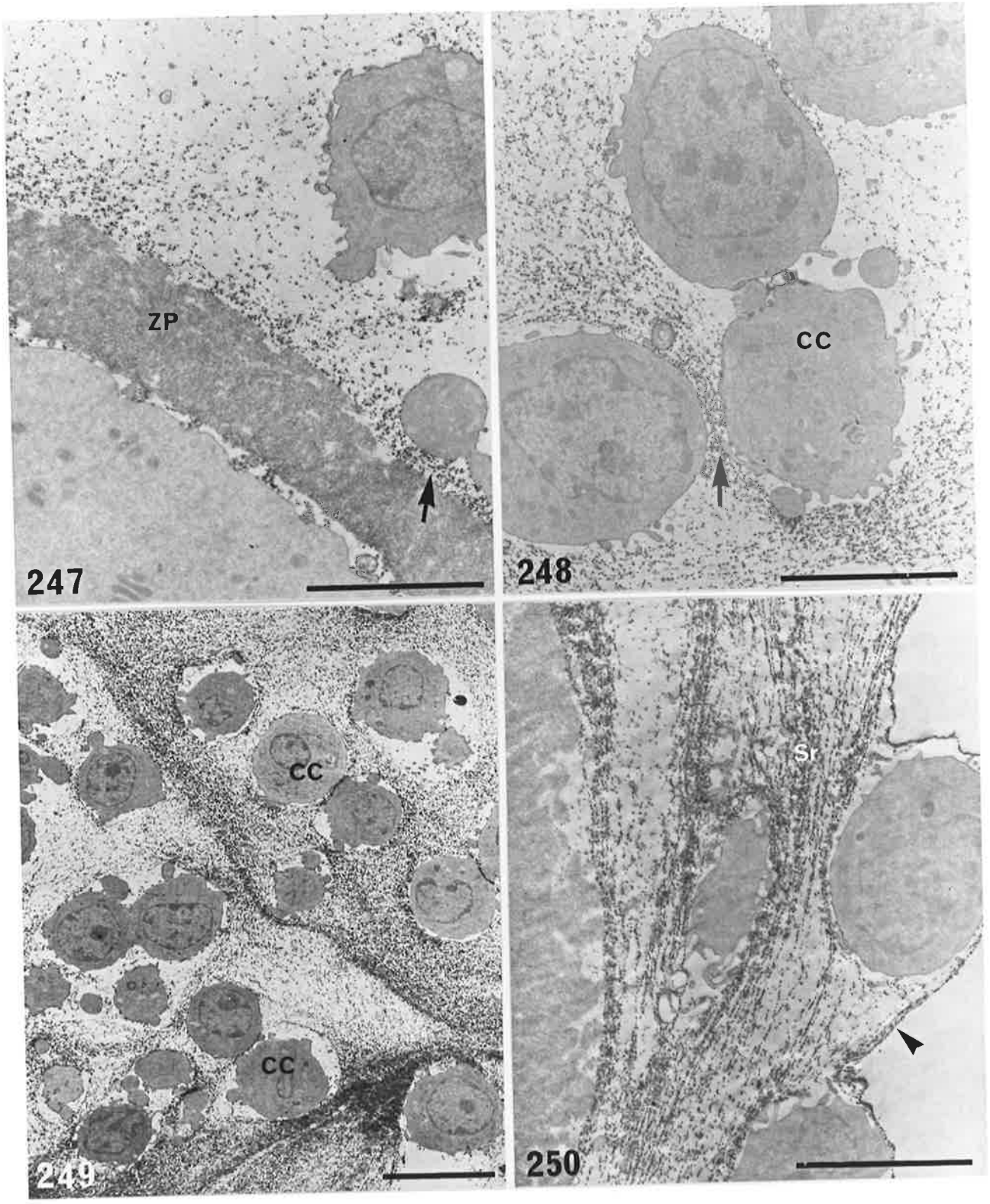
ZP
247
CC
248
CC
CC
249
Sr
250

PLATE 51

Figs. 251-256. Ultrastructure of the ECM. Ruthenium red fixation. Sections unstained (251-253), or stained with uranyl acetate and lead citrate (254-256).

Fig. 251. The cumulus matrix extends into the zona pores (Po). The filaments appear to link with the fibrillar elements of the zona pellucida (arrows).
Bar = 0.5 µm. x 43,970

Figs. 252,253. The extracellular matrix consists of many granules (Gr), cross-linked by fine filaments (F). The granules may occur in strands or aggregates (arrows).
Bar = 0.5 µm. x 43,970 (252)
0.2 µm. x 70,460 (253)

Figs. 254-256. High magnification of the granules and filaments. The granules (Gr) often join end-to-end, and attach to the surface of cummulus cell process (CC). The filaments (F) link individual granules or aggregates, and sometimes branch (arrow).
Bar = 0.1 µm. x 103,460

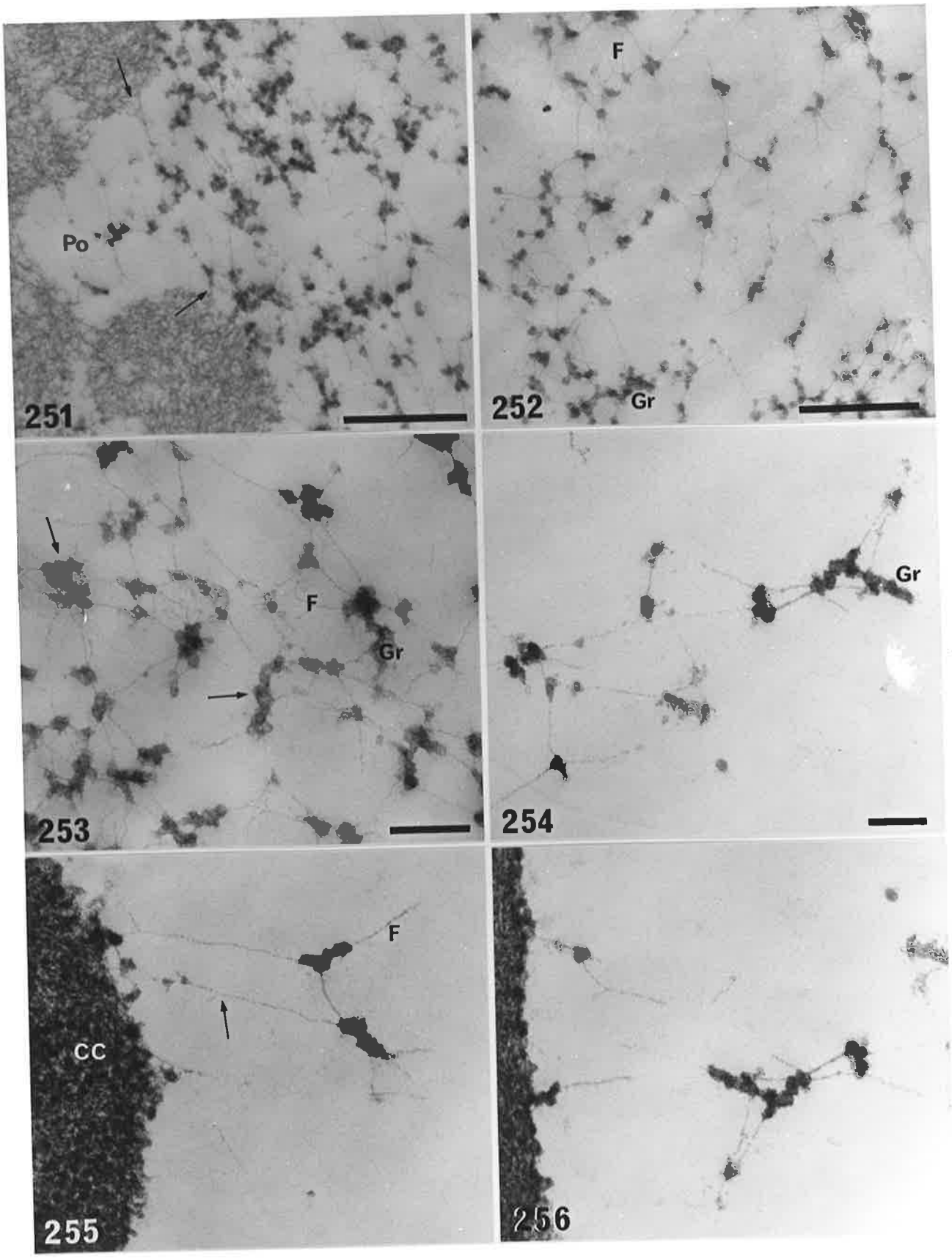
Po
251
F
Gr
252
F
Gr
253
Gr
254
CC
F
255
256

PLATE 52

Fig. 257. Plains mouse oocyte after culture with sperm for 8 hours. A female pronucleus (Pn) has formed, and a second polar body (PB) ejected. No spermatozoon is present in the vitellus.
Lacmoid. Bar = 50 µm. x 530

Fig. 258. Pre-incubated plains mouse sperm bind to zona-free mouse oocytes. The three hooks usually remain close together (arrows).
Lacmoid. Bar = 50 µm. x 530

Fig. 259. Zona-free laboratory mouse oocyte penetrated by laboratory mouse sperm. The two pronuclei (Pn), second polar body (PB) and part of the sperm tail (arrow) are shown.
Lacmoid. Bar = 50 µm. x 530

Fig. 260. Zona-intact laboratory mouse oocyte fertilized in vitro. There are two pronuclei (Pn) a sperm tail (arrow), and the second polar body (PB). The zona pellucida has been removed during staining.
Lacmoid. Bar = 50 µm. x 530

Fig. 261. Zona-free rat oocyte penetrated by plains mouse spermatozoon. The sperm head and middle piece (MP) have been incorporated, and nuclear decondensation has occurred (arrow). The ventral hooks and pseudoperforatorium are intact (arrowhead).
Lacmoid. Bar = 10 µm. x 1,320

Fig. 262. Polyspermic fertilization of a zona-free rat oocyte by rat sperm. Shown are the pronuclei (Pn) and sperm tail (arrow).
Bar = 50 µm. x 530

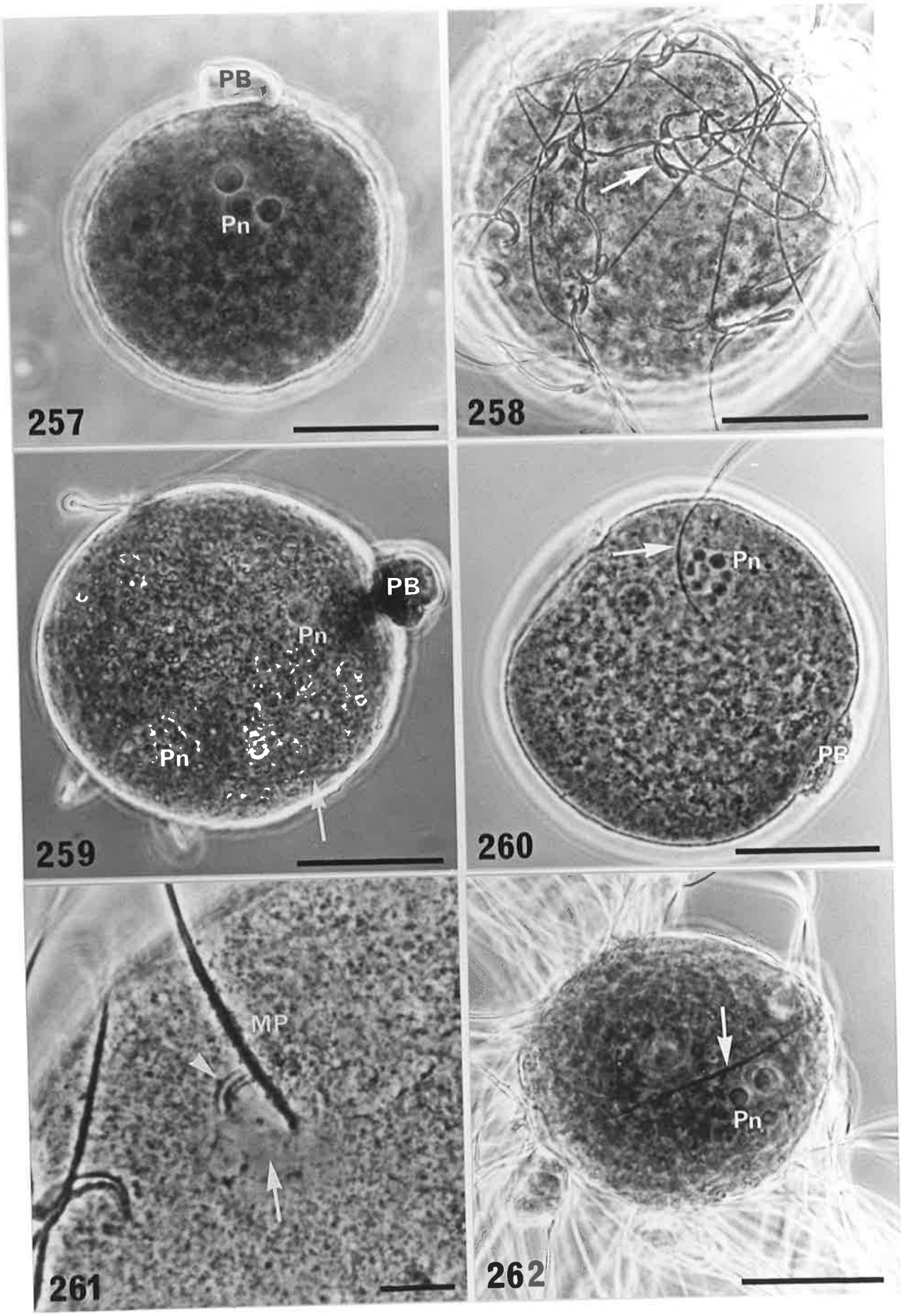
PB
Pn
257
258
PB
Pn
Pn
259
Pn
PB
260
MP
261
Pn
262

PLATE 53

Fig. 263. Plains mouse sperm cultured in TCM for 4 hours. The principal segment of the acrosome appears to have vesiculated, revealing the dorsal ridges (DR). The equatorial segment (ES) is present, but the plasma membrane is broken (arrow).
Bar = 0.5 µm. x 44,090

Fig. 264. Plains mouse sperm after incubation in HBT6 for 12 hours. The entire acrosome has been lost, leaving only the exposed inner acrosomal membrane (arrow).
Bar = 0.5 µm. x 44,090

Fig. 265. HBT6, 2 hours. A vesiculated acrosomal ghost occurs on the dorsal margin of the sperm head (arrow). The equatorial segment (ES) is largely intact, and fine bridging elements link the inner and outer membranes (white arrow).
Bar = 0.5 µm. x 48,700

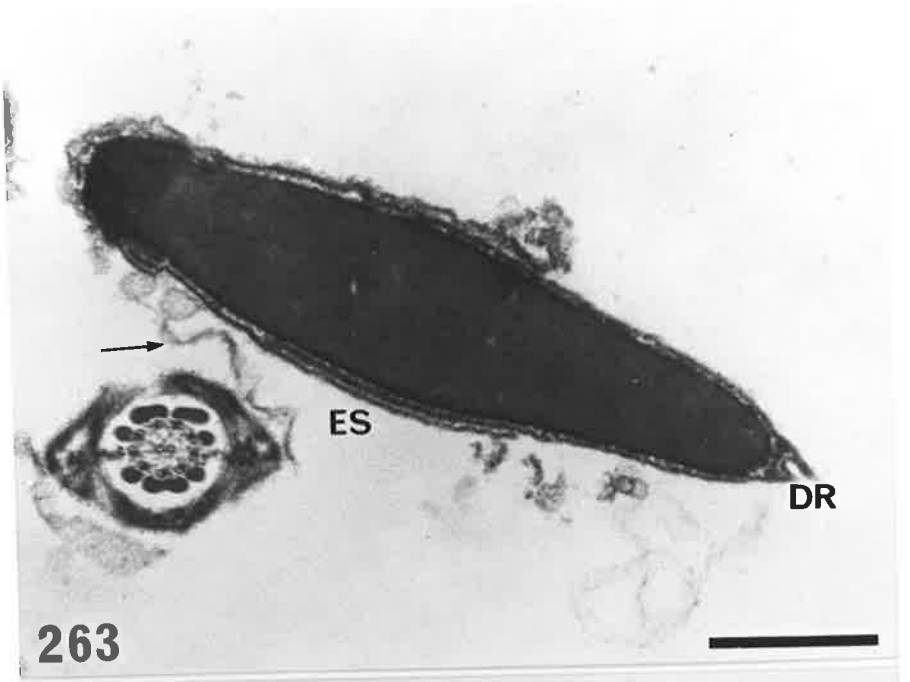

263

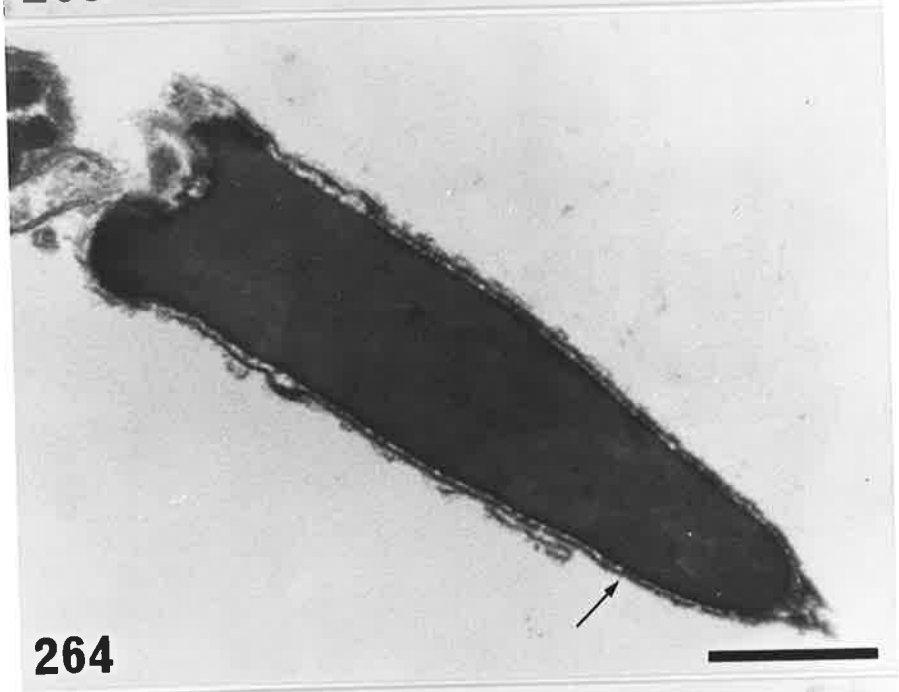

264

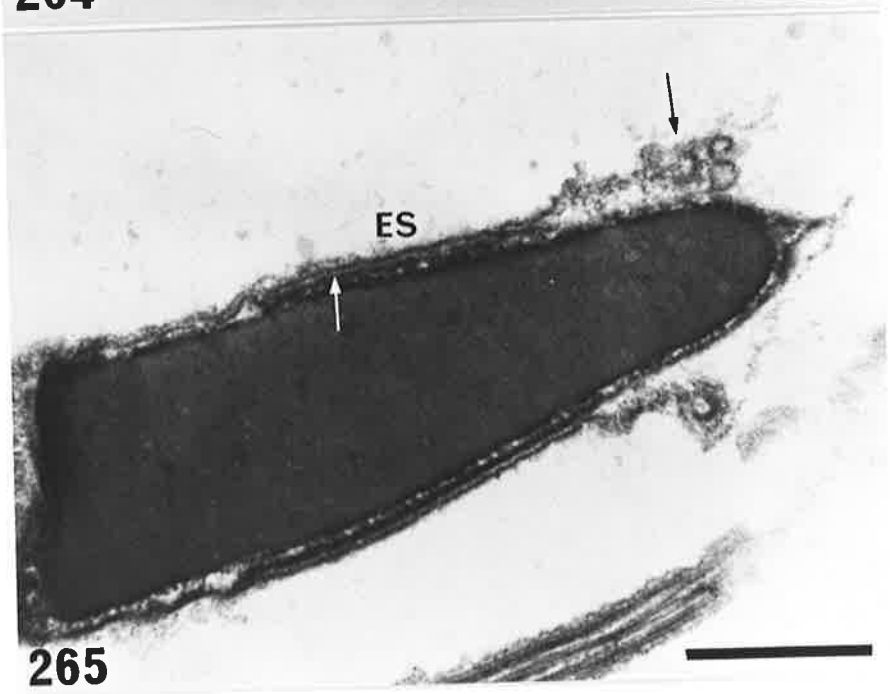

265